SKB

TECHNICAL REPORT 97-17

A site scale analysis of groundwater flow and salinity distribution in the Äspö area

Urban Svensson

Computer-aided Fluid Engineering AB

October 1997

SVENSK KÄRNBRÄNSLEHANTERING AB
SWEDISH NUCLEAR FUEL AND WASTE MANAGEMENT CO

P.O.BOX 5864 S-102 40 STOCKHOLM SWEDEN
PHONE +46 8 459 84 00
FAX +46 8 661 57 19

A SITE SCALE ANALYSIS OF GROUNDWATER FLOW AND SALINITY DISTRIBUTION IN THE ÄSPÖ AREA

Urban Svensson

Computer-aided Fluid Engineering AB

October 1997

This report concerns a study which was conducted for SKB. The conclusions and viewpoints presented in the report are those of the author(s) and do not necessarily coincide with those of the client.

Information on SKB technical reports from1977-1978 (TR 121), 1979 (TR 79-28), 1980 (TR 80-26), 1981 (TR 81-17), 1982 (TR 82-28), 1983 (TR 83-77), 1984 (TR 85-01), 1985 (TR 85-20), 1986 (TR 86-31), 1987 (TR 87-33), 1988 (TR 88-32), 1989 (TR 89-40), 1990 (TR 90-46), 1991 (TR 91-64), 1992 (TR 92-46), 1993 (TR 93-34), 1994 (TR 94-33), 1995 (TR 95-37) and 1996 (TR 96-25) is available through SKB.

A SITE SCALE ANALYSIS OF GROUNDWATER FLOW AND SALINITY DISTRIBUTION IN THE ÄSPÖ AREA

Urban Svensson
Computer-aided Fluid Engineering AB

October 1997

Keywords: numerical model, groundwater, site scale, density, stratification, Äspö HRL

ABSTRACT

The objective of the study is to develop, calibrate and apply a numerical simulation model of the Äspö area. An area of 1.8 x 1.8 km^2, centred around the Äspö Hard Rock Laboratory (HRL), gives the horizontal extent of the model. In the vertical direction the model follows the topography at the upper boundary and has a lower boundary at 1 000 metres below sea level.

The model is based on a mathematical model that includes equations for the Darcy velocities, mass conservation and salinity distribution. Gravitational effects are thus fully accounted for. A regional groundwater model was used to generate boundary conditions for vertical and bottom boundaries.

Transmissivities of fracture zones and conductivities for the rock in between, as used in the model, are based on field data.

An extensive calibration of the model is carried out, using data for natural conditions (i.e. prior to the construction of the Äspö HRL), drawdowns from a pumptest and data collected during the excavation of the tunnel. A satisfactory agreement with field data is obtained by the calibration.

Main results from the model include vertical and horizontal sections of flow, salinity and hydraulic head distributions for natural conditions and for completed tunnel. A sensitivity study, where boundary conditions and material properties are modified, is also carried out. The model is also used to describe some characteristic features of the site like infiltration rates, flux statistics at a depth of 450 metres, salinity of inflows to the tunnel and flow and salinity distributions in fracture zones.

The general conclusion of the study is that the model developed can simulate the conditions at Äspö, both natural and with Äspö HRL present, in a realistic manner.

ABSTRACT (Swedish)

Syftet med studien är att utveckla, kalibrera och tillämpa en numerisk simuleringsmodell för Äspö-området. Den modellerade arean är 1.8 x 1.8 km^2 centrerad runt Äspölaboratoriet. Vertikalt följer modellen områdets topografi på övre randen och har en nedre rand på ett djup av 1 000 meter under havsnivån.

Modellen baseras på en matematisk modell som innefattar Darcys ekvationer, konservering av massa och en ekvation för salthaltsfördelningen. Gravitationella effekter är inkluderade i dessa ekvationer.

Transmissiviteter för sprickzoner och konduktiviteter för det mer eller mindre intakta berget baseras på data från fältmätningar.

Modellen kalibreras mot fältdata för naturliga förhållanden (innan tunneln byggdes), ett pumptest och data från tunnelns konstruktionsskede. Genom mindre justeringar av transmissiviteter och konduktiviteter erhålls en god överensstämmelse med fältdata.

Huvudsakliga resultat från modellen är ett antal horisontella och vertikala snitt genom modellvolymen där flöde, salthalt och tryck redovisas. Detta för naturliga förhållanden och färdig tunnel. En känslighetsstudie, där randvärden och materialegenskaper varieras, genomförs också. Ett kapitel ägnas åt att beskriva några karakteristiska drag hos området, såsom det beskrivs av modellen. Till exempel beskrivs infiltrationens djupberoende och hur flöde och salthalt fördelar sig i sprickzoner.

Den generella slutsatsen från studien är att den utvecklade modellen simulerar förhållandena på Äspö på ett realistiskt sätt, både för naturliga förhållanden och med Äspölaboratoriet.

TABLE OF CONTENTS

1 INTRODUCTION

1.1 BACKGROUND

The Äspö Hard Rock Laboratory (HRL) is a laboratory for the development and testing of methods for detailed characterisation of the rock volume from excavated tunnels. Further, Äspö is a full scale laboratory for testing construction and handling techniques and for the demonstration of important parts of a repository system. Finally, it provides a multitude of data for development of our knowledge of important processes in deep crystalline bedrock and for testing of models for groundwater composition, groundwater flow and radionuclide migration.

A major milestone was reached 1996 with the completion of the pre-investigation and construction phases. The comprehensive research conducted has enabled valuable development and verification of site characterisation methods applied from the ground surface, boreholes and underground excavations. The hydrogeological characterisation of the area has in this context been revised and updated, see Rhén et al (1997). The updated conceptual models and data have motivated the present study and will form the basis for the numerical simulations to be presented.

In the safety assessment of a deep repository for spent nuclear fuel, it is expected that numerical simulation models will play an important role. The models can provide estimates of the groundwater flow around the repository and transport times, from the repository to the biosphere, for tracers. One of the problems when setting up such models concerns scales. We need to consider length scales from 10 metres (canister performance) to a regional scale of perhaps 10 km. Most of the models have so far been set up for a site scale, which typically covers a volume of $1 \times 1 \times 1$ km^3. At the vertical boundaries of the site scale model one needs to assume that the pressure and salinity distributions are known. Generally, it is not possible to account for a regional groundwater flow by these boundary conditions. The site scale model to be presented in this report uses boundary conditions obtained from a regional groundwater model, see Svensson (1997), and hence considers regional effects. It is expected that the site scale model will be used to generate boundary conditions to what is called a laboratory scale model (covering typically 0.5 x 0.5 x 0.5 km^3), which can be used to study details around the excavated tunnels. The present study is thus part of a larger modelling project, which attempts to cover the whole range of lengthscales mentioned.

1.2 SITE DESCRIPTION

The Äspö Hard Rock Laboratory is located near the Oskarshamn nuclear power plant on the east cost of Sweden, see Figure 1-1. The access tunnel starts on the mainland, goes under the Baltic and reaches the spiral part of the tunnel beneath the island of Äspö. The total length of the tunnel is 3600 metres and it reaches a depth of 450 metres below ground. A vertical elevator shaft connects the laboratory to the Äspö Research Village. In Figure 1-1 a black rectangle shows the boundaries of the site scale model.

Mean precipitation minus evapotranspiration, P-E, has been estimated to be about 200 mm/year for the region, Rhén et al (1997). For the island of Äspö one can expect that the groundwater recharge (i.e. P-E) is smaller as the distance to the sea is smaller (no storage of water in lakes and ponds during periods of heavy precipitation). A value of 100 mm/year will be used in this study.

Around the island of Äspö the Baltic has a salinity of about 0.6%. It is known from boreholes on Äspö that the fresh water lens below Äspö has a thickness of 100-200 metres under natural conditions; below this level the salinity increases to reach a value of about 2% at a depth of 800 metres below ground. As the water density increases with salinity we have a density stratified water below the Island of Äspö. This is an important feature of the groundwater flow system.

1.3 OBJECTIVES

The main objective of the study is to develop and establish an adequate model of the groundwater flow and salinity distribution in the Äspö area. With "adequate model" it is understood that the model should be well balanced with respect to expected use, available data, scientific basis and computational resources.

In order to meet the main objective of the study some specific objectives have been formulated:

- Consider the regional groundwater flow by using boundary conditions generated by a regional groundwater model.
- Put emphasis on the calibration process.
- Carry out sensitivity studies in order to establish that the model reacts to variations in input data in a reasonable way.
- Make the presentation of results, in form of figures, diagrams and tables, extensive.

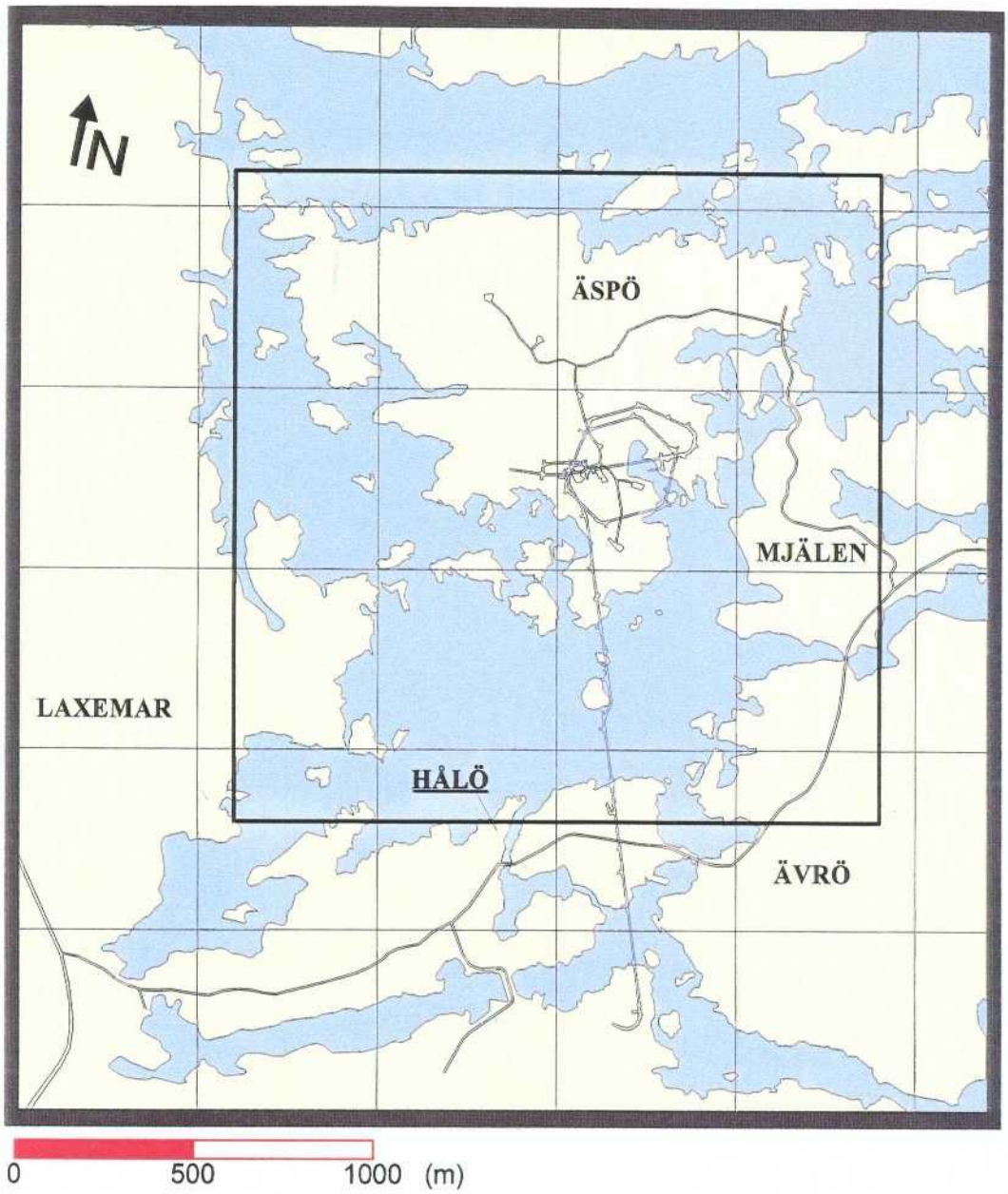

Figure 1-1. *The island of Äspö and the Äspö Hard Rock Laboratory. The black rectangle shows the model area. N is magnetic north.*

2 MATHEMATICAL MODEL

2.1 BASIC APPROACH AND ASSUMPTIONS

Groundwater models can be developed for a number of purposes; perhaps the most common one is that the rainfall - runoff relation is requested. As stated above, the objective of the present study is to understand the groundwater flow below the island of Äspö. With this in mind the following basic requirements for the simulation model have been formulated:

- It needs to be three-dimensional with high resolution in space. We need to be able to simulate the effect of the Äspö Hard Rock Laboratory (HRL) and at the same time resolve the general hydrology of the area.

- Variable density needs to be accounted for, as the salinity of the groundwater will vary in the domain.

- The model should predict a realistic groundwater level, as we expect a balance between the pressure generated by the water table and the pressure due to the internal density distribution.

We will further introduce some basic assumptions; some of which are motivated by the purpose of the study, others by the lack of information or data. The following assumptions are made:

- Flow, pressure and salinity fields are in a steady state. This assumption seems appropriate from the purpose of study. It may however be questioned if the salinity field will ever be in a steady state.

- Spatial uniformity. Due to lack of data we need to assume that precipitation and evapotranspiration are horizontally uniform. Variations in vegetation and soil types are also neglected.

- The unsaturated zone can be handled by the simple algorithm introduced in Svensson (1995).

The computational domain was introduced in Figure 1-1. The motives for the size and orientation of the domain can be summarised as follows:

- The orientation should follow the Äspö coordinate system, for simple and secure integration with the Äspö data base.

- The size should be comparable to the expected "radius of influence" of the Äspö HRL. From the drawdowns, due to the Äspö HRL, one can estimate this radius to about 1 km.

- The computational grid should not have more than 500 000 cells, in order to avoid extreme execution times on a low-end workstation.

These considerations led to a domain of 1.8 x 1.8 x 1.0 km^3, centred around the Äspö HRL, represented in a computational grid of 90 x 90 x 55 cells.

These are the basic requirements and assumptions of the model.

2.2 GOVERNING EQUATIONS

For the momentum balance it will be assumed that the Darcy law applies. For the salinity equation we will assume a balance between advective transport and dispersion, i.e. the time derivative is neglected.

Within these assumptions, and the ones in the previous section, the following set of equations can be formulated.

Momentum:

$$0 = -\frac{\partial p}{\partial x} - \frac{\rho g}{K_x} u \tag{1}$$

$$0 = -\frac{\partial p}{\partial y} - \frac{\rho g}{K_y} v \tag{2}$$

$$0 = -\frac{\partial p}{\partial z} - \frac{\rho g}{K_z} w - \rho g \tag{3}$$

Salinity balance:

$$\frac{\partial}{\partial x} us + \frac{\partial}{\partial y} vs + \frac{\partial}{\partial z} ws = \frac{\partial}{\partial x}\left(Dn \frac{\partial s}{\partial x} \right) + \frac{\partial}{\partial y}\left(Dn \frac{\partial s}{\partial y} \right) + \frac{\partial}{\partial z}\left(Dn \frac{\partial s}{\partial z} \right) \tag{4}$$

Mass balance:

$$\frac{\partial}{\partial x} \rho u + \frac{\partial}{\partial y} \rho v + \frac{\partial}{\partial z} \rho w = 0 \tag{5}$$

Equation of state:

$$\rho = \rho_0(1 + \alpha s) \tag{6}$$

Where *u, v, w* are Darcy velocities, *p* pressure, *s* salinity (in %, by weight), K_x, K_y, K_z conductivities, *D* hydraulic dispersion coefficient, *n* kinematic porosity, α a coefficient $\left(= 7.8 \times 10^{-3}\right)$, ρ_0 a reference density of water (= 1 000 kg/m^3), ρ density of water and *g* gravitational acceleration. The coordinate system is denoted *x, y, z* with *x* in the east direction, *y* north and *z* vertical upwards.

It is still unclear (at least to the author) how the hydraulic dispersion coefficient ought to be interpreted and determined in a fractured rock. For a general porous media, where a representative elementary volume can be defined, general tensor expressions are available, see Bear et al (1987). A further complicating factor is that we are going to apply the salinity equation in a discretized form, i.e. on our computational grid. A suggestion is that the dispersion coefficient should account for sub-grid mixing processes. Due to the uncertainty about the interpretation of the process we will assume that the dispersion coefficient is isotropic, proportional to the local velocity and the grid-size, hence:

$$D = \beta \Delta |\vec{U}| \tag{7}$$

where β is an unknown coefficient, Δ the grid-spacing and $|\vec{U}|$ the magnitude of the pore-velocity. As seen, the effect of molecular diffusion is also neglected in (7). As *D* is multiplied with *n* in equation (4) we will further assume that $n\,|\vec{U}|$ is equal to the magnitude of the Darcy velocity. A constant value of 2 metres was set for the product $\beta\Delta$.

2.3 GEOMETRIC FRAMEWORK AND MATERIAL PROPERTIES

Major fracture zones on Äspö are shown in Figure 2-1. The thick lines in the figure indicate regional fracture zones; these were used in the regional groundwater model, see Svensson (1997), and are in the site model essential for the connection of boundary conditions to the local fracture zone system. The fracture zones are assumed to be two-dimensional and planar. Data about the fracture zones are given by Rhén et al (1997); here we only reproduce the map of the fracture zones, see Figure 2-1, and their transmissivities, see Table 2-1.

The hydraulic conductivity for the rock mass in between the fracture zones has been estimated from borehole tests. Rhén et al

(1997) have compiled and analysed the field data and found that the Äspö area can be divided into *Rock block domains*; these are illustrated in Figure 2-2. It is well-known that the hydraulic conductivity and its standard deviation depends on the test scale. Rhén et al provide data for various test scales and also scaling laws that can be used to obtained data for a given scale. These data and scaling laws were used to obtained the hydraulic conductivities for *Rock block domains* given in Table 2-2.

The computational domain is $1.8\times1.8\times1.0\,\mathrm{km}^3$, which is represented in a grid with a total of 445 500 cells $(90\times90\times55)$. Part of the grid is shown in Figure 2-3. As can be seen the grid follows the topography (boundary-fitted grid), but has a uniform cellsize (= 20 metres) in the horizontal plane. The vertically non-uniform grid is restricted to the top 100 metres of the domain. For this part of the grid we start with a cellsize distribution (from groundlevel downwards) as follows: 0.5, 1.0, 1.5, 2.0, 5.0, 10.0 and 4 x 20.0 metres. This sequence of cells is then stretched/compressed to follow the topography, which means that the cell-sizes in the sequence are somewhat smaller below the Baltic and somewhat larger below land. Below 100 metres the cellsize is 20 metres in all three directions. It should be noted that the grid follows the sea-bed and not the free surface of the Baltic.

Conductivities for the top five cell layers, i.e. down to 10 metres, are given a special interpretation. One reason for this is that the soil cover can be expected to have a conductivity which is high, but rapidly decreasing with depth. Another is that small ephemeral rills and channels need to be accounted for by the conductivity of the near ground surface cells. The conductivity of the top five cell layers will be considered as calibration parameters and we can thus not assign any values to these at this stage.

A further modification of the conductivity field and fracture zone transmissivities is needed to account for unsaturated conditions. A method to predict the depth of the unsaturated zone was introduced in Svensson (1995). Here a brief account of the basic idea of the method will be given.

- Neglect capillary forces, which means that the pressure in the unsaturated zone will be equal to the atmospheric pressure (set to zero).

- The unsaturated zone is partly blocked by air and hence provide higher resistance to flow. Introduce a resistance factor, ϕ, in the balance of forces. The vertical balance, equation (3), then reads:

$$0 = -\frac{\partial p}{\partial z} - \frac{\rho g}{K_z} w\phi - \rho g \qquad (8)$$

- For $\phi = 1$ a negative pressure is predicted for the unsaturated zone. The problem is to find a ϕ - field that gives zero pressure in the unsaturated zone and, of course, has a value of 1.0 in the saturated zone. This can be achieved by an iterative procedure, see Svensson (1995) for details and applications.

Below the Baltic a clay layer of a few meters thickness is normally found. This was considered in the model by prescribing a conductivity of 10^{-9} m/s to a 3 metres thick layer, centred 5 metres below the sea bed.

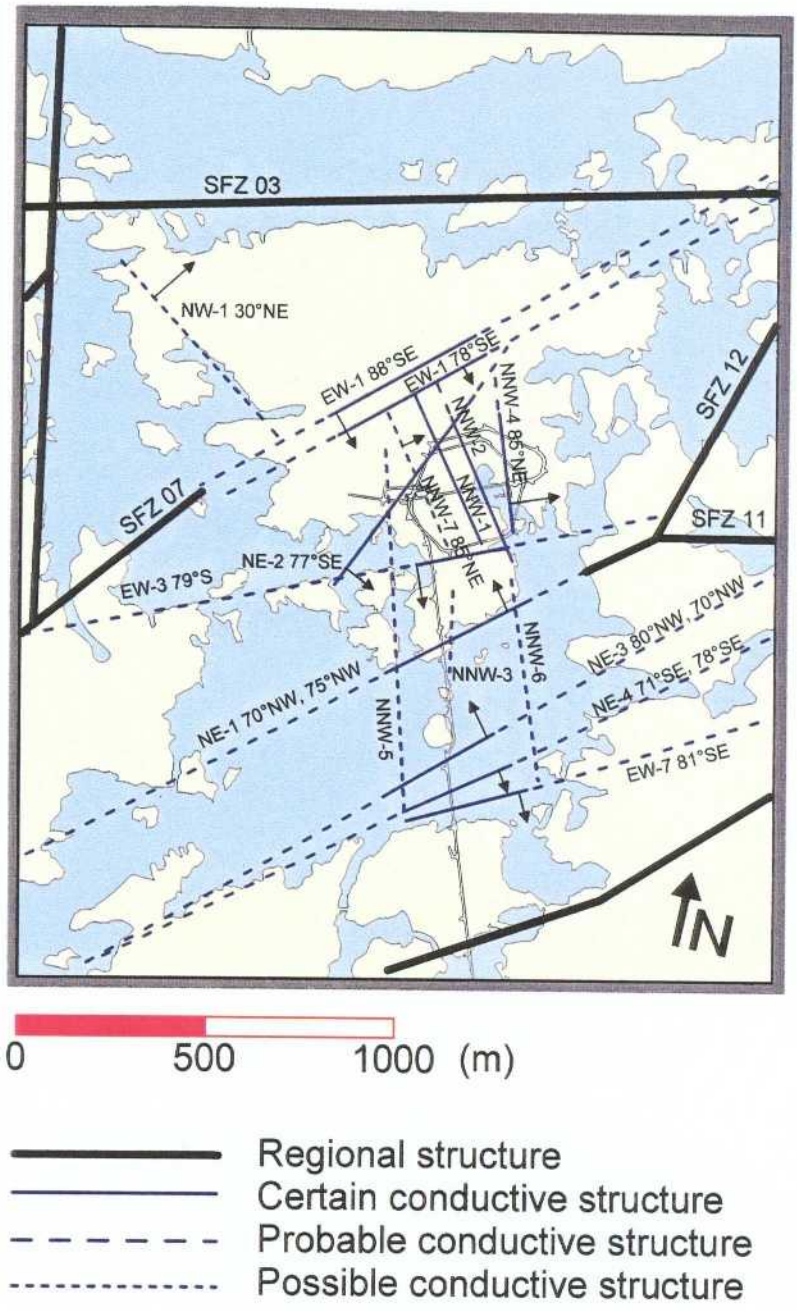

Figure 2-1. *Major fracture zones in the area, after Rhén et al (1997).*

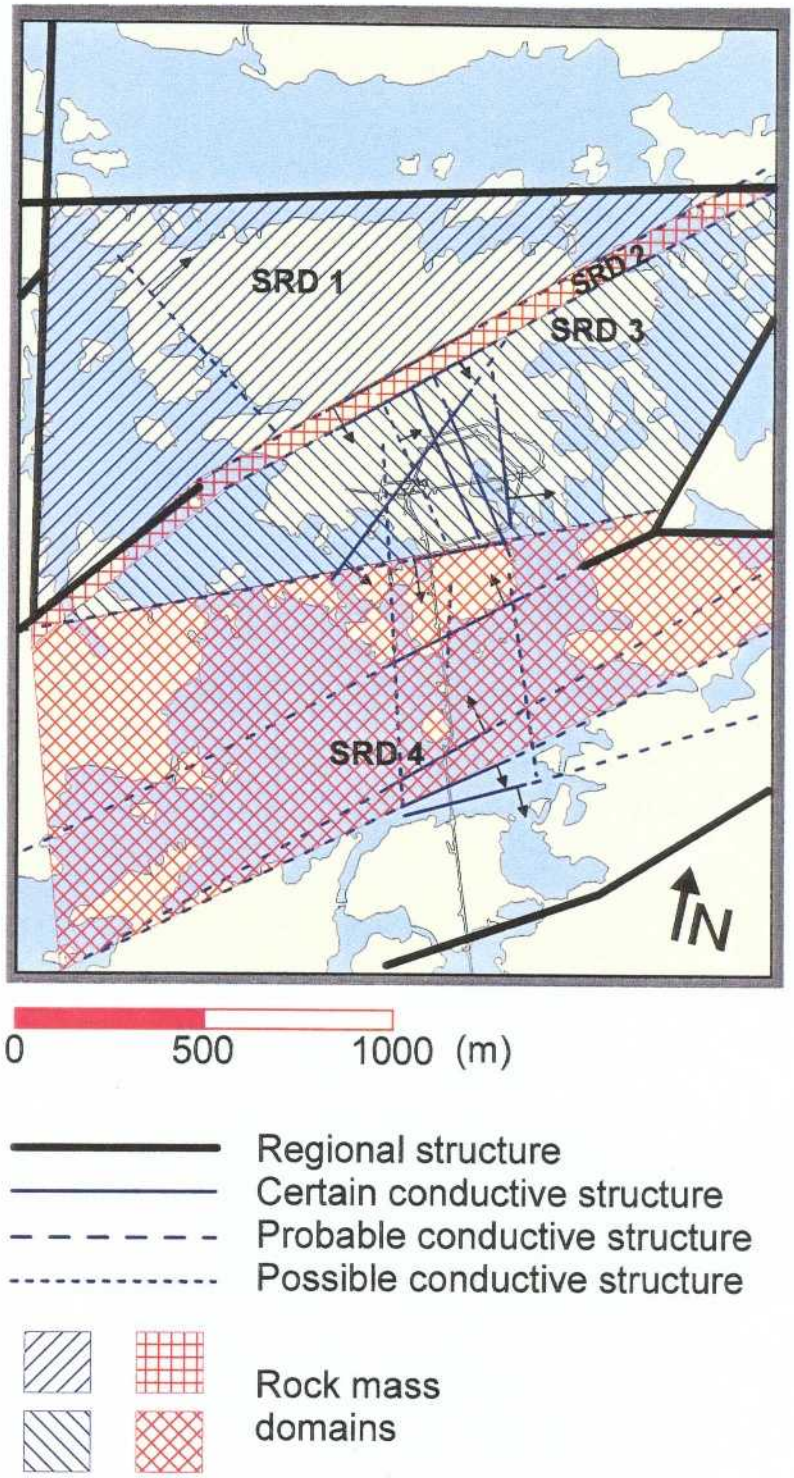

Figure 2-2. *Rock block domains, for further details see Rhén et al (1997).*

Table 2-1. Transmissivities of conductive structures on Äspö, after Rhén et al (1997).

Fracture zone	Transmissivity x 10^{-5}[m^2/s]
NW1	0.041
EW1, 88°	0.052
EW1, 78°	1.2
EW3	1.7
NE2	0.012
NE4	3.1
EW7	1.5
NE3	32.0
NE1	22.0
NNW1	0.86
NNW2	2.4
NNW3	2.0
NNW4	6.5
NNW5	0.4
NNW6	1.4
NNW7	0.75
NNW8	0.84
SFZ03	0.3
SFZ07	0.3
SFZ11	0.3
SFZ12	10.0

Table 2-2. Hydraulic conductivities for rock block domains, based on data and scaling laws from Rhén et al (1997). Scale: 20 m.

Rock block domain	Depth range (metres)	Log_{10} (K)	Standard deviation s(Log_{10} (K))
SRD1	0-600	- 8.10	0.70
SRD2	0-600	- 7.18	1.17
SRD3	0-600	- 8.83	1.01
SRD4	0-600	- 6.36	1.51
SRD1-4	600→	- 8.25	1.61
SRD5	see Rhén et al (1997)	- 7.68	1.37

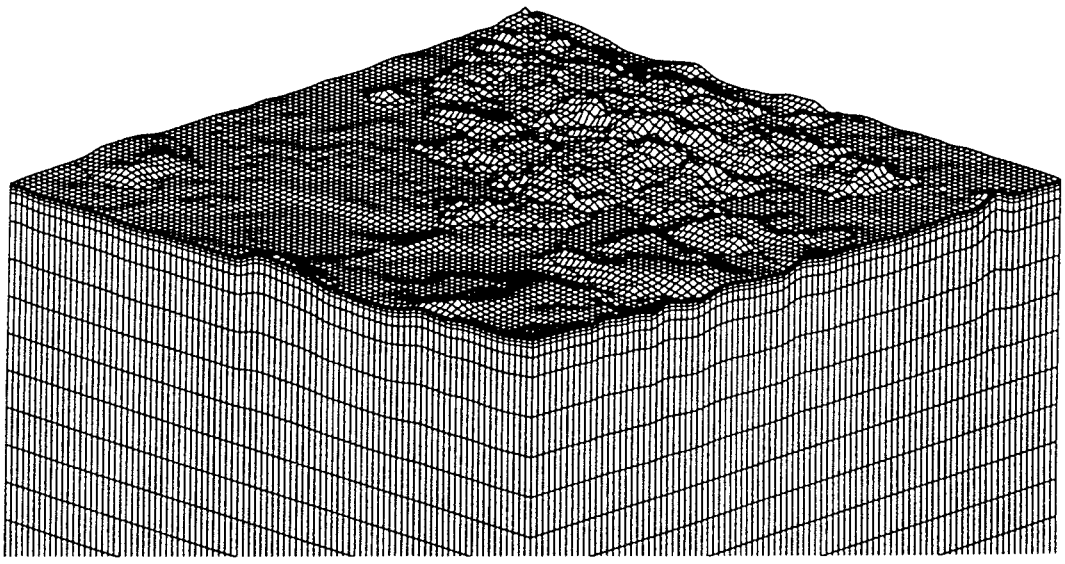

Figure 2-3. *Computational grid close to ground. 100 metres below sea level a uniform grid is used. The vertical scale has been stretched in the figure. View from south-east.*

2.4 SPATIAL ASSIGNMENT METHOD

The conductivity and transmissivity data given in the previous section need to be assigned to the computational grid. The main steps in this procedure are:

- Generate a conductivity randomly for each computational cell using the geometric mean values and standard deviations given in Table 2-2. No correlation is assumed between the cells.

- Generate cell wall conductivities by calculating a geometric mean between the cell and its neighbour. This is done for all cell walls and hence gives a locally anisotropic conductivity, i.e. for a given cell all cell wall conductivities are different.

- Calculate the length of the fracture zone crossings for each cell wall. Modify the cell wall conductivity with respect to the transmissivity of the fracture zones.

- Modify the conductivity for the top five layers. This is done as a condition; "if the cell wall conductivity is smaller than the prescribed conductivity for the cell layer, the prescribed value is used".

- Finally, modify conductivities with respect to unsaturated conditions. As this modification depends on the pressure, which is part of the calculation, it needs to be done during the iteration process.

Further details about the third point can be found in Svensson (1997).

The method outlined for the unsaturated zone may result in a vertical column of cells that has very low conductivities on all vertical cell walls. As we have a recharge at ground level an isolated column of water may result if, at some level, a low vertical conductivity is generated. The remedy to this problem was to prescribe a minimum vertical conductivity, equal to 5×10^{-9} m/s, above the spiral part of the tunnel, down to a depth of 140 metres.

2.5 BOUNDARY CONDITIONS

At the top boundary a net recharge of 100 mm/year is specified above sea level. Below the Baltic Sea a hydrostatic pressure is prescribed, with respect to the local water depth, and the salinity is fixed to the salinity of the Baltic (= 0.6%).

At the vertical and bottom boundaries pressure and salinity fields from the regional groundwater model are used. In a first attempt to incorporate these fields, pressure and salinity were prescribed in the

first plane of cells at each boundary. However, this proved to be inconsistent as, since the conductivity field is given, the resulting Darcy velocities parallel to the boundaries will then also be prescribed. The mass conservation equation will then require a perpendicular (to the boundary) flux which is then also is fixed; this is unrealistic. Instead the pressure fields are prescribed not in the cells but at the external boundary of the cells, see Figure 2-4. The pressure field is then linked to the first plane of cells through a conductivity of 5×10^{-7} m/s.

The inflow to the cell will then be calculated as:

$$Q = A \times K \frac{\Delta P}{\Delta X_i} \tag{9}$$

where A is the cell area at the boundary, K the conductivity mentioned, ΔP the pressure difference between the external pressure and the pressure in the cell and ΔX_i the distance from the cell centre to the boundary.

However, a further problem was encountered due to the different resolutions in the regional- and site-model. The problem is illustrated in Figure 2-4. As the resolution is higher in the site-model a "local" pressure field, not found in the regional model, will be present in the first plane of cells in the site-model. The final procedure adopted is to apply a zero flux condition for the top 100 metres of the model and a prescribed external pressure below this level. For salinity the values from the regional model are prescribed at the first plane of cells, for the whole depth.

When the Äspö HRL is included in a simulation we need to consider the inflows to the tunnel. These inflows are not boundary conditions in the usual meaning; a more relevant name is perhaps "distributed mass sinks". The measured inflows to tunnel sections need to be assigned to computational cells with a fracture zone crossing. Based on the measured data given by Rhén et al (1997), the distributions given by Table 2-3 have been estimated. Distributions are given for the two tunnel front positions to be considered in this report.

2.6 NUMERICAL TOOL AND OUTPUT PARAMETERS

The system of equations is solved by the general equation solver PHOENICS, Spalding (1981). PHOENICS is based on a finite-volume formulation of the basic equations and embodies a wide range of coordinate systems (cartesian, body-fitted, cylindrical, etc) and numerical techniques (higher order schemes, solvers, etc).

The basic output parameters from the model are pressure, salinity and Darcy velocities. It is however simple to generate additional output parameters like hydraulic head and density.

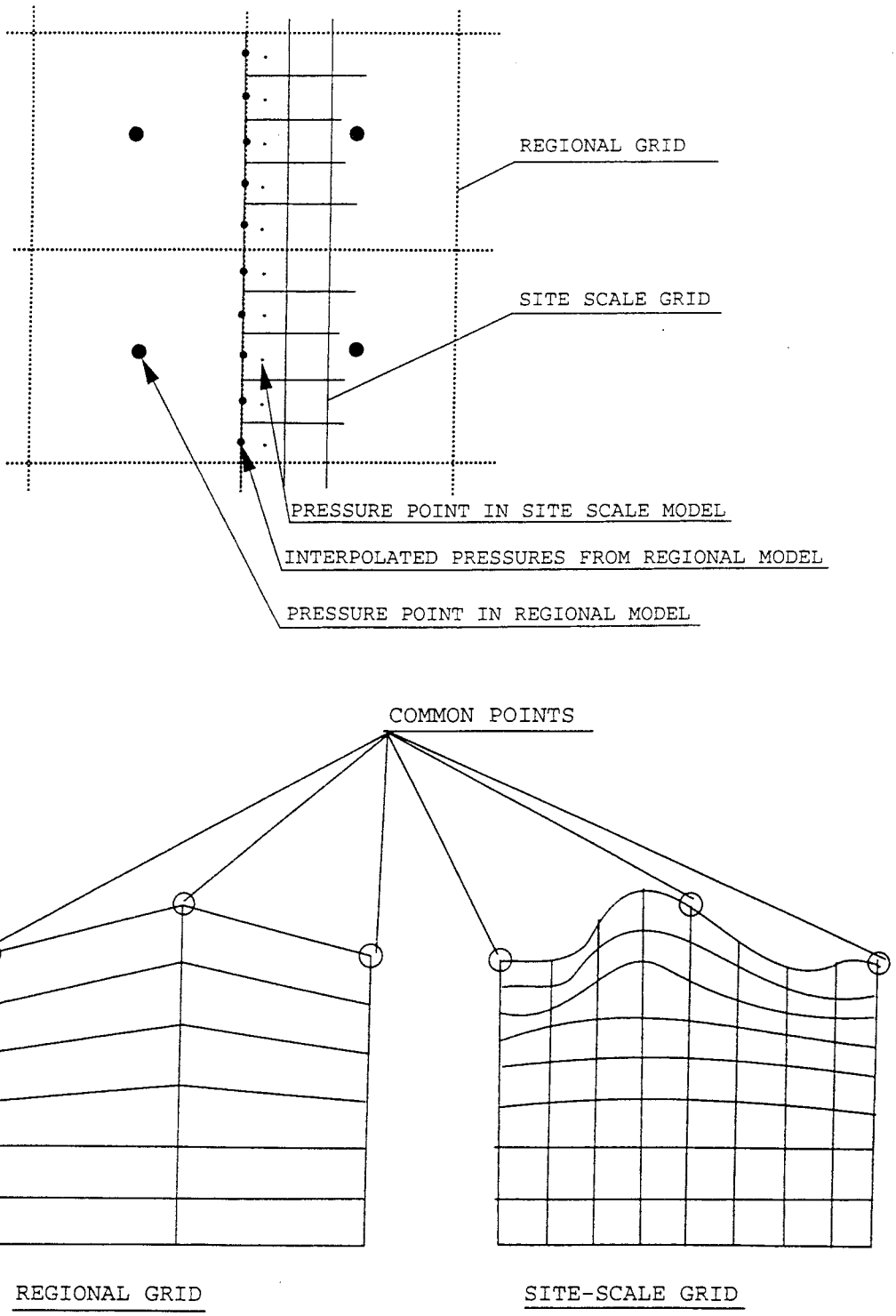

Figure 2-4. *The introduction of boundary conditions from a regional model.*
- Linking regional pressures to the site scale (top).
- Illustration of a problem due to different resolution of the topography in the two model scales.

Table 2-3. Inflows to Äspö HRL. Measured inflows at two tunnel front positions and assigned fracture zones for withdrawal. Basic data from Rhén et al (1997).

Tunnel section (m)	Measured inflow l/s		Selected zone(s) for withdrawal
	Tunnel front 2875 (m)	Tunnel front 3600 (m)	
0-850	2.36	1.90	NE4
850-1030	5.52	5.52	NE3
1030-1160	1.58	1.40	NNW3
1160-1310	7.26	7.00	NE1
1310-1460	2.03	2.03	EW3
1460-1584	0.61	0.61	NE2
1584-1745	0.34	0.27	NNW7
1745-1883	0.52	0.36	NNW1, NNW2
1883-2028	0.63	0.47	NNW4
2028-2178	0.92	0.70	NNW4
2178-2357	1.15	1.42	NNW1, NNW2
2357-2496	0.07	0.17	NE2
2496-2699	0.93	0.93	NNW7
2699-2875	0.59	0.38	NNW1, NNW2
2875-2994		1.12	NNW4
2994-3179		2.33	NNW4
3179-3426		0.96	NNW1, NNW2
3426-3600		0.46	NNW5
Shaft	3.05	1.54	NNW7
	Σ 27.56	Σ 29.57	

3 CALIBRATION

3.1 INTRODUCTION

A groundwater model is normally calibrated by adjusting conductivities and transmissivities to meet some predefined conditions or criteria, for example the drawdown due to a pumptest. In this study a fairly extensive calibration process will be carried out using data for natural conditions, a long term pumptest (called LPT2) and the drawdown by the Äspö HRL.

Natural conditions mean conditions prior to the start of the construction of the Äspö HRL. The data of interest are the groundwater level on Äspö and the salinity distribution below Äspö as measured in boreholes on Äspö. The name and location of the boreholes are given in Figure 3-1.

The LPT2 experiment was performed in 1990. Borehole KAS06, see Figure 3-1, was chosen for pumping and drawdown was observed in about 100 packed-off borehole sections. The inflow distribution to borehole KAS06 was estimated in the experiment and this information was used to distribute the total inflow to fracture zones crossing KAS06, see Table 3-1. The inflow data and further information about LPT2 can be found in Rhén et al (1992) and Gustafson and Ström (1995).

During the construction of the Äspö HRL, the pressure was monitored in the borehole sections mentioned above. The drawdown at tunnel front position 2875 metres can be found in Rhén et al (1994); these data will be used for the present calibration.

Table 3-1. Inflow distribution to KAS06 during the LPT2 experiment, as used in the simulation model.

Borehole section (m)	Prescribed inflow (l/s)	Fracture zone
0-200	0.34 (15%)	EW3
200-300	0.45 (20%)	NNW1
300-600	1.46 (65%)	NNW2

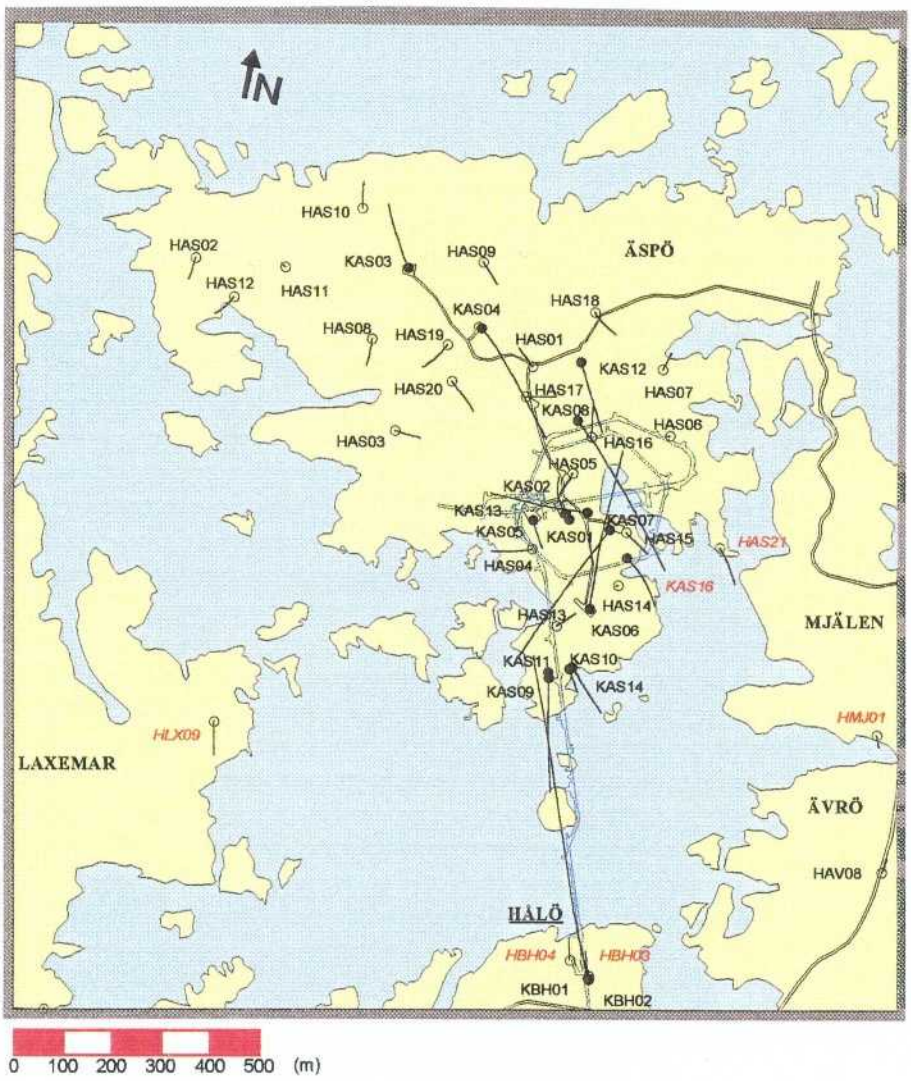

Figure 3-1. *Boreholes in the Äspö area.*

3.2 CALIBRATION CRITERIA

The following calibration criteria were chosen:

- The model should simulate the natural water table on Äspö.
- The calculated vertical salinity distribution below Äspö under natural conditions should be correct.
- The measured drawdowns during the LPT2 experiment should be reproduced.
- The measured drawdowns when the tunnel front was at position 2875 metres should be correctly simulated.
- The drawdown for tunnel front position 3600 metres (completed tunnel) should be close to the drawdown for position 2875 metres.

3.3 CALIBRATION PROCESS

The objective of the calibration process is to adjust the conductivities and transmissivities so as to meet the calibration criteria. There is no established technique or strategy, at least not known to the author, how this should be achieved in an effective way. The present calibration is thus based on a trial and error approach, where the outcome of many trial calculations are studied and an intuitive knowledge about the behaviour is developed. During the calibration process a few guidelines were however formulated:

- Collect uncertainty limits and additional information about the transmissivities and conductivities, in order to be able to modify these within accepted limits. An example of "additional information" used in the present work is that "the conductivity values given in Table 2-2 are probably to low due to conductive features with a scale larger than the cell size. These features introduce correlations not accounted for in the present model" (personal communication, Ingvar Rhén (1997)).
- Identify major disagreements in the comparison with the measured data. These disagreements should require significant (i.e. well outside uncertainty limits) changes in the basic input data.
- When the major disagreements have been removed the fine-tuning starts. As the LPT2 experiment and the spiral part of the tunnel are in the same area it seems reasonable to start the fine-tuning at the centre of the spiral and work outwards.

- Study the three basic situations (natural conditions, LPT2 experiment and 2875 metres position) at the same time and try to understand which changes affect the different situations most. It is for example clear that the conductivities of the top five layers have a stronger influence on the natural groundwater level than on the LPT2 experiment.

These guidelines were followed in the calibration process. Two major disagreements were identified:

- The fracture zone NNW7 has too low transmissivity for the prescribed inflow to the elevator shaft at tunnel front position 2875 metres. In order to increase the transmissivity around the elevator shaft the transmissivities for NNW7 and NE2 were increased with more than an order of magnitude (details below).

- The conductivity of the rock block domain south of Äspö, SRD4, was found to be too high. In order to get agreement with field data the conductivity was decreased (details below).

After these major corrections, the fine-tuning was performed. It should be stated that the adjustments made at this stage can be made in several ways and should thus not be considered as suggestions for updating the original input data.

3.4 MAIN RESULTS

The conductivities and transmissivities that resulted from the calibration process are summarised in Tables 3-2, 3-3 and 3-4.

We shall now return to the calibration criteria and see how well these are met by the calibrated model.

The measured and calculated groundwater levels for natural conditions are shown in Figure 3-2. As seen the agreement is very close and the comparison needs no further comments.

The calculated salinity in various borehole sections are in Table 3-5 compared to measured values, all for natural conditions. The measurements are given in Forsmark and Rhén (1994) and are strictly valid for a borehole section. In Table 3-5 a depth is given, which is an estimate of the "point of application" for the salinity value. The general trend in the comparison is that the model predicts too low salinities close to ground but too high salinities below, say, 500 metres below sea level. Field data thus suggest that the salinity is more dispersed, than the model predicts. It is then tempting to increase the dispersion coefficient in order to improve the comparison. However, in the author's view the result calls for a discussion about the possible physical processes behind the disagreement; such a discussion will be given in Section 7.

Measured and calculated drawdowns during the LPT2 experiment are given in Table A-1, Appendix A. The mean error is –0.01 m and also the point by point agreement is acceptable.
The corresponding comparison for tunnel front at 2875 metres is shown in Table A-2, Appendix A. Also this comparison is regarded as satisfactory; only three borehole sections have an error larger than 10 metres and the mean error is 0.05 metres.

The final criteria concerns the mean drawdowns at tunnel front position 3600 metres (completed tunnel), which should be about the same as for 2875 metres. A calculation for complete tunnel, using the tunnel inflows given in Table 2-3, gave a mean drawdown of 21.1 metres for the borehole sections given in Table A-2. The mean drawdown for 2875 metres is 19.6 metres and the mean drawdowns can thus be regarded as being close.

3.5 ADDITIONAL RESULTS AND DISCUSSION

In this section some additional results and aspects of the calibration procedure will be discussed.

For practical purposes only one realisation of the conductivity field was used in the calibration. With the objective to study how various realisations affect the drawdowns for the 2875 metres position and the LPT2 experiment four more realisations of the conductivity field were used. The result can be studied in Tables A-3 and A-4, Appendix A. The general conclusion from this study is that large variations may result for individual boreholes or sections, see for example K07-J6 and K08-M2 for LPT2 and borehole KAS11 for the 2875 metres position, but the general patterns remain. A close inspection of the results showed, as expected, that the borehole sections which responded with large variations are not in direct contact with a fracture zone.

The boreholes in Figure 3-1 named HASxx were not used in the calibration process. The reason for this is that they are generally rather shallow and not well connected to the fracture zone system. From the above discussion it is then clear that it may be questionable to tune fracture zone transmissivities with reference to these boreholes. However, for completeness the comparisons for these boreholes are also reported, see Tables A-5 and A-6, Appendix A.

The water table for tunnel front position 2875 metres has been constructed from the drawdowns in shallow borehole sections, by Rhén et al (1997). Their figure is in Figure 3-3 compared with the simulated water table, based on the pressure field 40 metres below ground. As can be seen a fairly good agreement is found.

Table 3-2. Fracture zone transmissivities modified during the calibration process. Original values in brackets.

Name	Transmissivity 10^{-5} * [m^2/s]
EW3	1.2 (1.7)
NE2	0.8 (0.012)
NE1	30.0 (22.0)
NNW1	3.0 (0.86)
NNW2	1.0 (2.4)
NNW7	8.0 (0.75)
NNW8	0.1 (0.84)

Table 3-3. Rock domain hydraulic conductivities as modified during the calibration process. Original values in brackets.

Name	Conductivity $Log_{10}(K)$
SRD1	-7.8 (-8.10)
SRD2	-7.1 (-7.18)
SRD3	-8.7 (-8.83)
SRD4	-7.6 (-6.36)

Table 3-4. Conductivities for the top five cell layers as given by the calibration process.

Layer (m)	Conductivity m/s
0-0.5	10^{-3}
0.5-1.5	10^{-3}
1.5-3.0	$5. \times 10^{-4}$
3.0-5.0	10^{-5}
5.0-10.0	$3. \times 10^{-7}$

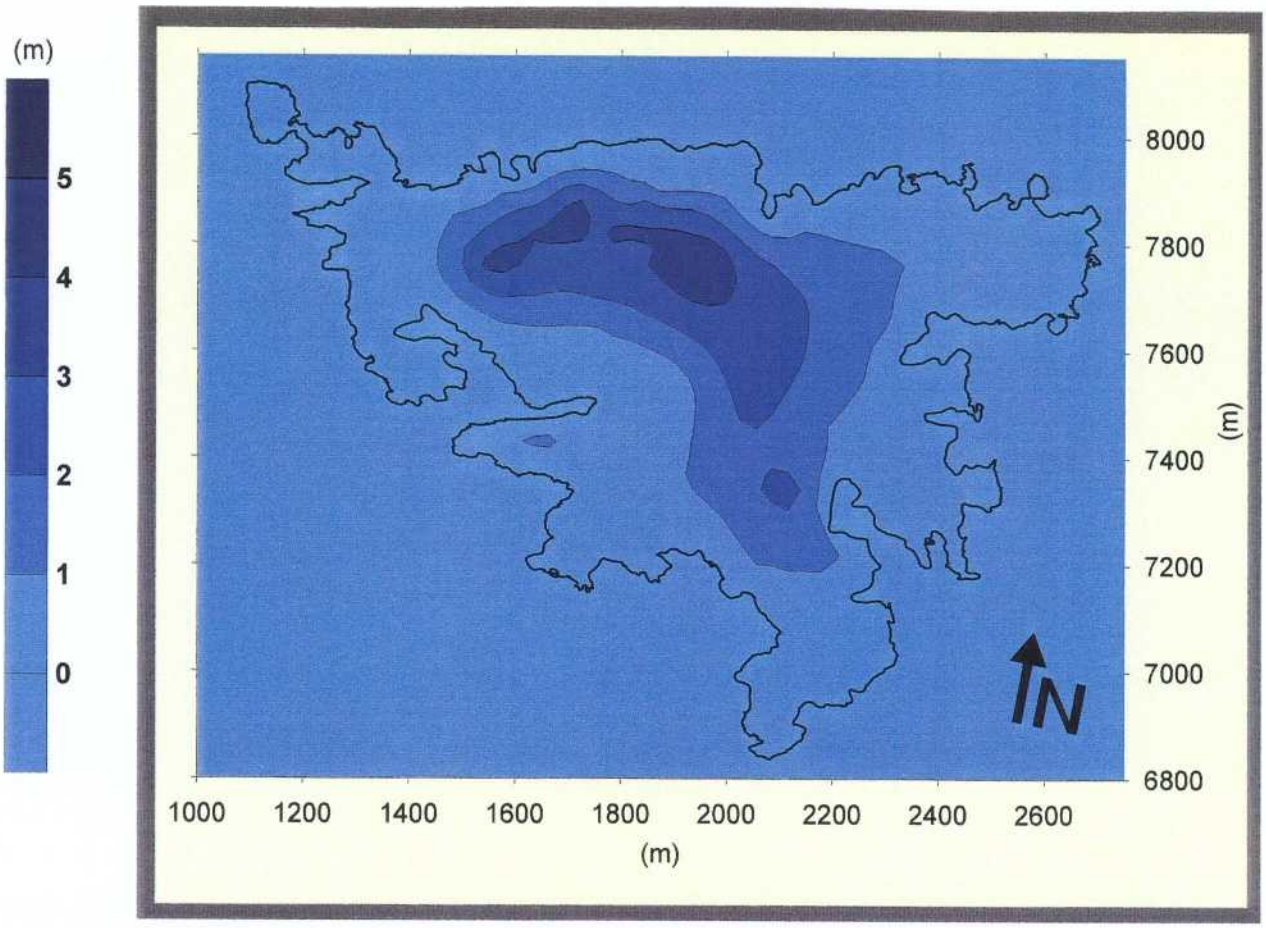

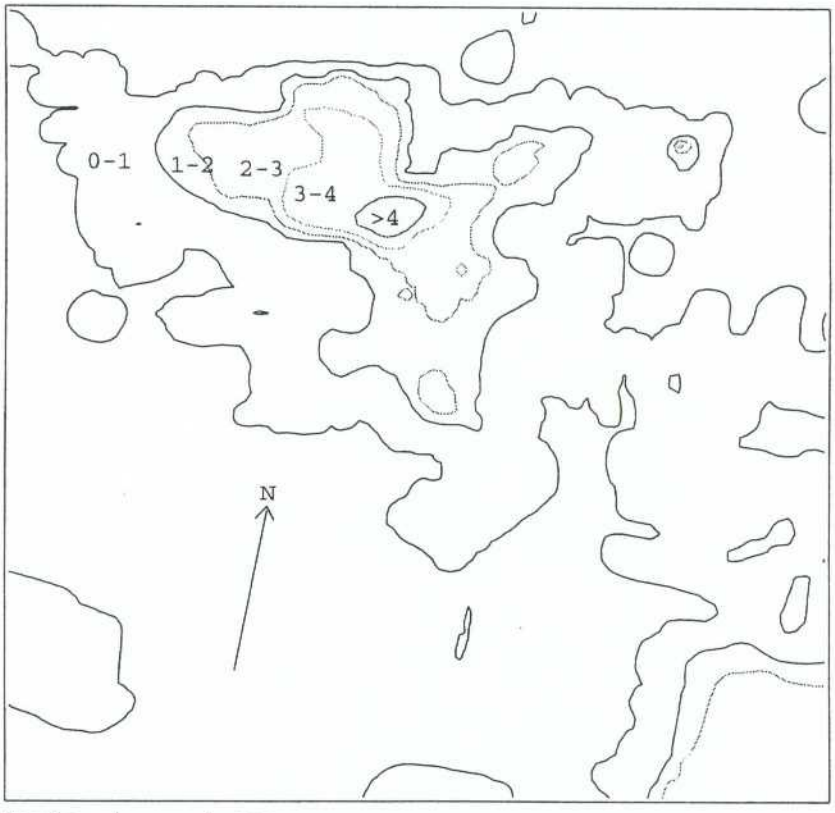

Figure 3-2. *Measured (top) and calculated water table for natural conditions.*

Table 3-5. Comparison between measured and calculated salinity in borehole sections. Natural conditions.

Borehole section	Depth M b s l	Measured salinity %	Calculated salinity %	Error
KAS02A	52.00	0.38	0.00	-0-38
KAS02B	191.00	0.73	0.00	-0.73
KAS02C	311.00	0.95	0.06	-0.89
KAS02D	540.00	0.98	1.08	0.10
KAS02E	829.00	1.42	2.45	1.03
KAS02F	879.00	1.58	2.67	1.09
KAS03A	51.00	1.21	0.00	-0.21
KAS03B	210.00	0.22	0.00	-0.22
KAS03C	349.00	0.86	0.55	-0.31
KAS03D	517.00	0.90	0.86	-0.04
KAS03E	606.00	0.65	1.28	0.63
KAS03F	676.00	1.12	1.49	0.37
KAS04A	142.00	0.05	0.00	-0.05
KAS04B	151.00	0.10	0.00	-0.10
KAS04C	185.00	0.12	0.00	-0.12
KAS04D	235.00	0.25	0.00	-0.25
KAS04E	277.00	0.53	0.00	-0.53
KAS04F	343.00	0.93	0.42	-0.51
KAS05A	81.00	0.08	0.00	-0.08
KAS05B	270.00	0.12	0.01	-0.11
KAS05C	310.00	0.62	0.12	-0.50
KAS05D	429.00	0.78	0.78	0.00
KAS05E	459.00	0.90	0.82	-0.08
KAS06A	81.00	0.32	0.37	0.05
KAS06B	183.00	0.49	0.16	-0.33
KAS06C	259.00	1.03	0.26	-0.77
KAS06D	293.00	1.00	0.58	-0.42
KAS06E	334.00	1.01	0.69	-0.32
KAS06F	376.00	1.08	0.70	-0.38
KAS07A	47.00	0.45	0.03	-0.42
KAS07B	107.00	0.54	0.01	-0.53
KAS07C	210.00	0.67	0.00	-0.67
KAS07D	295.00	0.66	0.50	-0.16
KAS07E	362.00	1.01	0.68	-0.33
KAS07F	463.00	0.85	0.81	-0.04
KAS08A	52.00	0.70	0.00	-0.70
KAS08B	148.00	0.66	0.00	-0.66
KAS08C	313.00	0.90	0.68	-0.22
KAS08D	455.00	1.02	0.70	-0.32
Mean error %:	-0.21			

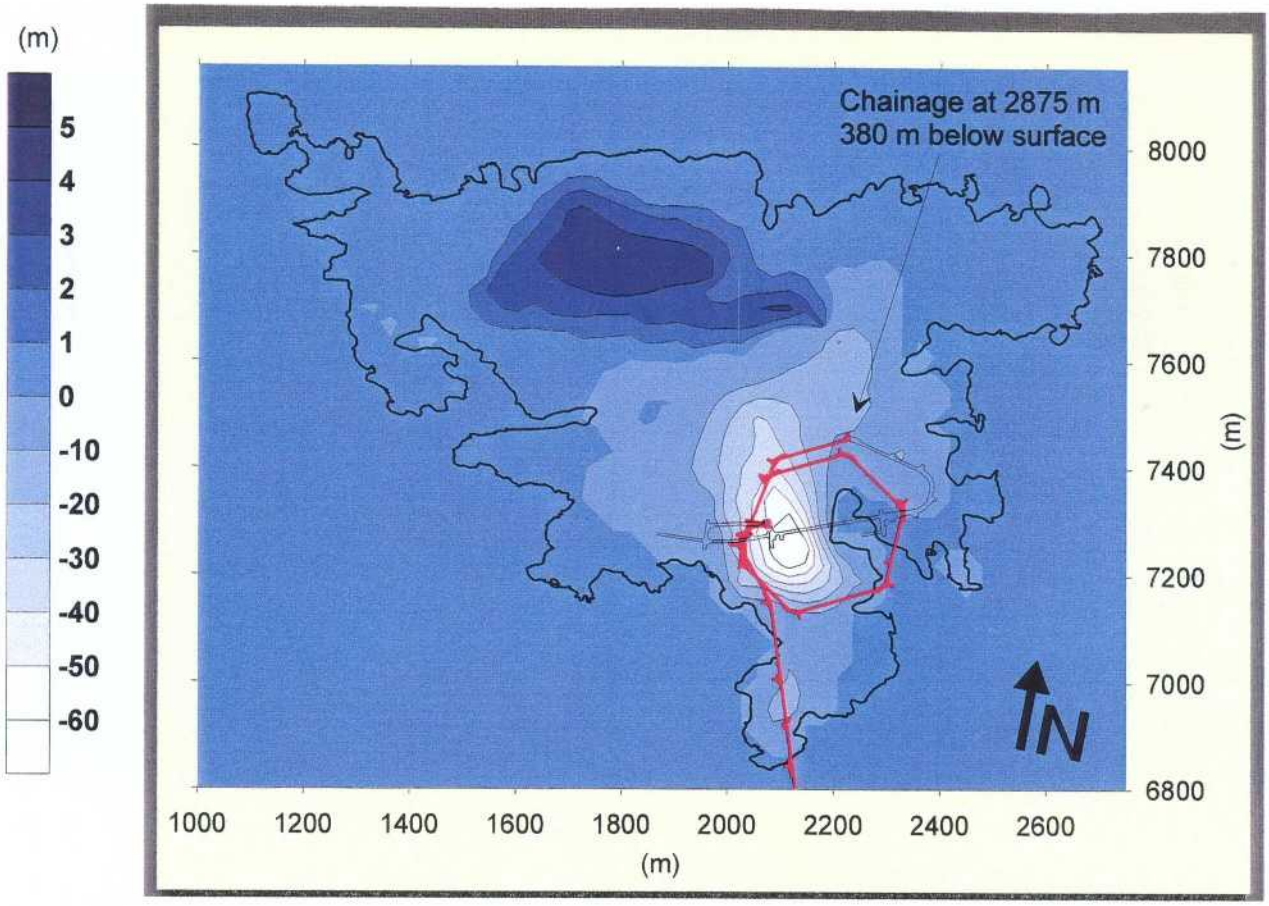

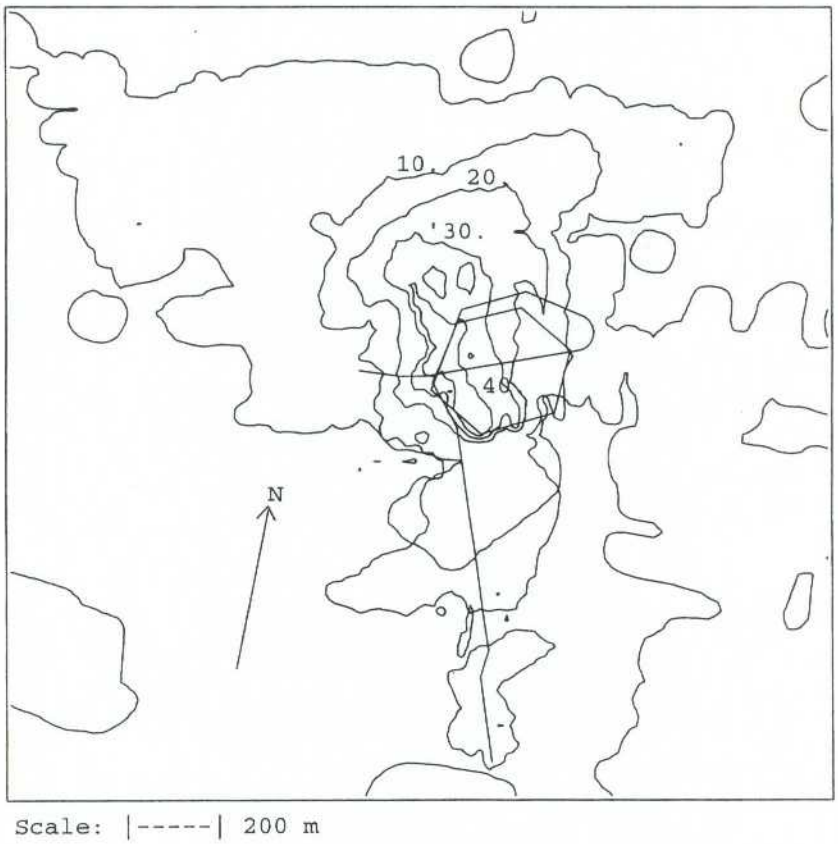

Figure 3-3. *Comparison between measured (top) and calculated water table for tunnel front at 2875 metres. Figure based on field measurements from Rhén et al (1997).*

4 MAIN RESULTS

4.1 INTRODUCTION

In the presentation of results we will concentrate on two situations; natural conditions and completed tunnel. For these two situations the distribution of freshwater head, flux and salinity (these are the main variables chosen to illustrate the simulations) will be presented in a number of vertical and horizontal sections.

For each of the two situations, ten realisations of the stochastic part of the conductivity field were used. For most of the figures the mean values will be used. The ten realisations also give the opportunity to show statistical distributions of a variable. This will however not be done in this report.

The conductivity field is an input to the simulations and thus not a part of the results. It may however be instructive, as a background, to show a visualisation of a conductivity field. In Figure 4-1 the vertical conductivity field, which includes the fracture zones, is shown. The conductivity interval is chosen to illustrate the fracture zones and part of the stochastic conductivity field. By comparing Figure 4-1 with the maps of major fracture zones (Figure 2-1) and rock block domains (Figure 2-2), one can identify the features in the figure.

4.2 NATURAL CONDITIONS

In Figure 4-2 the predicted water table is shown together with the topography, as represented in the model. The water table, as all results in this section, is an average based on ten realisations of the conductivity field. A comparison with Figure 3-2, which is based on one realisation, shows that the different realisations do not influence the water table. This is to be expected as the top five layers have a deterministic conductivity.

The horizontal flow at various depths is shown in Figures 4-3, 4-4 and 4-5. Close to ground, see Figure 4-3 (top), most of Äspö is unsaturated, but already at 4 metres below ground most of the area is saturated. At deeper levels the flow pattern is governed by the fracture zone system.

The vertical flow distribution at various depths is shown in Figures 4-6, 4-7 and 4-8. At a depth of 0.5 metres the flow is downwards on the whole of Äspö, except for a thin region along the coastline. At 5 metres below ground the downward flow is found in areas

with high elevation, while the upward flow is in areas closer to the coastline. Further down the distribution is determined by the fracture zone system.

Two vertical sections through Äspö HRL are shown in Figure 4-9. The freshwater lens below Äspö, as indicated by the 0.1% isoline, is found to be about 300 metres deep.

The freshwater hydraulic head in two vertical sections can be studied in Figure 4-10. The freshwater hydraulic head is calculated as $p/\rho_0 g - h$, where p is pressure, ρ_0 freshwater density, g acceleration due to gravity and h the depth below mean sea level. As seen in Figure 4-10 it is the water table on Äspö and the boundary condition at the western boundary that provides the driving force for the flow. The influence of the western boundary is also clearly seen in Figure 4-11, where a horizontal section at a depth of 450 metres is shown.

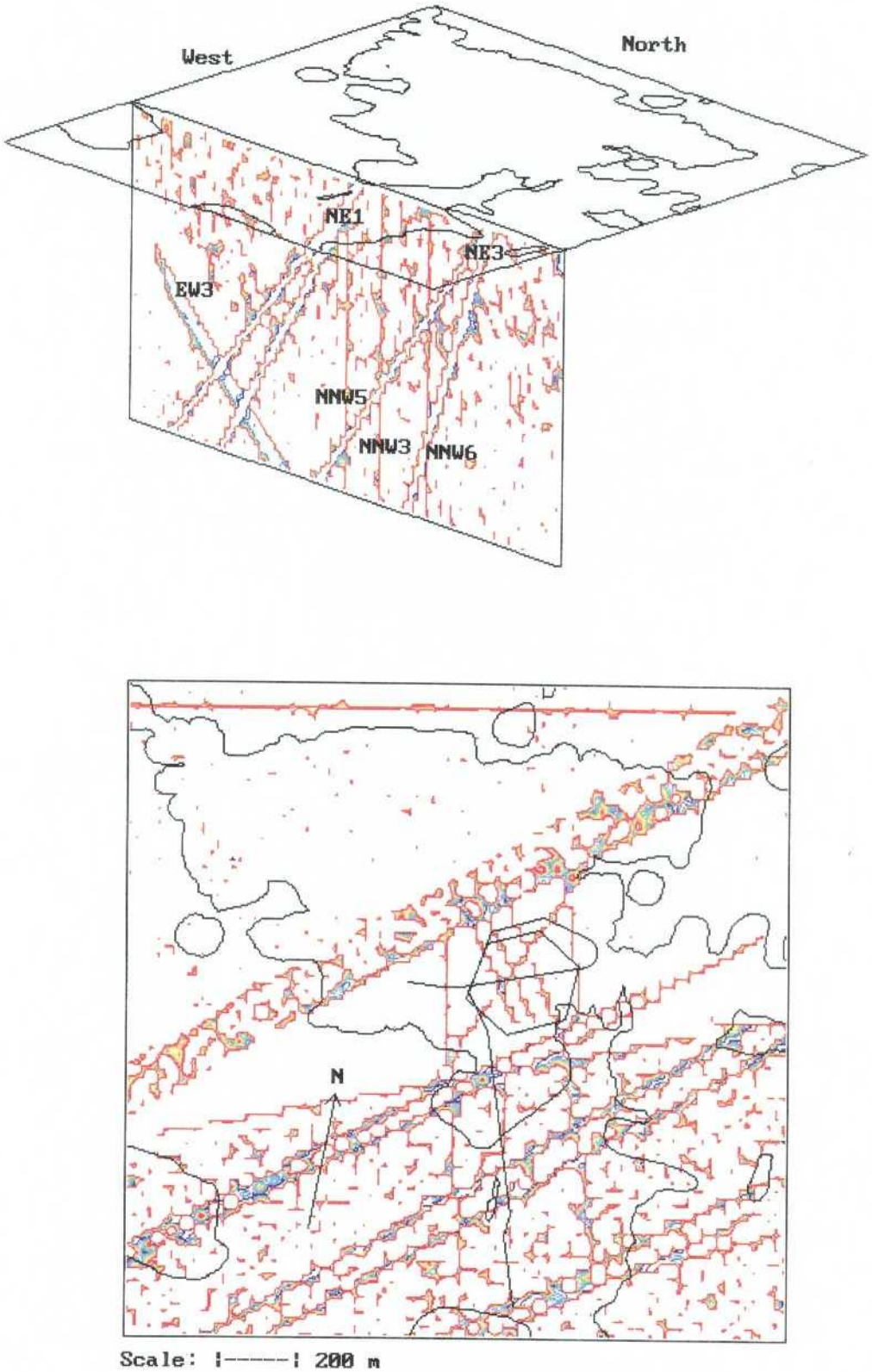

Figure 4-1. *Illustration of conductivity field. Perspective view (top) and horizontal section at a depth of 450 metres.*
Plotted conductivity interval: $10^{-7} \rightarrow 10^{-4}$ m/s.

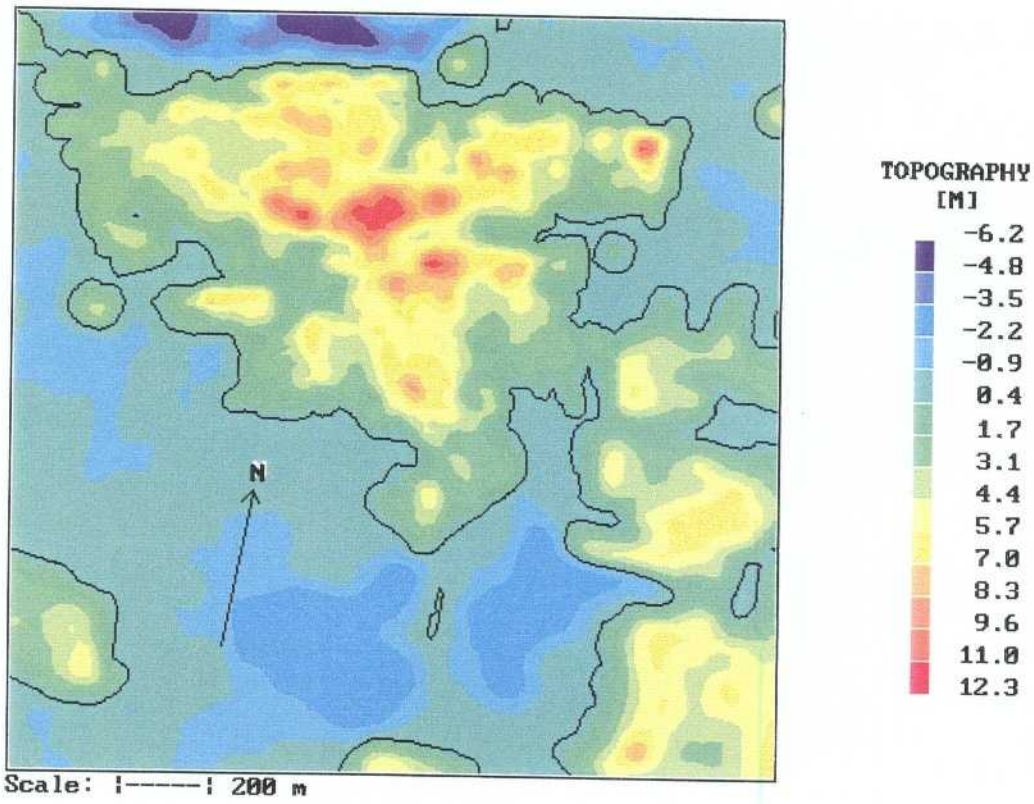

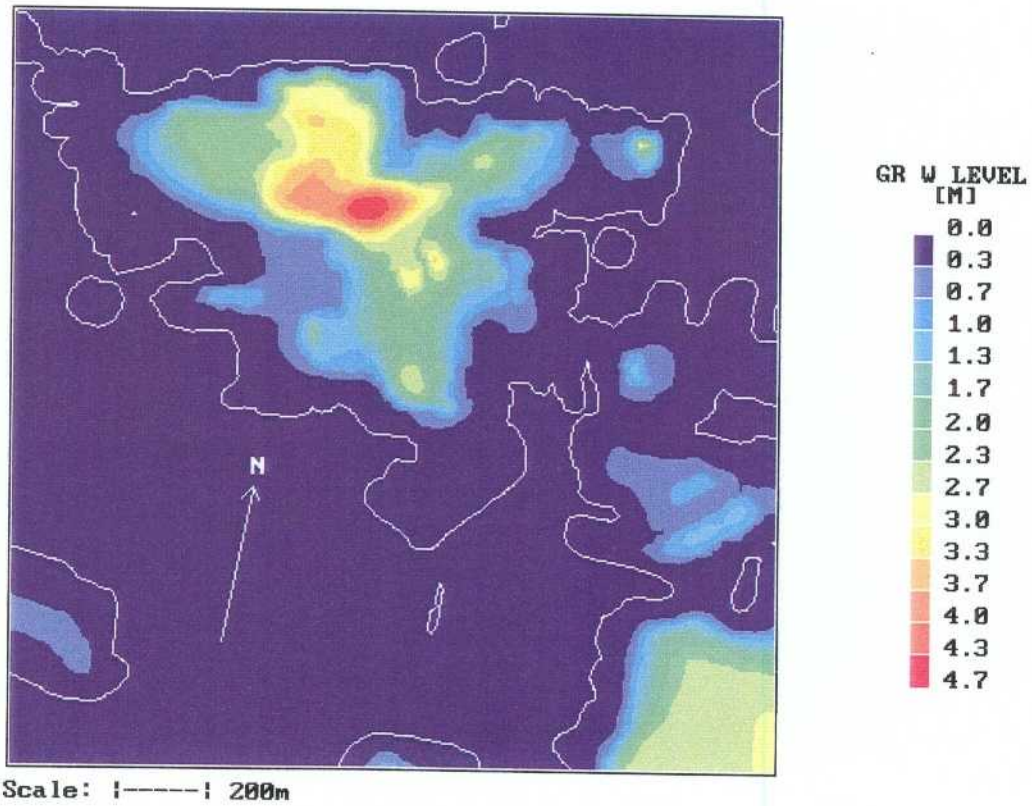

Figure 4-2. *Topography (top) and predicted water table (metres above sea level) for natural conditions.*

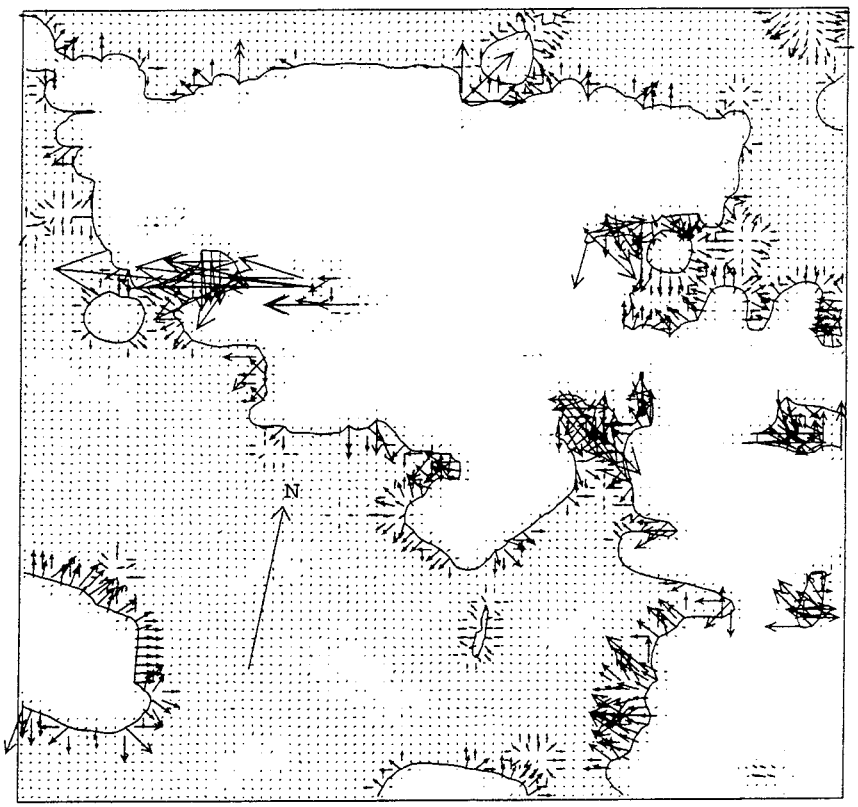

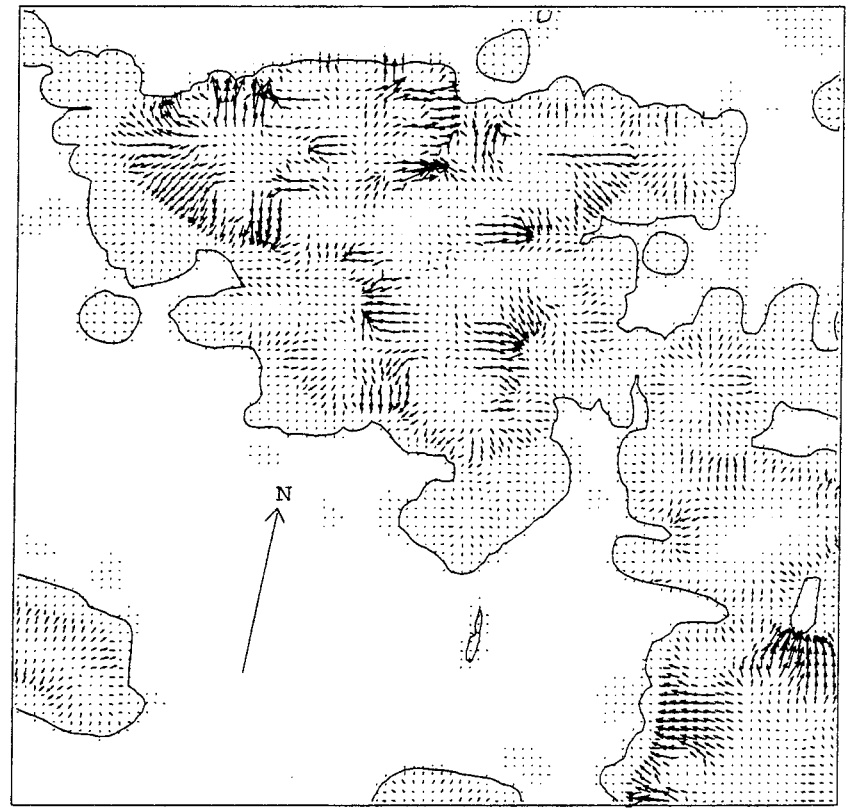

Figure 4-3. *Horizontal flow at 0.25 metres (top) and four metres depth below ground. Natural conditions.*
Darcy velocity scale: ⟶ 1 x 10^{-6} *m/s.*

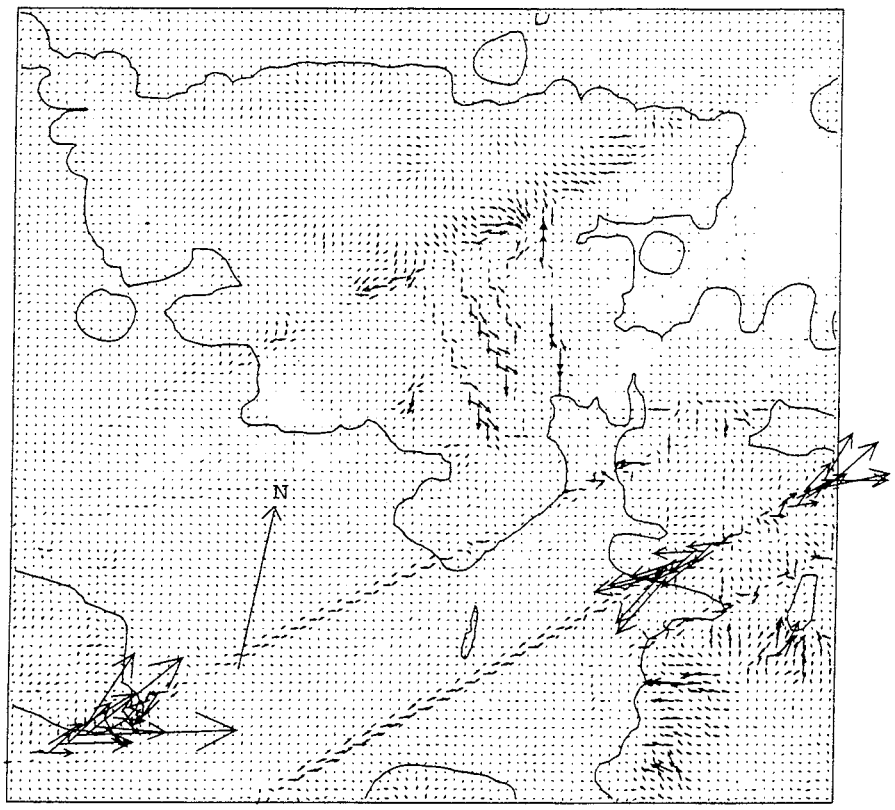

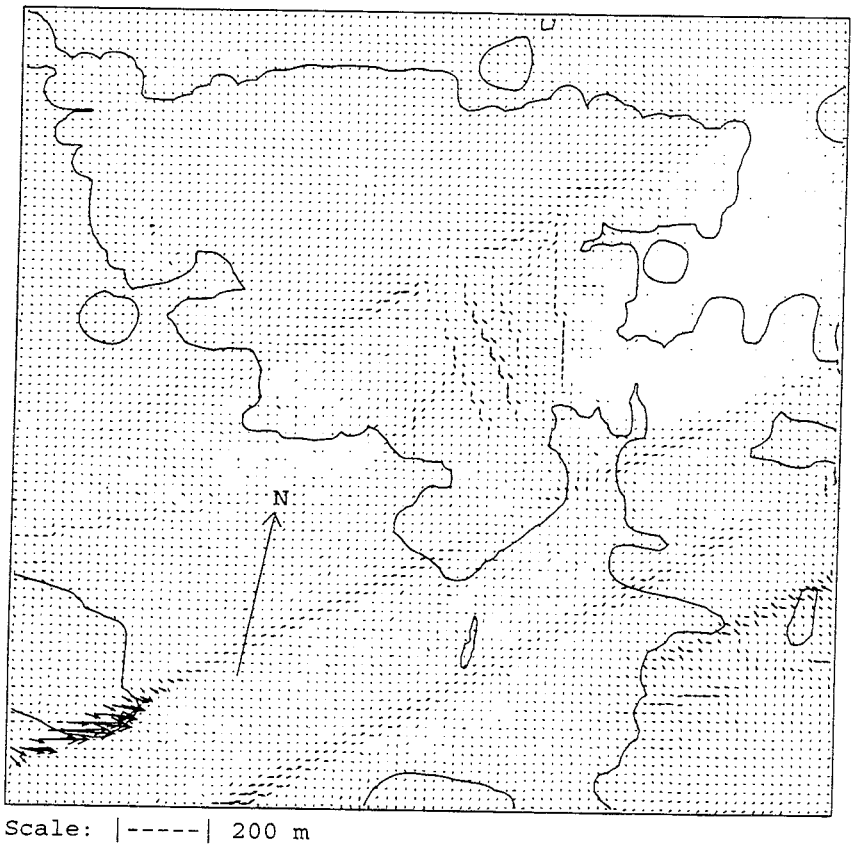

Figure 4-4. *Horizontal flow at* 15 *metres (top) and* 100 *metres depth. Natural conditions.*
Darcy velocity scale: ⟶ 5 x 10^{-8} *m/s.*

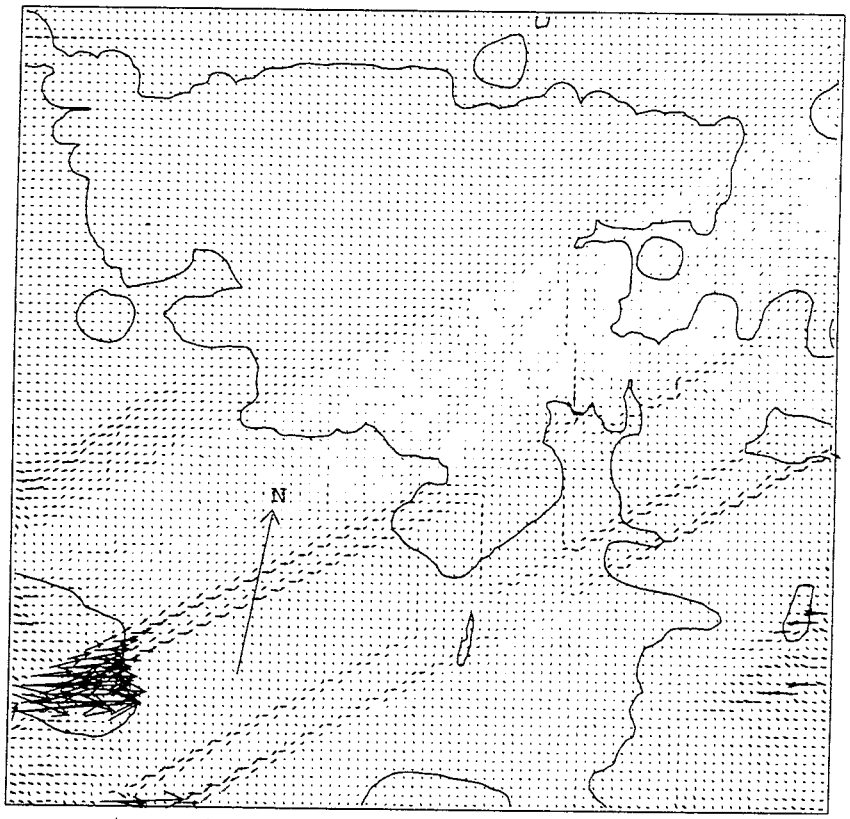

Figure 4-5. *Horizontal flow at 450 metres depth. Natural conditions.*
Darcy velocity scale: ⟶ 1 x 10^{-8} *m/s.*

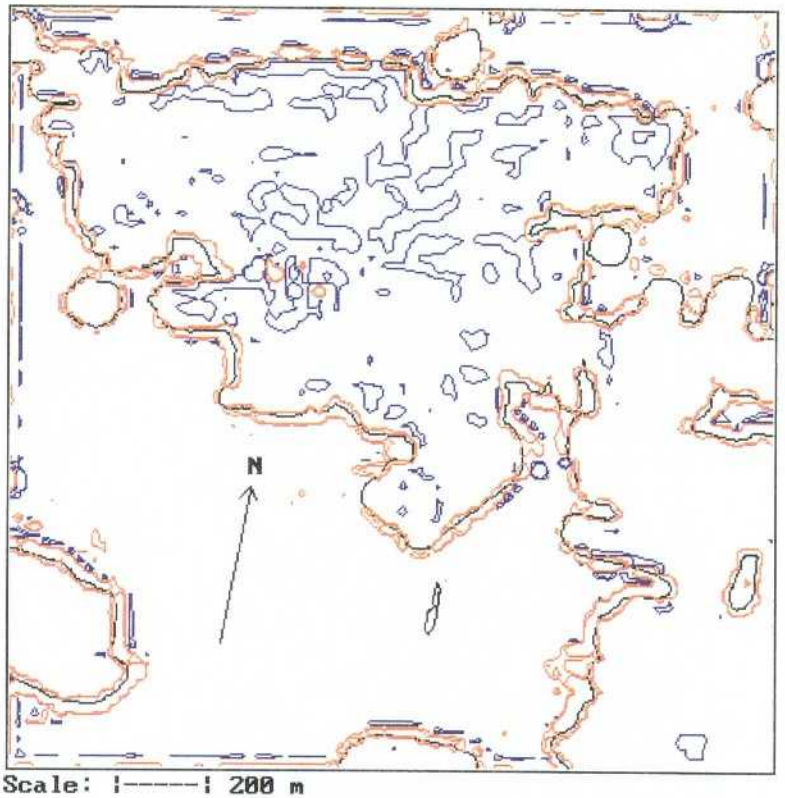

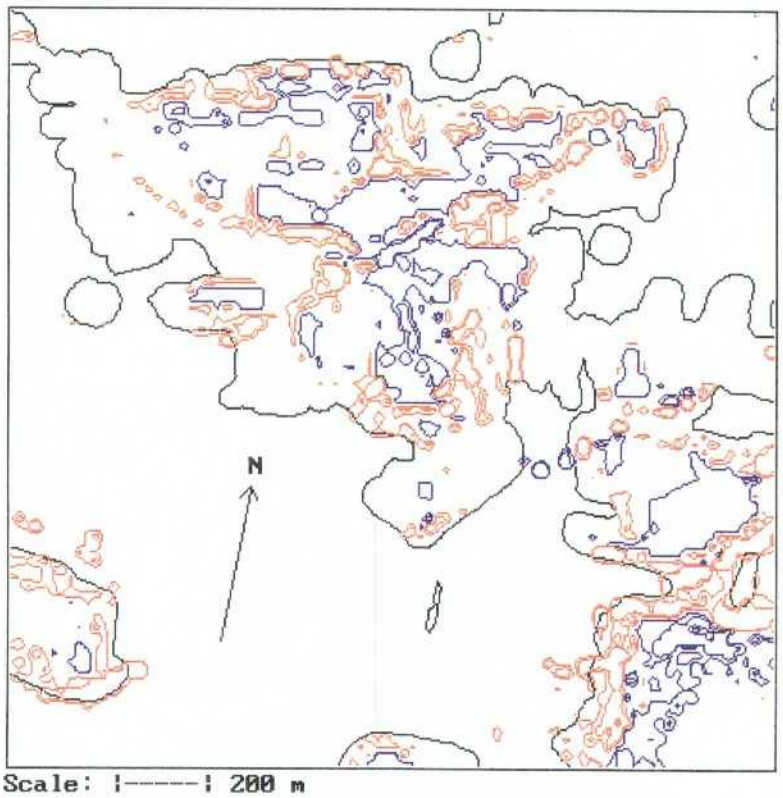

Figure 4-6. *Vertical flow at* 0.5 *metres (top) and 5.0 metres depth. Natural conditions. Blue colour indicates downward and red upward flow. Isoline values:* 100 *and* 200 *mm/year (top).*
50 *and* 100 *mm/year (bottom).*

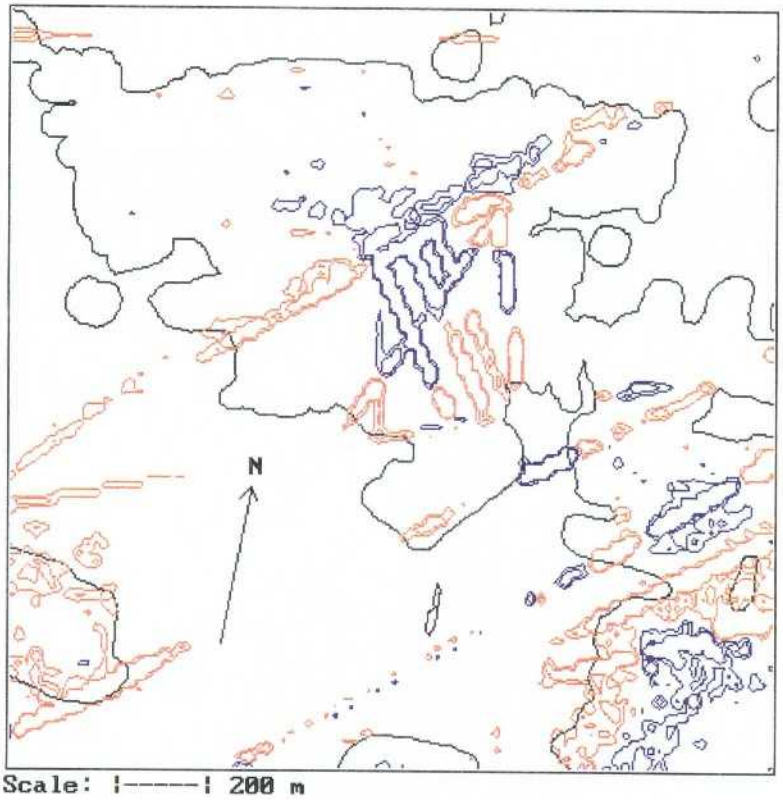

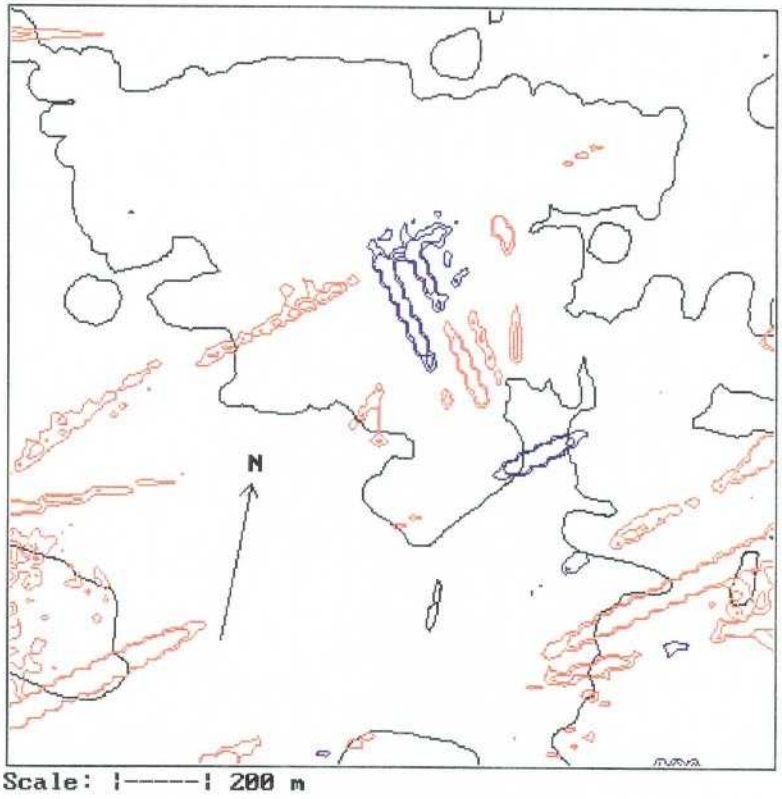

Figure 4-7. *Vertical flow at* 20 metres *(top) and at* 100 *metres depth. Natural conditions. Blue colour indicates downward and red upward flow. Isoline values:* 25 *and* 50 *mm/year.*

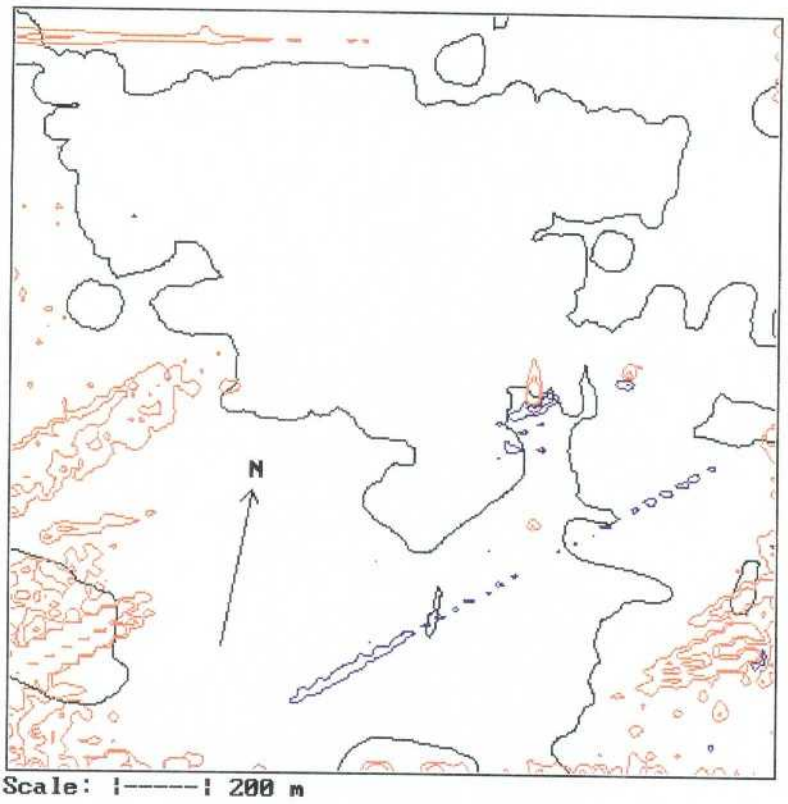

Figure 4-8. *Vertical flow at* 450 metres *depth below ground. Natural conditions. Blue colour indicates downward and red upward flow. Isoline values:* 3 *and* 10 *mm/year.*

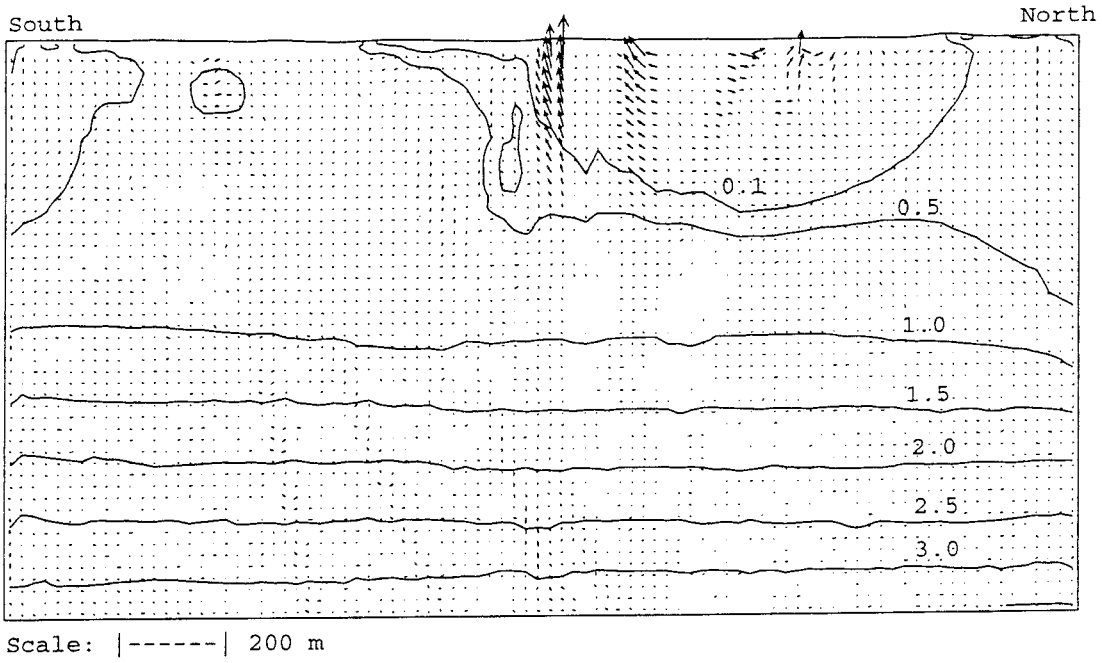

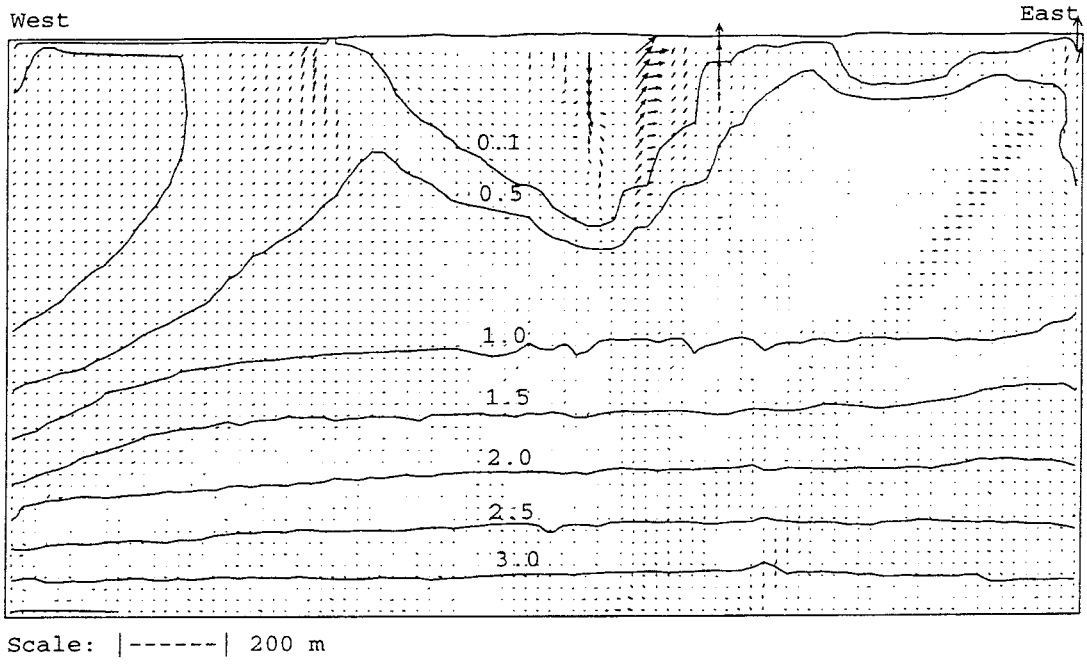

Figure 4-9. *North-South (top) and East-West vertical sections through Äspö HRL. Flow and salinity fields (in %). Natural conditions.*
Darcy velocity scale: ⟶ 2 x 10^{-8} *m/s.*
(Note: flow from ground to 20 metres depth not shown).

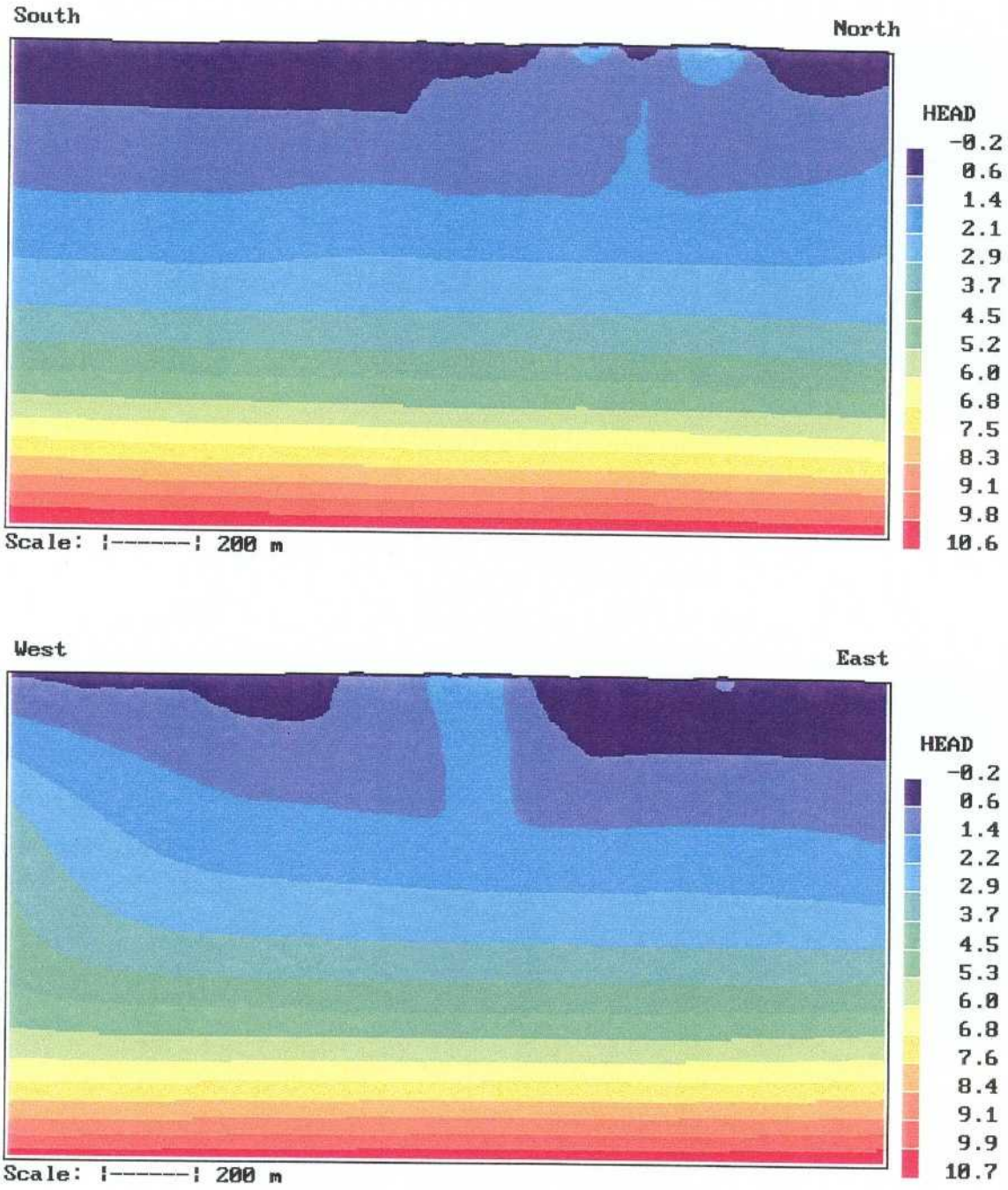

Figure 4-10. *Hydraulic head in two vertical sections through Äspö HRL. Natural conditions.*

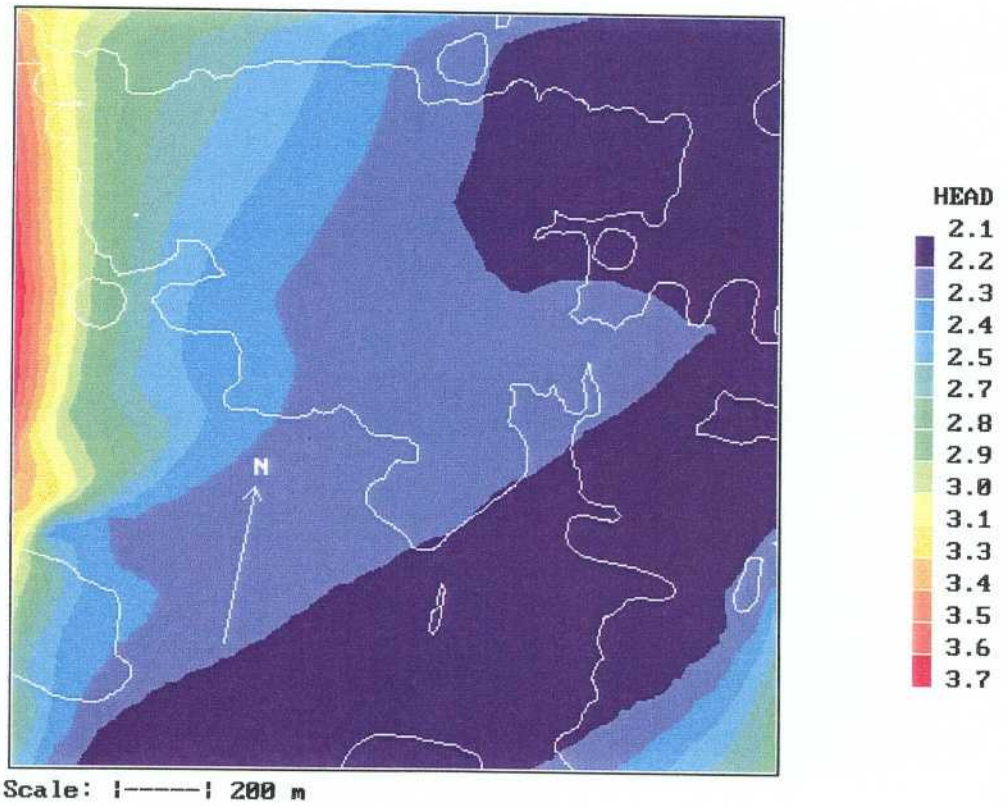

Figure 4-11. *Hydraulic head at a depth of 450 metres below ground level. Natural conditions.*

4.3 COMPLETED TUNNEL

Results for tunnel front at 3600 metres, i. e. completed tunnel will be presented in this section. The same sections and variables, as for natural conditions, are used and direct comparisons are thus possible. All results to be presented represent the mean of ten realisations of the conductivity field.

The water table is shown in Figure 4-12. The main drawdown is in the fracture zones while the water table on northern Äspö is fairly unaffected. Note that this water table is based on the calculated phreatic surface. If it had been based on the pressure drops at some depth, like in Figure 3-3, a smoother surface would have been obtained.

The horizontal flow at various depths is shown in Figures 4-13, 4-14 and 4-15. Close to ground large areas are unsaturated (only vertical flow) and the flow on southern Äspö is from the Baltic. At deeper levels the flow is in the fracture zones and directed towards the tunnel crossings.

The vertical flow distributions are shown in Figures 4-16, 4-17 and 4-18. Close to ground we see a strong downward flow on southern Äspö, with its maximum along the coast. At 5 metres below ground it is only the north coast of Äspö that has a small discharge area. At 20 and 100 metres depth, see Figure 4-17, the downward flow is concentrated to the fracture zones. Figure 4-18 shows the vertical flow at 450 metres below ground. As we are now at or below all inflows to the tunnel it is not surprising that we find large areas of upward flow.

Two vertical sections through the Äspö HRL, showing the salinity and flow field, can be found in Figure 4-19. The upconing effect below the tunnel is a dominant feature, caused by the tunnel. In the east-west section it is interesting to note that water of salinity 0.1% may reach the tunnel from the west. The fresh water found in the tunnel inflows may thus have its origin in the Laxemar area.

The distribution of freshwater hydraulic head is shown in two vertical sections, Figure 4-20, and one horizontal section at a depth of 450 metres below sea level, Figure 4-21. The minimum value found (-84 metres) is at a point where a fracture zone crosses the tunnel. The inflow is prescribed at this cell and a pressure that generates the given inflow is calculated.

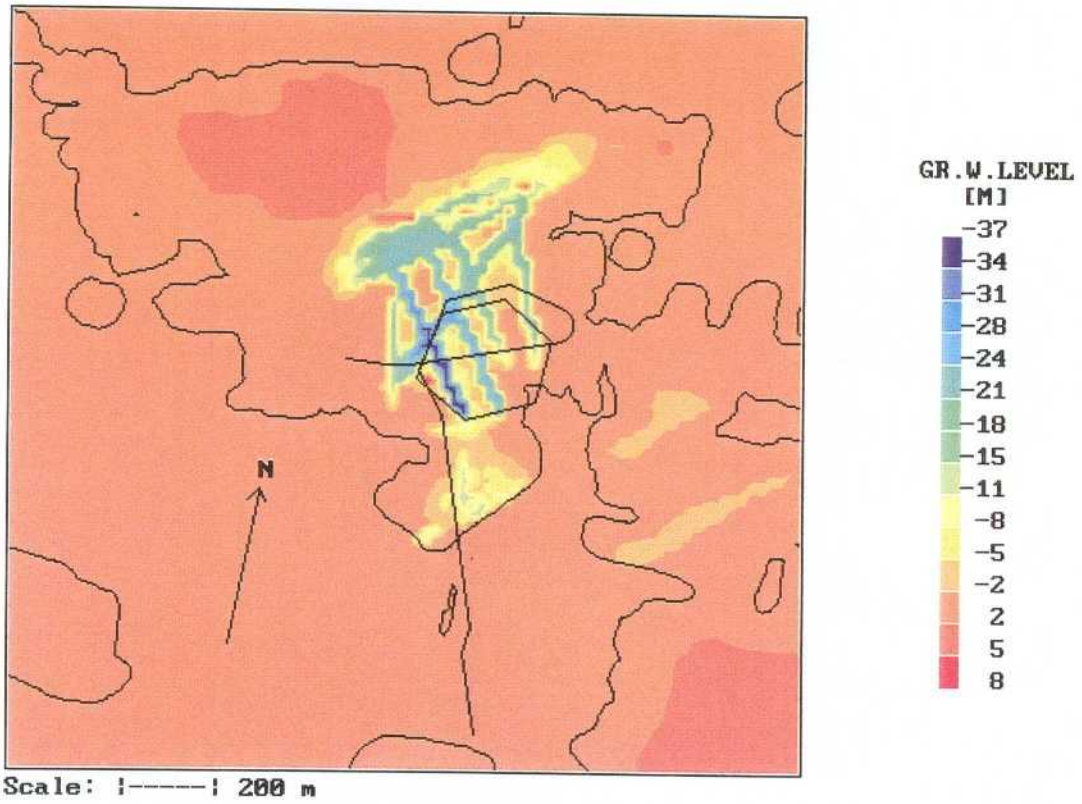

Figure 4-12. *Water table for completed tunnel.*

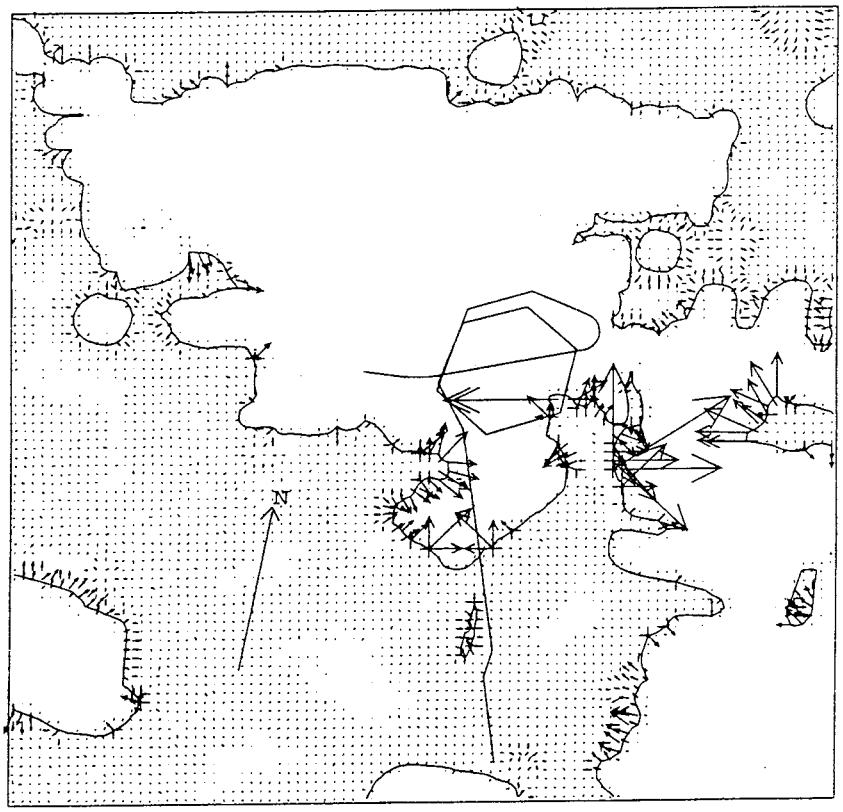

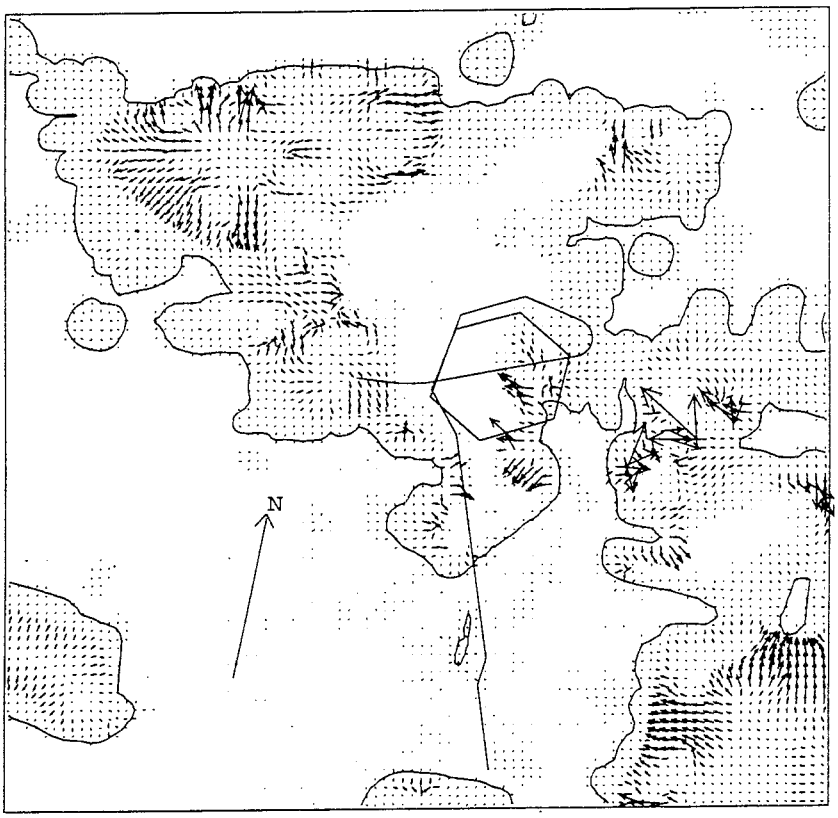

Figure 4-13. *Horizontal flow at* 0.25 *and* 4 *metres depth, with complete tunnel.*

Darcy velocity scale: ⟶ $\begin{cases} 2\times10^{-6} \text{ m/s (top)} \\ 10^{-6} \text{ m/s (bottom)} \end{cases}$

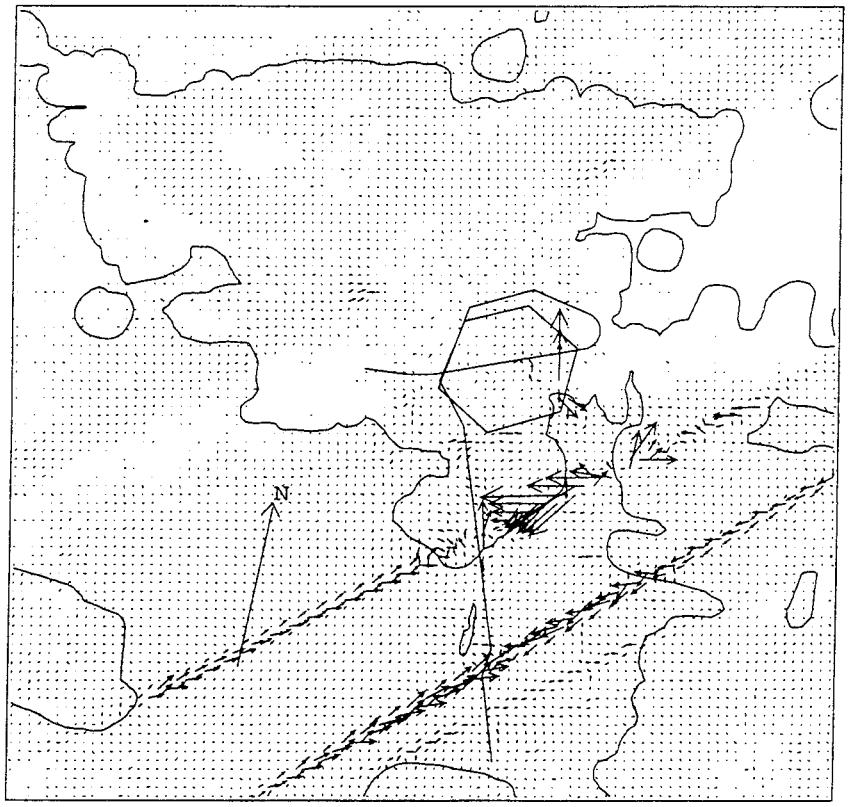

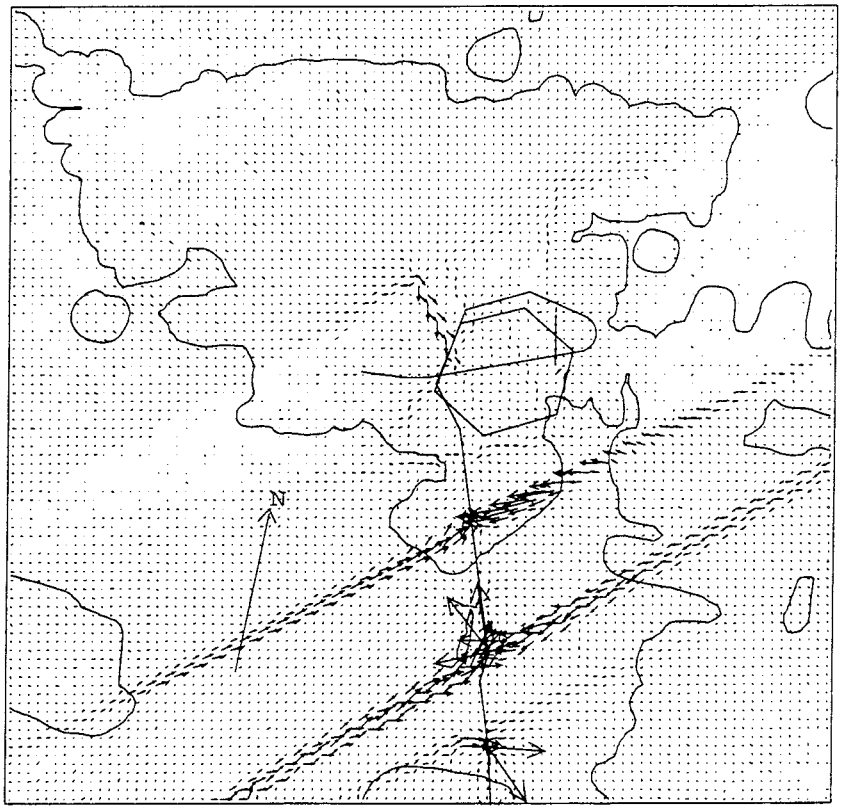

Figure 4-14. *Horizontal flow at 15 and 100 metres depth, with complete tunnel.*
Darcy velocity scale: ⟶ 10^{-6} m/s.

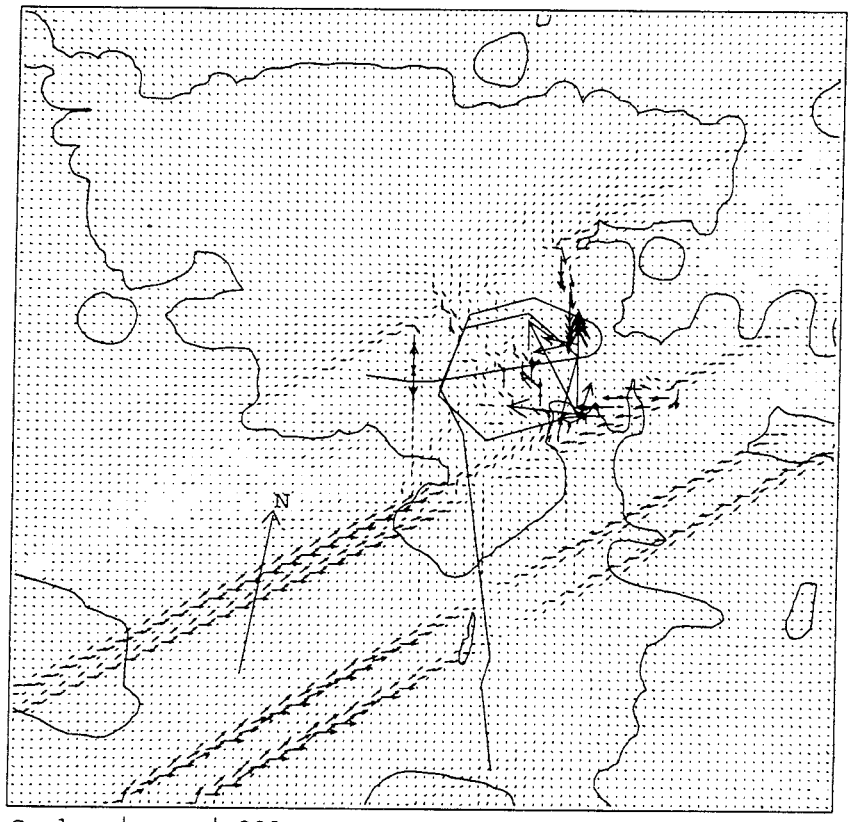

Figure 4-15. *Horizontal flow at 450 metres depth, with complete tunnel.*
Darcy velocity scale: ⟶ 5 x 10^{-7} m/s.

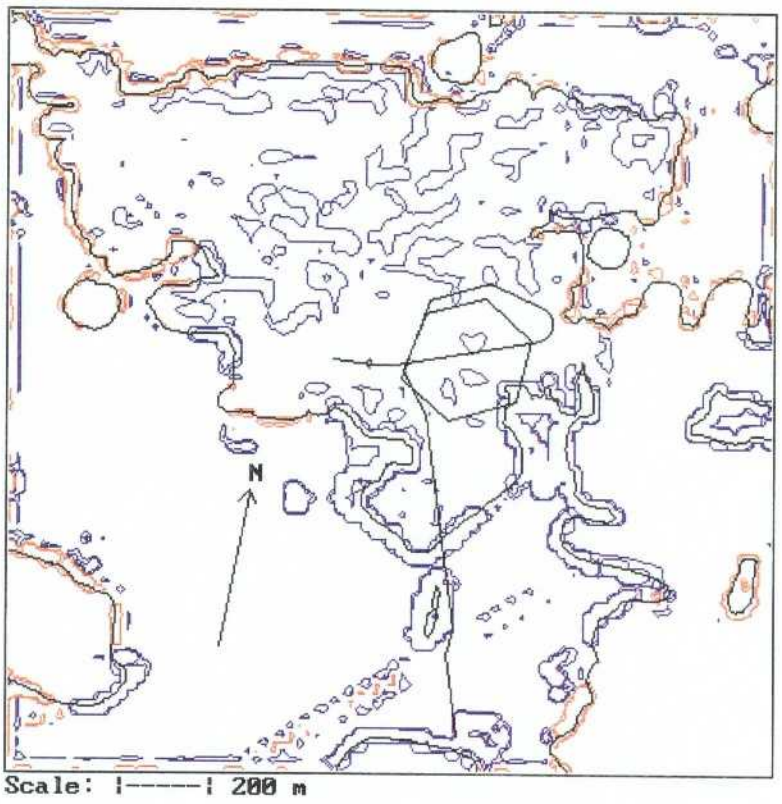

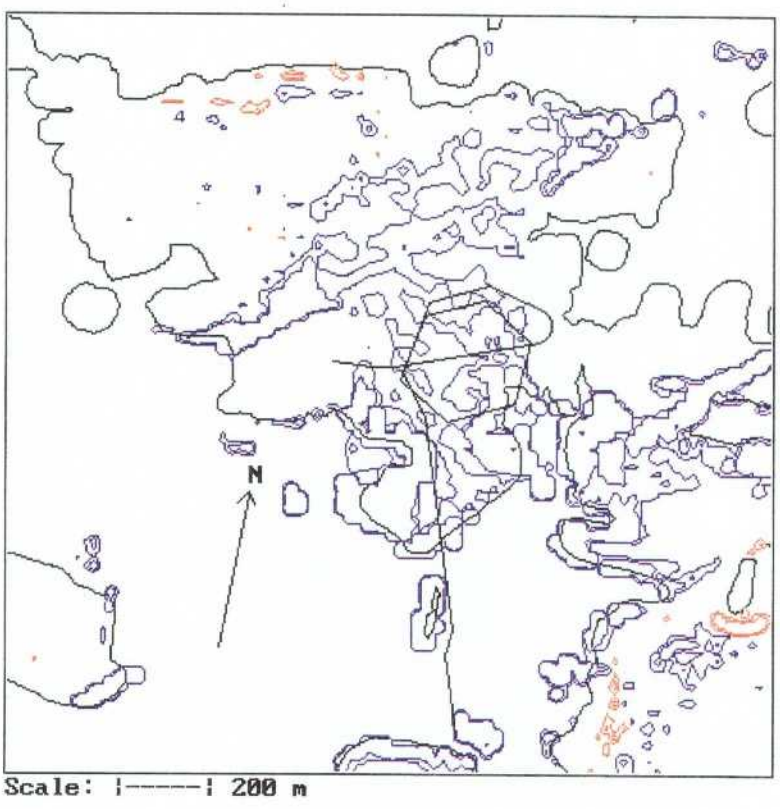

Figure 4-16. *Vertical flow at* 0.5 *and* 5 *metres depth, with complete tunnel. Isoline value:* ± 100 *and* ± 200 *mm/year. Red colour indicates upward flow, blue downwards.*

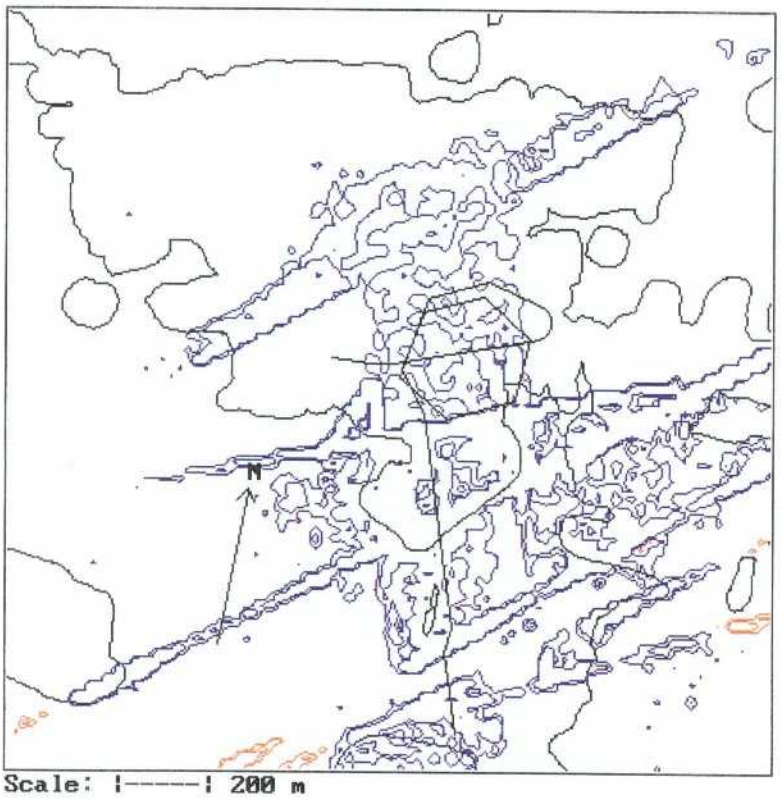

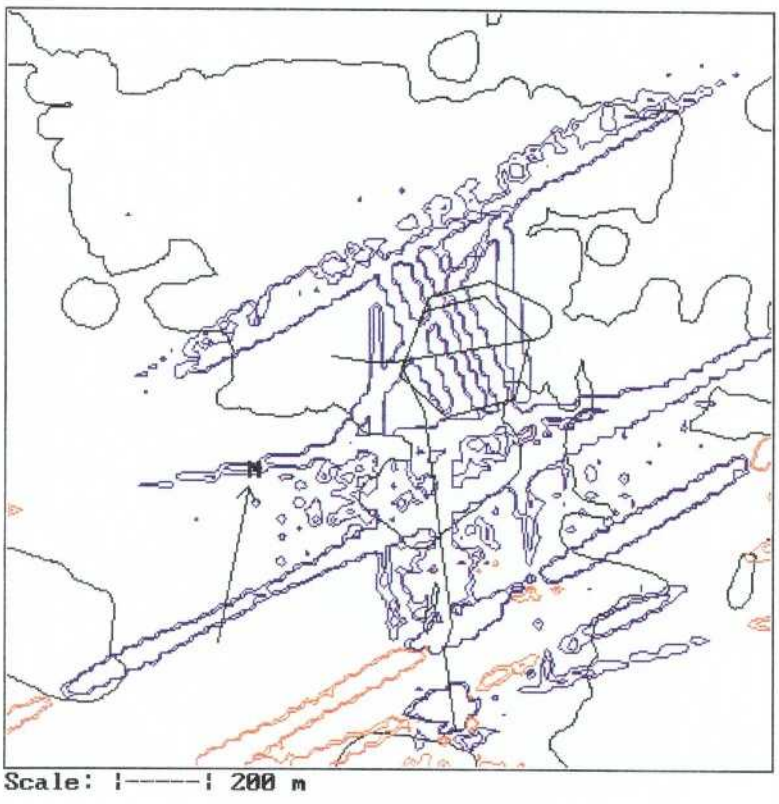

Figure 4-17. *Vertical flow at* 20 *and* 100 *metres depth, with complete tunnel.*
Isoline value: ± 100 *and* ± 200 *mm/year.*
Red colour indicates upward flow, blue downwards.

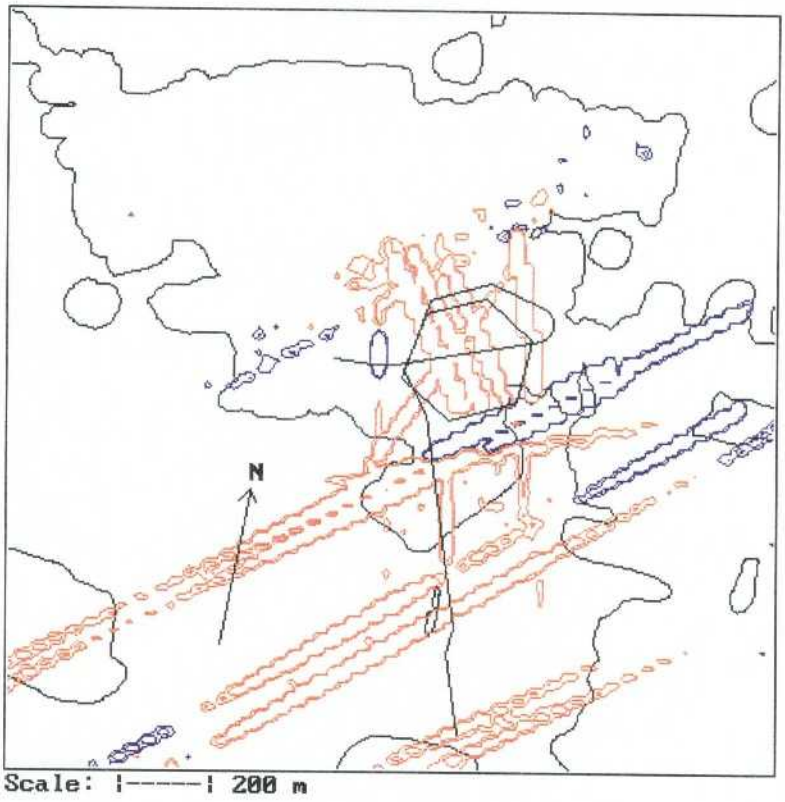

Figure 4-18. *Vertical flow at* 450 *metres depth, with complete tunnel.*
Isoline value: ± 400 *and* ± 800 *mm/year.*
Red colour indicates upward flow, blue downwards.

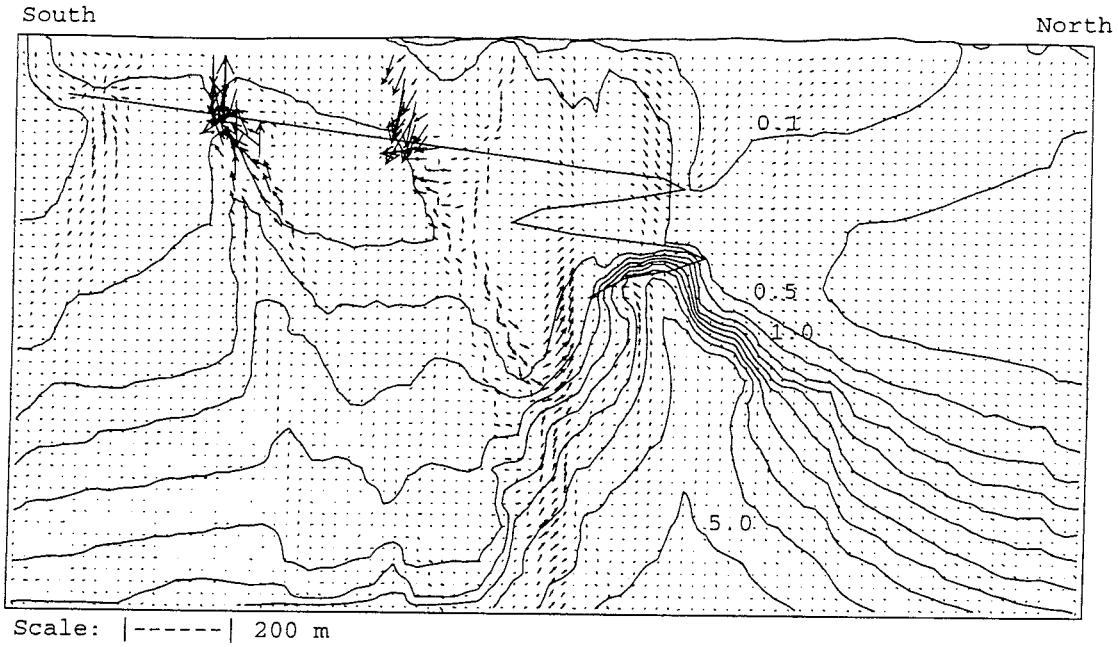

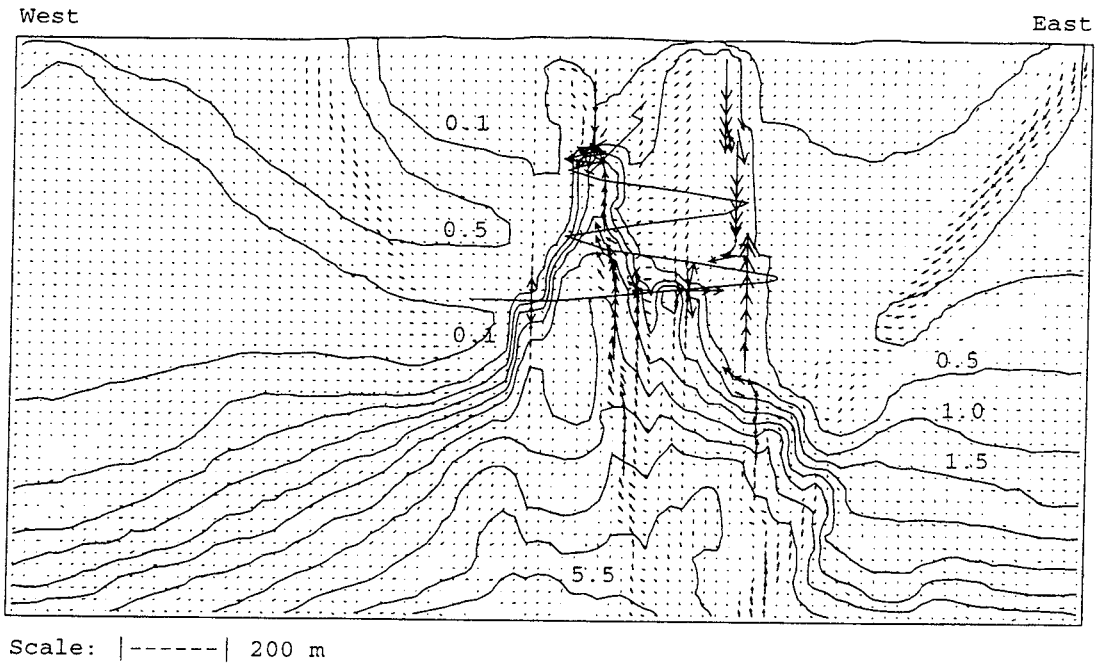

Figure 4-19. *Two vertical sections, through the Äspö HRL, showing salinity (in %) and flow for complete tunnel. Darcy velocity scale:* ⟶ 5 x 10^{-7} m/s. *(Note: flow from ground to 20 metres depth not shown).*

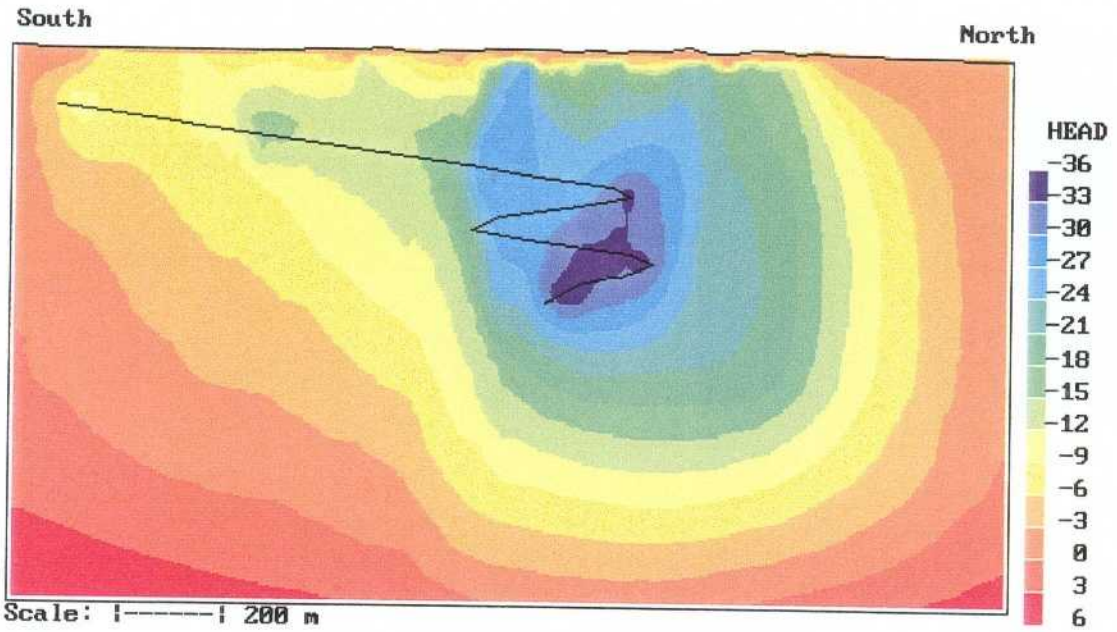

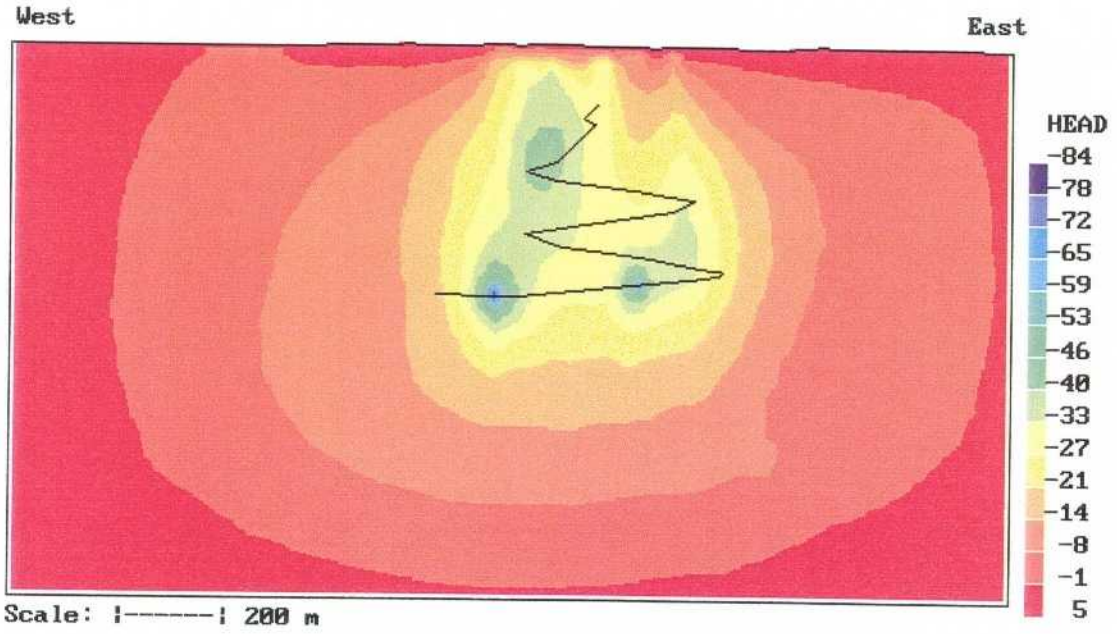

Figure 4-20. *Two vertical sections, through the Äspö HRL, showing the hydraulic head, with complete tunnel.*

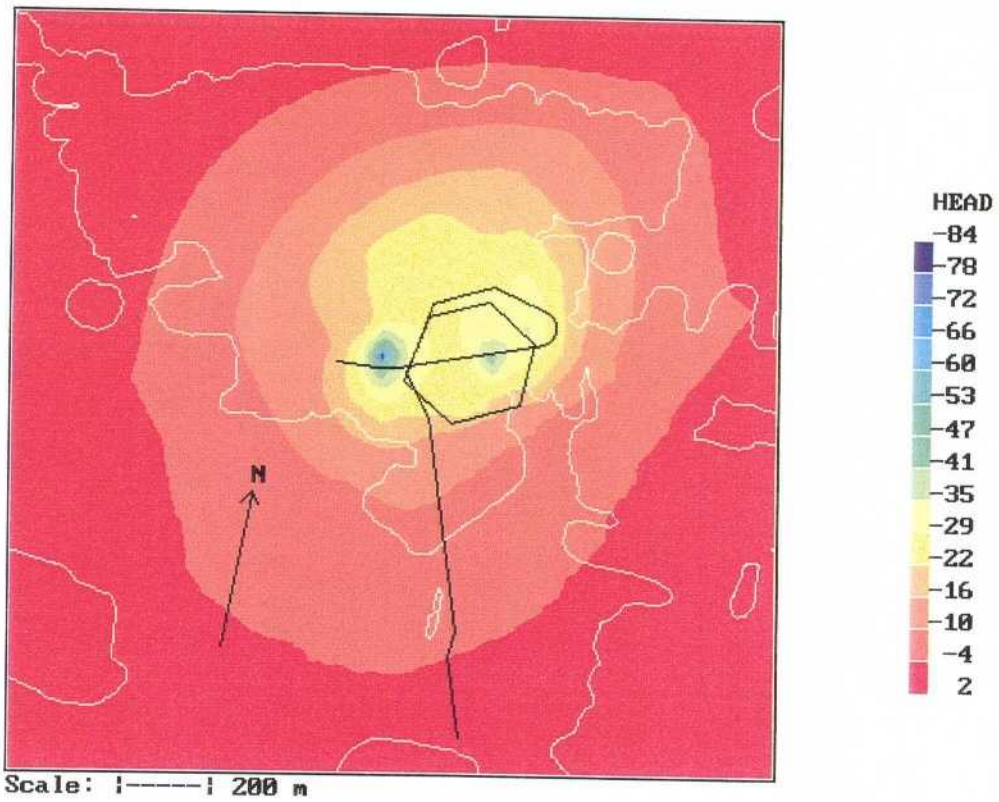

Figure 4-21. *Horizontal hydraulic head distribution at a depth of* 450 *metres, with complete tunnel.*

5 SENSITIVITY TESTS

5.1 INTRODUCTION

The accuracy of a groundwater simulation is to a large extent determined by how well boundary conditions and material properties are known. For the Äspö HRL we probably know these input data better than for most other sites, but they still constitute the main sources of uncertainty. In this chapter a series of sensitivity tests, which are all related to boundary conditions and material properties, will be presented. We will focus on two situations, natural conditions and tunnel front at 2875 metres, which will allow comparisons with measured data.

5.2 RECHARGE AT UPPER BOUNDARY

The standard value for precipitation minus evapotranspiration, P-E, used is 100 mm/year. In order to study the sensitivity to this value two runs, with 50 and 200 mm/year, were performed. The result can be studied in Figures 5-1 and 5-2, which should be compared with the corresponding ones for 100 mm/year (Figures 4-2 and 4-9). The groundwater level is found to be increased/decreased, as compared to the reference situation, with about 1 metre for the two values of P-E tested. It is interesting to note the response in the depth of the fresh water lens below Äspö, see Figure 5-2. For P-E = 50 mm/year the depth is about 200 metres, while it is about 360 metres for 200 mm/year.

5.3 VERTICAL AND BOTTOM BOUNDARY CONDITIONS

In the present model the boundary conditions for vertical and bottom boundaries are obtained from a regional groundwater model. Different sets of boundary conditions are used for natural conditions and with the tunnel present. It is thus expected that the influence of the tunnel, if there is such an influence, is taken care of. The next case to be discussed aims to answer if there is an influence from the tunnel on the boundary conditions. This is done by using the boundary conditions for natural conditions in a simulation with the tunnel front at 2875 metres.

The calculated mean drawdown in the borehole sections used in the calibration process is 17.0 metres, while the mean drawdown with correct boundary conditions is 19.6 metres. It is thus concluded that the tunnel affects boundary conditions in a model of the present size.

5.4 MATERIAL PROPERTIES

Next the sensitivity to the assigned conductivity and transmissivity values will be evaluated. Four cases are defined by multiplying or dividing all conductivities, as given in Tables 2-2 and 3-3, or transmissivities, as given in Tables 2-1 and 3-2, with a factor of two. When conductivities are modified, the top five cell layers and the clay layer below the Baltic are included.

The result can be found in Tables A-7 and A-8, Appendix A. As seen in Table A-7 the modified transmissivities will generate a major change in the drawdown magnitude; for the case with reduced transmissivities almost all drawdowns will be larger than the measured ones while the opposite is true for the case with increased transmissivities. The result for conductivities is found in Table A-8. Increasing the conductivities will result in drawdowns that are too small in nearly every borehole section. Decreasing the conductivities gives a more complex response as borehole sections close to the inflows to the tunnel will get a increased drawdown, while borehole sections without a good contact with the fracture zone system will get a reduced drawdown.

5.5 CONCLUDING REMARKS

The sensitivity studies presented show that the simulation model is sensitive to the modified boundary conditions and material properties. The next question is then if modifying P-E, conductivities and transmissivities with a factor of 2.0 is a large or small modification. There is of course no general answer to this question; the best answer is probably that these modifications are generally within the uncertainty limits of the input data.

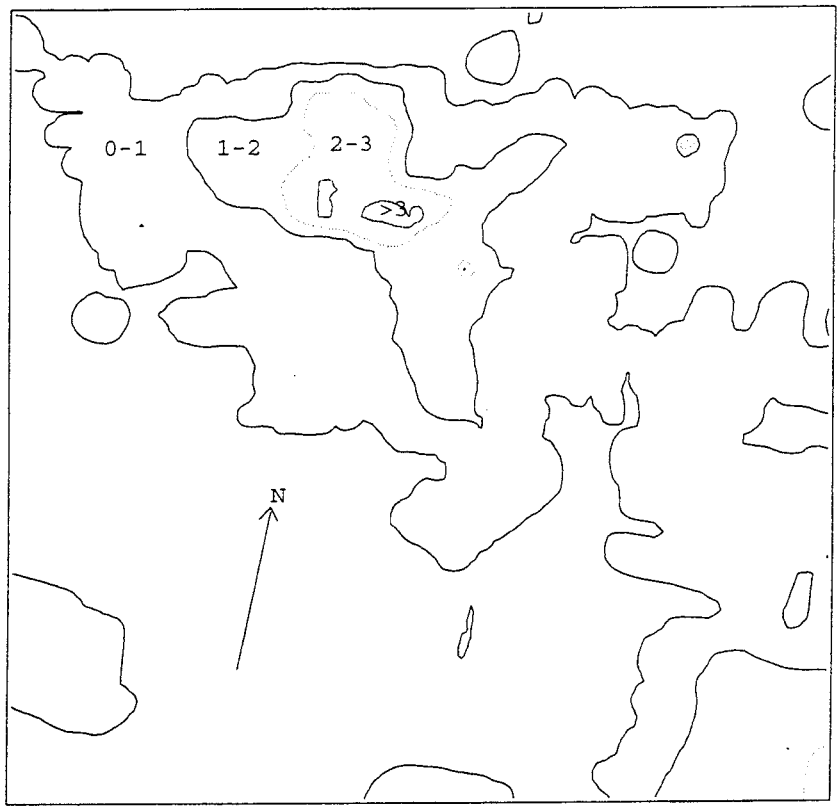

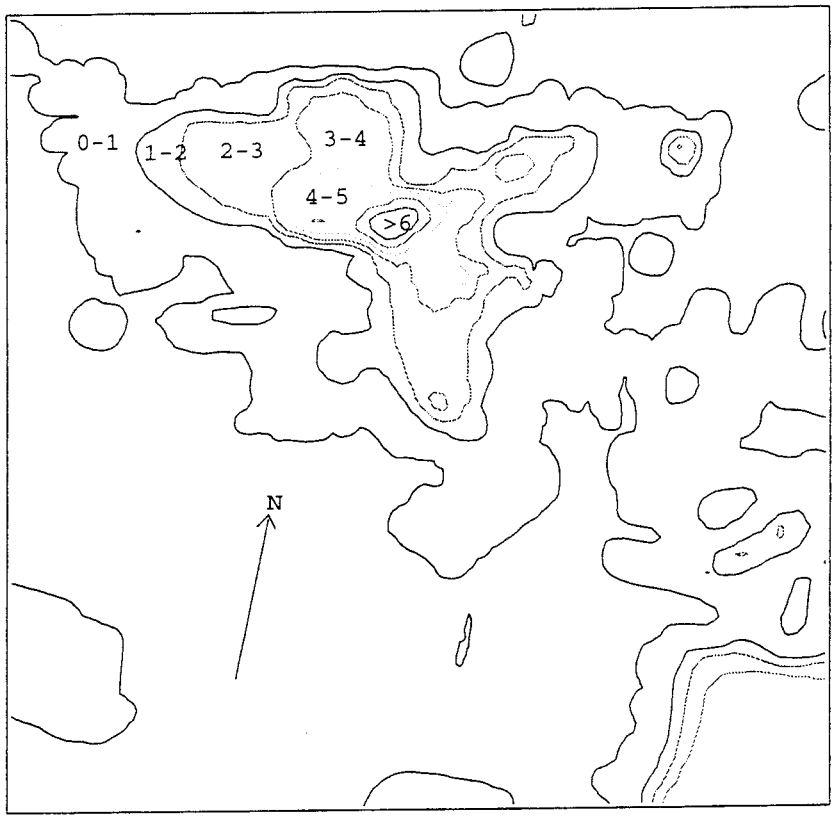

Figure 5-1. *Water table for* P-E = 50 *mm/year (top) and* 200 *mm/year. Natural conditions.*

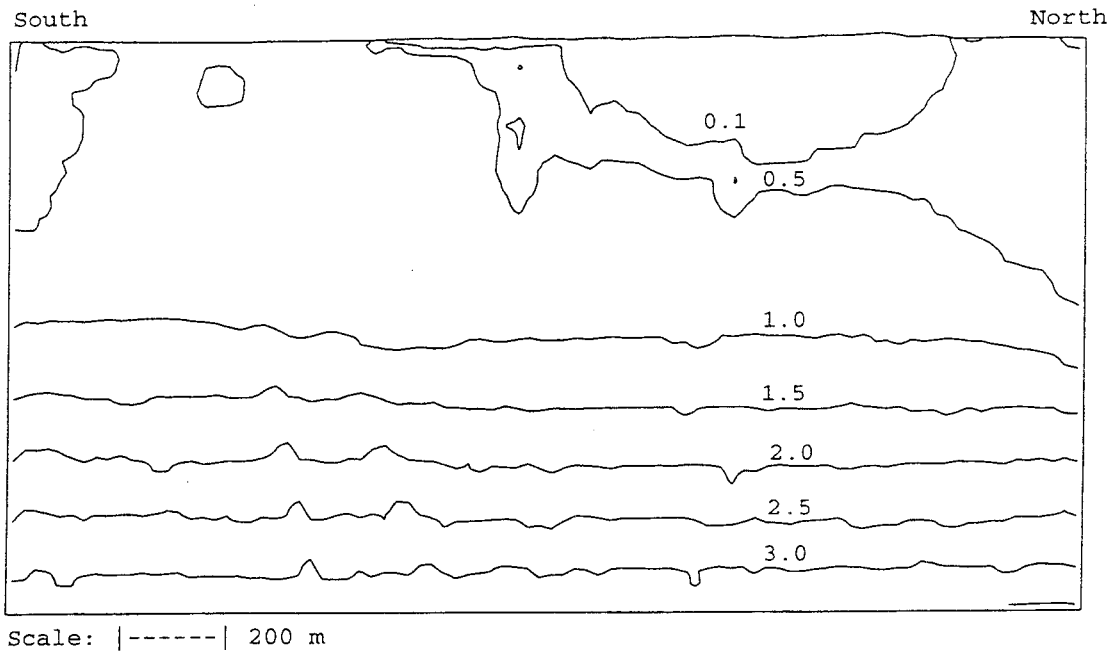

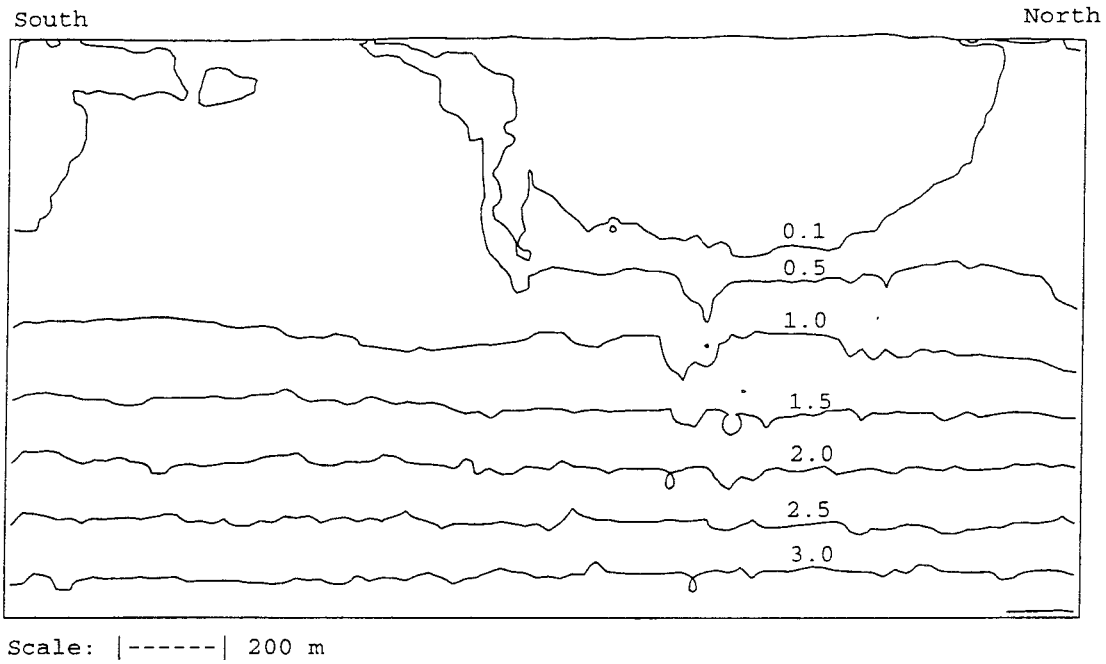

Figure 5-2. *Two vertical sections through Äspö HRL showing the salinity distribution for* P-E = 50 *mm/year (top) and* 200 *mm/year. Natural conditions.*

6 THE MAIN CHARACTERISTICS OF THE SITE

6.1 INTRODUCTION

In this chapter some gross features, as given by the simulation model, of the site will be discussed. It is expected that these features are not depending on a particular realisation of the conductivity field or a fine-tuned transmissivity.

6.2 INFILTRATION

The infiltration on southern Äspö and the whole of Äspö are summarised in Table 6-1. The infiltration is integrated over an area defined by the coastline of Äspö. This area is used for all depths shown in Table 6-1. Southern Äspö is in this context defined as south of the y-coordinate 7500 metres (in the Äspö coordinate system), which is just north of the spiral part of the tunnel. This coordinate line is drawn in Figure 1-1.

As can be seen the infiltration on southern Äspö is larger than the surface recharge when the tunnel is present, which means that there is a significant contribution from the sea. This is not surprising as the surface recharge on southern Äspö is about 1 l/s and the inflow to the spiral part of the tunnel is about 10 l/s. At 450 metres below ground the flow is upwards as indicated by the negative sign. This depth is right below the tunnel and the upward flow is thus a flow towards the tunnel.

For natural conditions a week mean upward flow is found already at 5 metres below ground. This prevails down to 450 metres, even if the flow is very week at this level. It should be noted that it is the net infiltration that is given in Table 6-1. The number –0.7% for "whole of Äspö at 100 m depth" is the net result of a upward flux of 3.8% and a downward flux of 3.1%

The pattern indicated by Table 6-1 is the same as earlier given by Figures 4-6, 4-7, 4-8, 4-16, 4-17 and 4-18.

Table 6-1. Infiltration, expressed as % of recharge (=100 mm/year)

	Depth below ground				
	0.5 m	5 m	10 m	100 m	450 m
Natural conditions whole of Äspö	83.8	0.4	-0.5	-0.7	-0.2
Southern Äspö	89.4	-3.2	-3.2	-1.6	-0.18
Complete tunnel whole of Äspö	91.8	134.2	132.3	222.9	-142.3
Southern Äspö	98.9	264.1	260.5	519.4	-358.9

Table 6-2. Volume and salt fluxes over the boundaries of a box with coordinates:
X: 1840 → 2440 (m)
Y: 7100 → 7500 (m)
Z: -600 → -200 (m)

CASE	Boundary Flux					
	WEST	EAST	SOUTH	NORTH	BOTTOM	TOP
Natural conditions						
Net flux (l/s)	-4×10^{-4}	6.9×10^{-3}	9×10^{-3}	-8×10^{-4}	-10^{-3}	10^{-3}
Positive flux	3×10^{-3}	7×10^{-3}	9.8×10^{-3}	6×10^{-3}	10^{-3}	2×10^{-2}
Negative flux	3.4×10^{-3}	10^{-4}	8×10^{-4}	6.8×10^{-3}	2×10^{-3}	1.9×10^{-2}
Max Darcy vel (m/s)	4×10^{-10}	10^{-9}	2×10^{-9}	8×10^{-10}	2×10^{-10}	3×10^{-9}
Min Darcy vel (m/s)	-2×10^{-9}	-9×10^{-11}	-2×10^{-10}	-2×10^{-9}	-4×10^{-10}	-10^{-9}
Salt flux (g/s)	0.19	0.47	0.69	0.18	-0.15	0.12
Complete tunnel						
Net flux (l/s)	0.69	-1.71	1.26	-1.77	2.31	-2.87
Positive flux	0.69	0.00	1.39	0.15	2.53	0.13
Negative flux	0.00	1.71	0.13	1.92	0.22	3.00
Max Darcy vel (m/s)	9×10^{-8}	7×10^{-11}	2×10^{-7}	6×10^{-8}	3×10^{-7}	8×10^{-8}
Min Darcy vel (m/s)	-2×10^{-13}	-10^{-7}	-6×10^{-8}	-2×10^{-7}	-8×10^{-8}	-10^{-7}
Salt flux (g/s)	2.19	-7.98	9.95	-14.08	76.71	-14.75

6.3 INTEGRATED FLUXES

The general flow pattern in the domain can be characterised by what can be called a box analysis. The idea is to place a control volume somewhere in the domain and study the fluxes over the boundaries. Two such boxes were used, one centred around the spiral with dimensions 600 x 400 x 400 m^3 and the other of almost the same size as the model domain.

Table 6-3. Volume and salt fluxes over the boundaries of a box with coordinates:
X: 1120 → 2880 (m)
Y: 6280 → 8080 (m)
Z: -880 → -100 (m)

CASE	Boundary Flux					
	WEST	EAST	SOUTH	NORTH	BOTTOM	TOP
Natural conditions						
Net flux (l/s)	0.54	-0.18	0.00	-0.02	-0.01	0.74
Positive flux	0.56	0.03	0.01	0.01	0.04	0.89
Negative flux	0.02	0.21	0.01	0.03	0.05	0.15
Max Darcy vel (m/s)	2×10^{-8}	6×10^{-9}	5×10^{-9}	6×10^{-10}	2×10^{-9}	6×10^{-8}
Min Darcy vel (m/s)	-5×10^{-9}	-10×10^{-8}	-8×10^{-9}	-5×10^{-10}	-10^{-9}	-2×10^{-9}
Salt flux (g/s)	1.11	-0.44	-0.19	-0.02	-0.19	1.20
Complete tunnel						
Net flux (l/s)	2.51	-2.65	4.90	-0.59	1.73	-16.86
Positive flux	2.51	0.00	4.91	0.00	2.47	1.05
Negative flux	0.00	2.65	0.01	0.59	0.75	17.91
Max Darcy vel (m/s)	7×10^{-8}	10^{-9}	2×10^{-7}	10^{-10}	6×10^{-8}	3×10^{-7}
Min Darcy vel (m/s)	-5×10^{-10}	-10^{-7}	-4×10^{-9}	-9×10^{-9}	-5×10^{-8}	-5×10^{-8}
Salt flux (g/s)	8.14	-5.27	7.63	-2.92	85.03	-91.26

The result can be studied in Tables 6-2 and 6-3. For the small box, Table 6-2, it is found that the net fluxes under natural conditions are very small; the positive and negative fluxes are however of the same magnitude and the circulation can thus be larger than the net flux indicates. For complete tunnel the fluxes are of course several orders of magnitude larger and fluxes are also more uniform. The large box, see Table 6-3, is almost of the same size as the model domain and the fluxes thus give the general circulation in the domain. For natural conditions the general pattern is that the flow is from east and west and leaves at the top. This is also true for the fluxes of salt. The fluxes of volume and salt for complete tunnel gives an average salinity of the inflows to the tunnel of 0.69%.

6.4 SALINITY OF INFLOWS TO TUNNEL

The salinity of the inflows to the tunnel is given in Table 6-4. The salinity varies from 0.11 to 3.04 % and both these values are found in NNW1. This variation is larger than found from field measurements; a point that will be discussed further in the discussion section. The salinity distribution in two vertical sections can be studied in Figure 4-19.

Table 6-4. Salinity of inflows to Äspö HRL. The salinities are given for the fracture zone crossings, selected for withdrawal (see Table 2-3).

Tunnel section (m)	Salinity (%)	Fracture zone
0-850	0.27	NE4
850-1030	0.31	NE3
1030-1160	0.33	NNW3
1160-1310	0.55	NE1
1310-1460	0.61	EW3
1460-1584	0.79	NE2
1584-1745	0.41	NNW7
1745-1883	0.11 0.23	NNW1 NNW2
1883-2028	0.61	NNW4
2028-2178	0.64	NNW4
2178-2357	0.89 0.62	NNW1 NNW2
2357-2496	0.97	NE2
2496-2699	2.54	NNW7
2699-2875	1.97 1.37	NNW1 NNW2
2875-2994	1.25	NNW4
2994-3179	1.08	NNW4
3179-3426	3.04 1.92	NNW1 NNW2
3426-3600	0.95	NNW5
Shaft	0.42	NNW7

6.5 FLOW AND SALINITY 450 METRES BELOW GROUND

Understanding the changes brought about by the tunnel is one of the key tasks in the Äspö HRL project. In order to study the implications from the present modelling exercise we will study the flow and salinity distributions, and some statistics, at a depth of 450 metres below ground. We will restrict ourselves to the area given by the small box, introduced in section 6.3, with the purpose to get good resolution close to the tunnel.

In Figures 6-1 and 6-2 the fluxes are given for natural conditions and completed tunnel. The fluxes are plotted for each computational cell, which gives the pattern with small squares. For natural conditions the fluxes are very small but the fracture zone system can still be identified in the figure. For the tunnel case the x- and y-components are towards the tunnel while the vertical component is upwards (450 metres is below the lowest part of the tunnel). Also for this case the magnitude of the flux-vector (called RES Flux in the figure) indicates the fracture zone system. The statistics of the fluxes are summarised in Figure 6-3 and Table 6-5. As can be seen, the tunnel increases the fluxes with 2-3 orders of magnitude.

The corresponding analysis for salinity is given in Figure 6-4 and Table 6-6. As can be expected the salinity field is very uniform for natural conditions, while the tunnel generates areas with high salinity due to the upconing effect discussed earlier in the report.

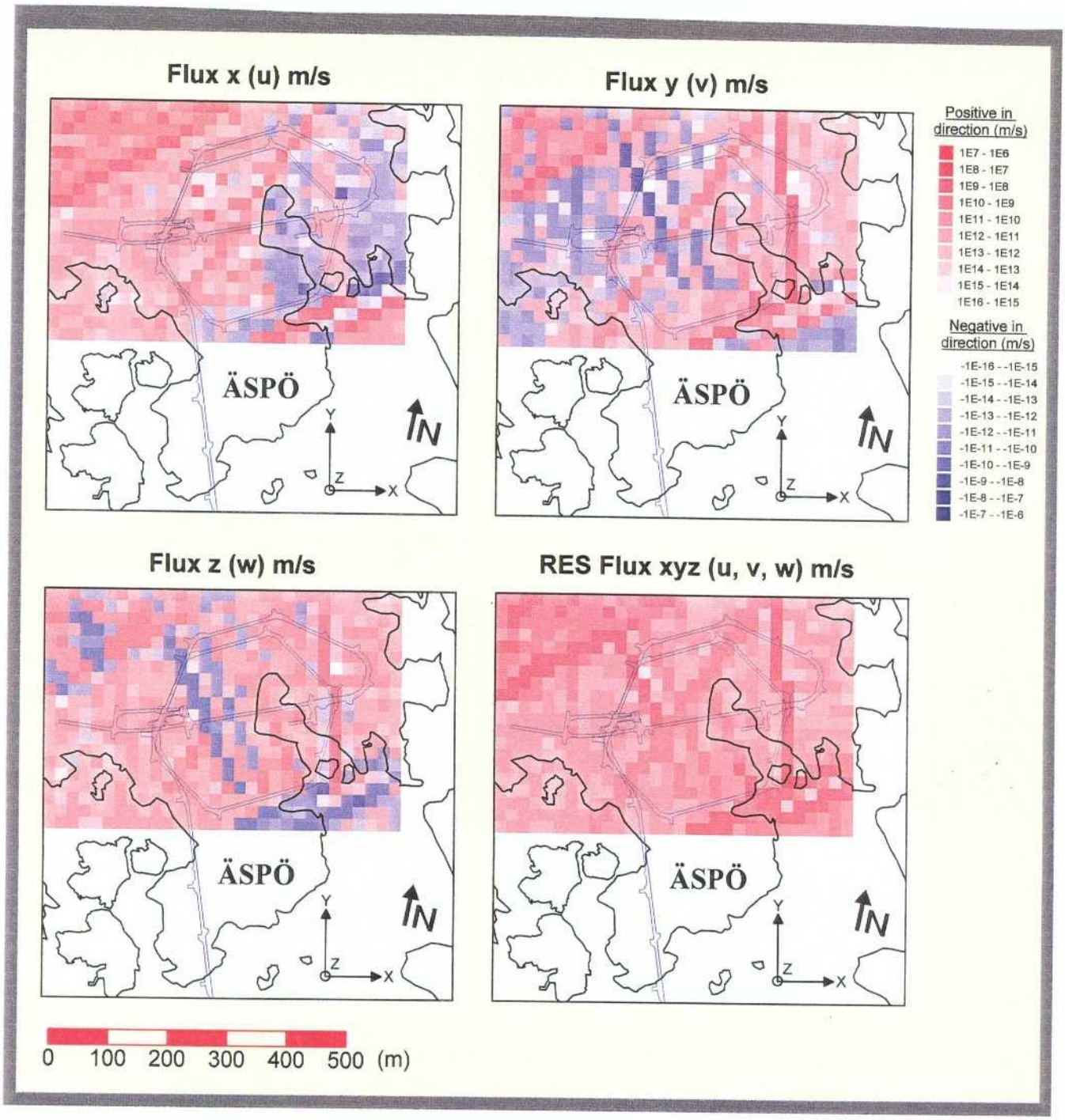

Figure 6-1. *Darcy fluxes at a depth of 450 metres. Natural conditions.*

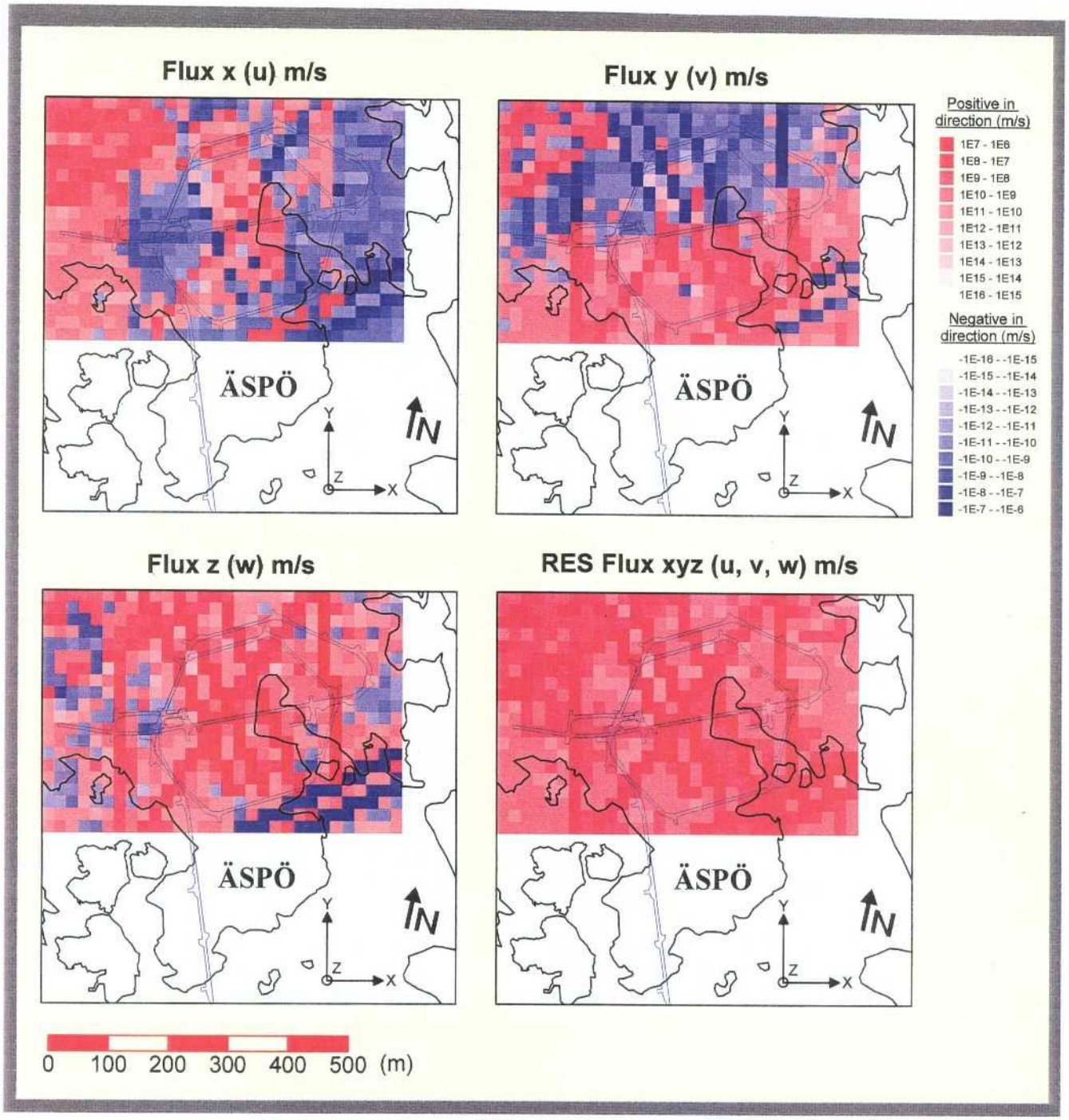

Figure 6-2. *Darcy fluxes at a depth of 450 metres. Complete tunnel.*

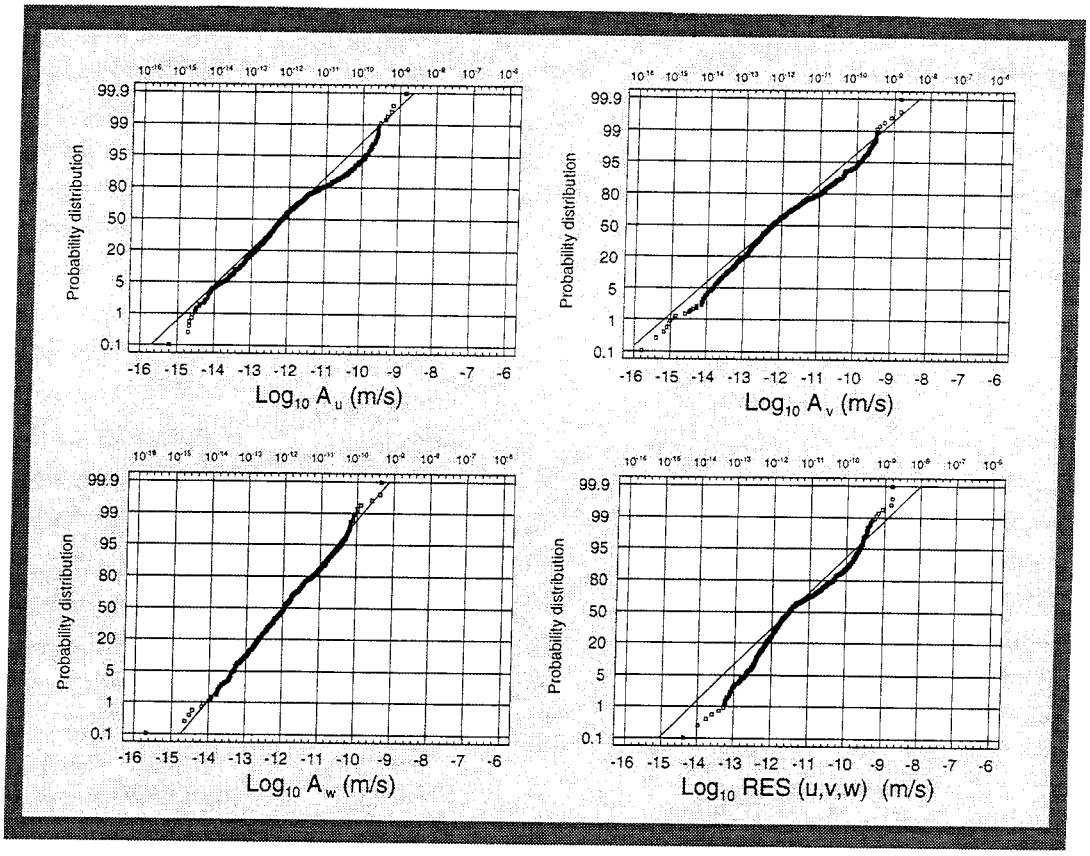

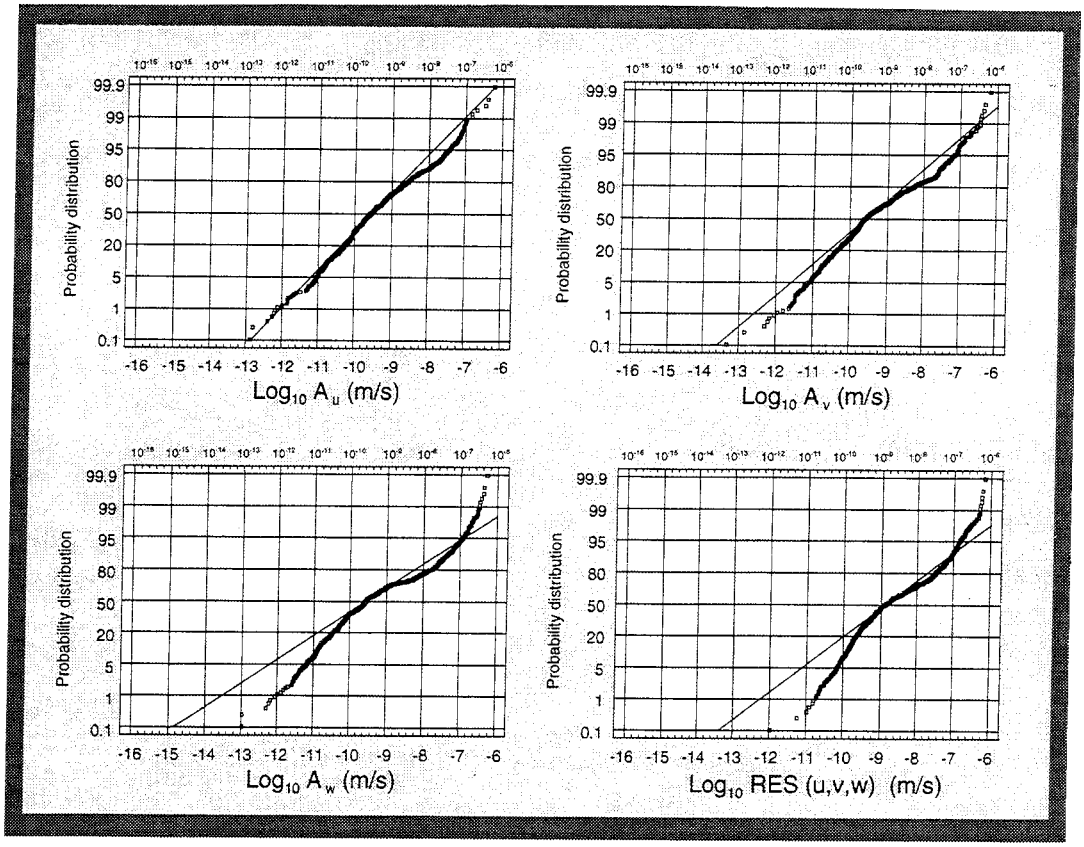

Figure 6-3. *Statistics for the absolute values of the flux components and the magnitude at a depth of 450 metres. Natural conditions (top) and complete tunnel.*

Table 6-5. Statistics of absolute values of fluxes at a depth of 450 metres.

Case	Component (X)	Mean (X) (m/s)	Median (X) (m/s)	Min (X) (m/s)	Max (X) (m/s)	s Log_{10} (X)
Natural conditions	A_u	9.7E-13	6.8E-13	6.2E-16	1.4E-09	1.19
	A_v	8.7E-13	5.8E-13	1.6E-16	1.5E-09	1.25
	A_w	1.2E-12	1.1E-12	2.1E-16	4.5E-10	0.92
	RES (u, v, w)	4.7E-12	2.9E-12	4.3E-15	1.6E-09	1.01
Complete tunnel	A_u	3.8E-10	2.8E-10	1.4E-13	5.8E-07	1.15
	A_v	4.6E-10	2.7E-10	4.8E-14	6.3E-07	1.27
	A_w	5.4E-10	2.8E-10	1.1E-13	5.0E-07	1.42
	RES (u, v, w)	2.3E-09	1.4E-09	1.1E-12	6.9E-07	1.15

Table 6-6. Statistics of salinity at a depth of 450 metres.

Case	Component (X)	Mean (X) (%)	Median (X) (%)	Min (X) (%)	Max (X) (%)	s Log_{10} (X)
Natural conditions	Salinity	0.78	0.78	0.66	0.85	0.04
Complete tunnel	Salinity	1.38	0.73	0.05	4.54	1.36

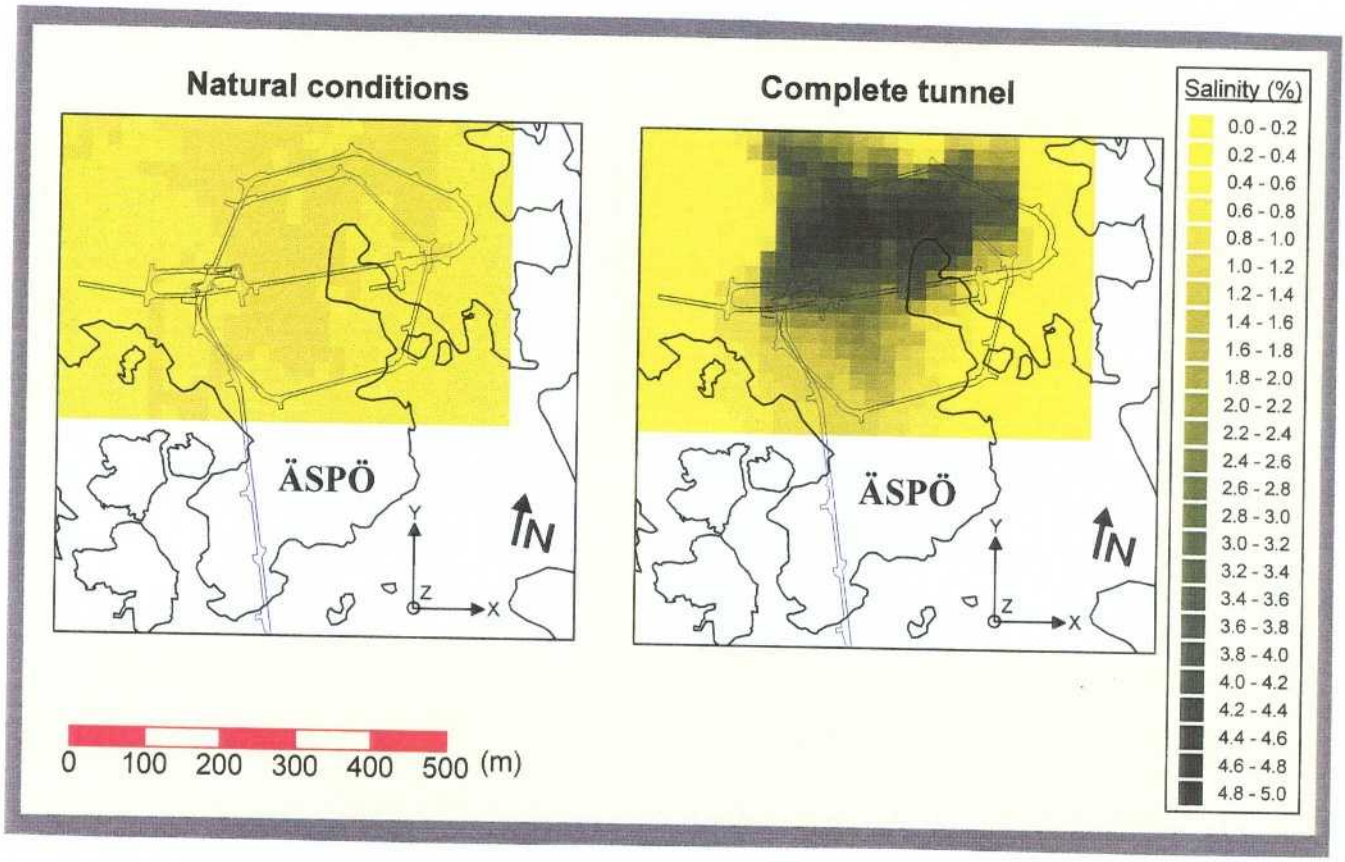

Figure 6-4. *Salinity distribution at a depth of 450 metres for natural conditions and complete tunnel.*

6.6 FLOW AND SALINITY DISTRIBUTION IN FRACTURE ZONES

All results presented hitherto show that most of the flow takes place in the fracture zones. This is due to the basic structure model used and may, or may not, be a good representation of the actual conditions. In any case it is of interest to study the calculated distributions of flow and salinity in the fracture zones. Three fracture zones, NE1, NNW1 and NNW4 will be discussed for natural conditions and for complete tunnel. These are shown in Figure 6-5, where also a volume which gives the "bounding box" of the illustrations is outlined. In the vertical direction the interval –600 to –200 metres is considered. In Figure 6-5 the salinity distribution at a depth of 600 metres, for complete tunnel, is also shown. This field gives the lower boundary for the fracture zones to be discussed next.

The flow and salinity distributions in NE1 are found in Figure 6-6. In this and the following figures we will not give a scale for the flux vector as these are three-dimensional and may have a component perpendicular to the fracture zone. For natural conditions we see that the salinity in NE1 is about 0.6%, which may be an indication of Baltic water. For complete tunnel the flow and salinity distributions are governed by the inflow to the tunnel. It is interesting to note that water of very low salinity enters the tunnel from the west. This may be fresh water from the Laxemar area. In this and the following figures the cutting plane is red when outside the bounding box. This is of course not an indication of 0.% salinity.

We next study the conditions in NNW1, see Figure 6-7. For natural conditions the freshwater lens is found above the spiral part of the tunnel, while water with a salinity of 0.6 % is found south of NNW1. Note that NNW1 only extends to the southern part of the spiral, but the cutting plane is limited by the bounding box. For complete tunnel we can find four crossings with the tunnel and these will generate the distribution shown.

The final fracture zone to be discussed is NNW4, see Figure 6-8. The view is now from east and the tunnel is seen as two lines. Also for NNW4 one should note that the fracture zone is only a part of the cutting plane, see Figure 6-5. For natural conditions we find a salinity field dominated by water with a salinity of 0.6 % and large fluxes in NE1 (south of NNW4) and in the fresh water lens. For complete tunnel we see that the upper crossings with the tunnel receive water mainly from above while the lower crossings extracts water from all directions.

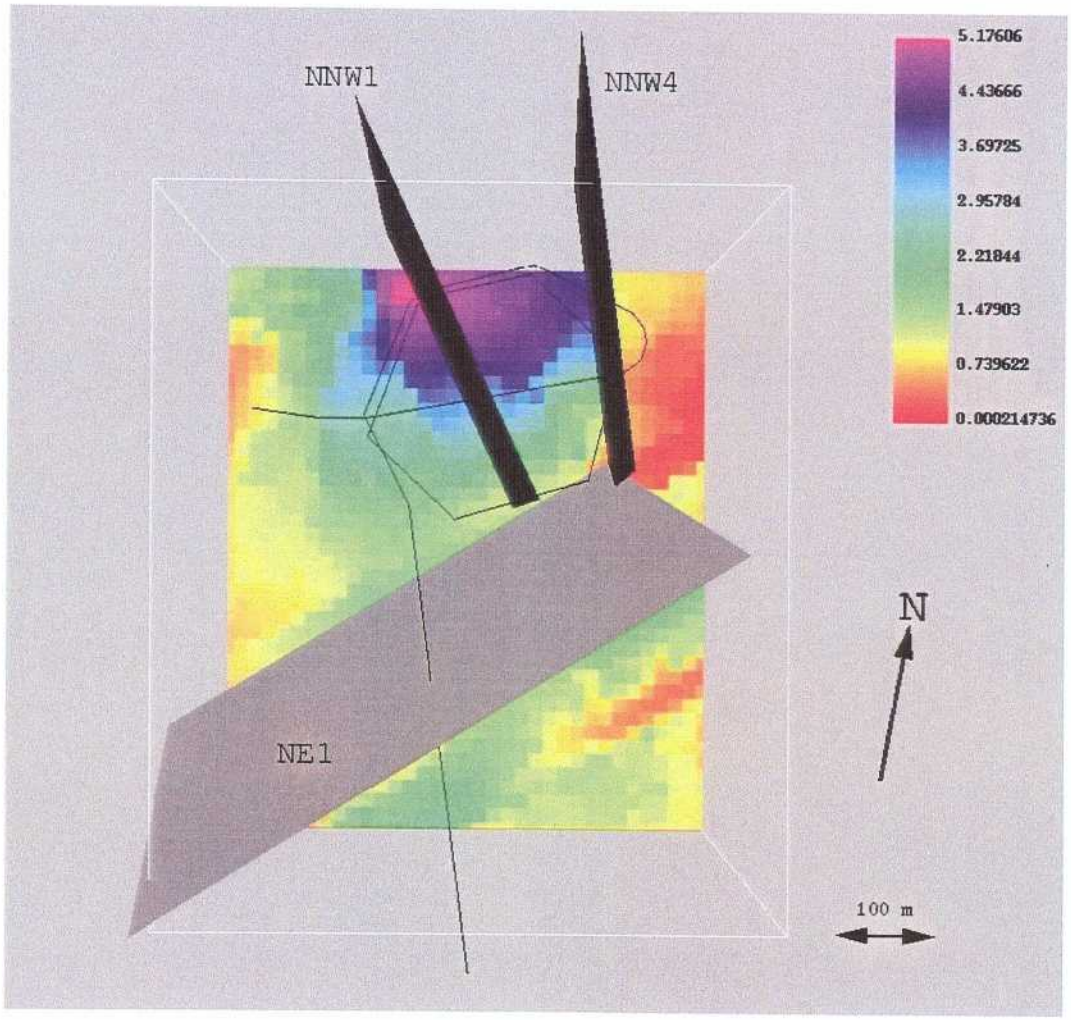

Figure 6-5. *Orientation figure for flow and salinity in fracture zones. Salinity (in %) distribution at a depth of 600 metres for complete tunnel.*

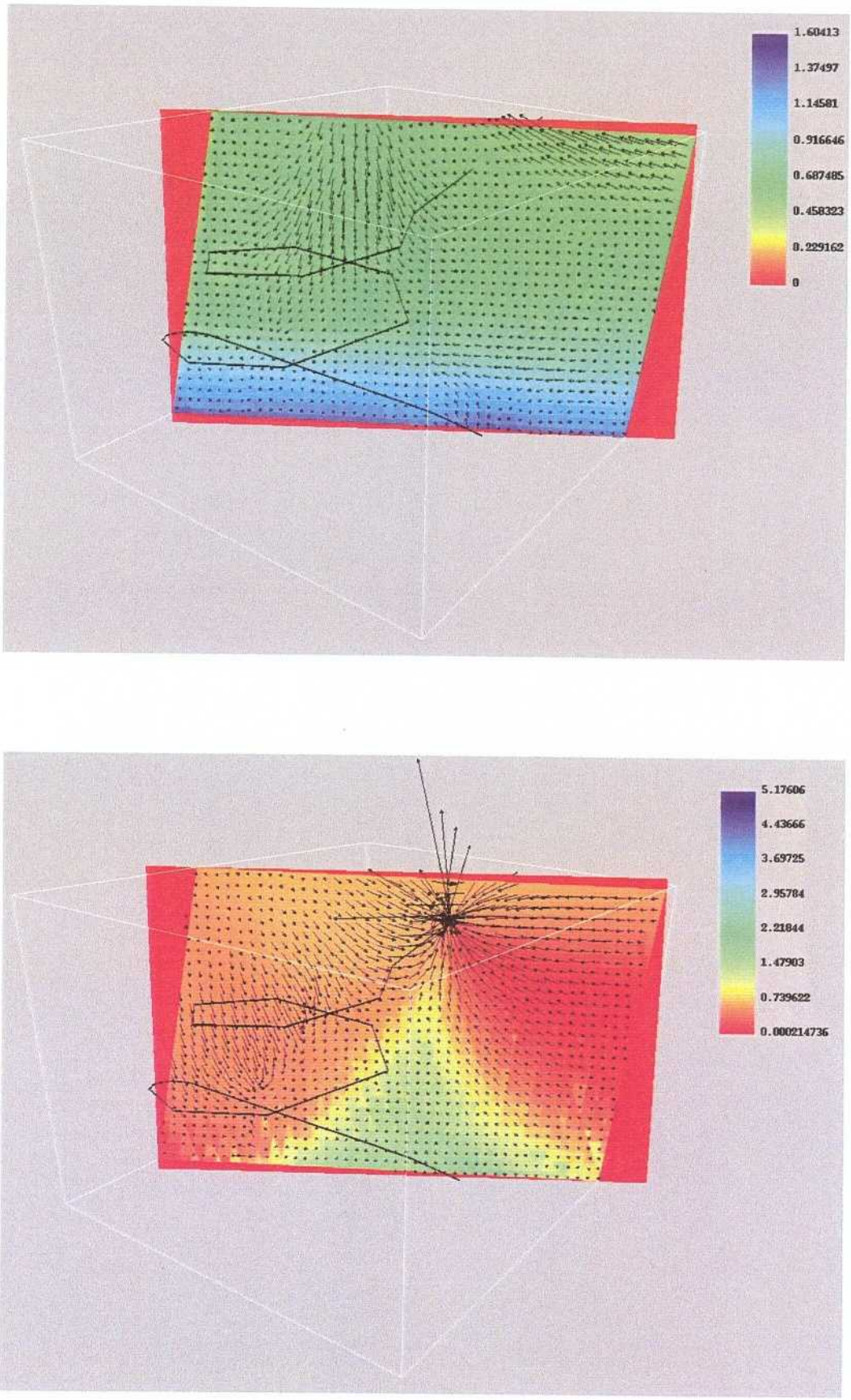

Figure 6-6. *Flow and salinity (in %) distribution in NE1. View from North. Natural conditions (top) and complete tunnel. Depth interval:* -600 → -200 *metres.*

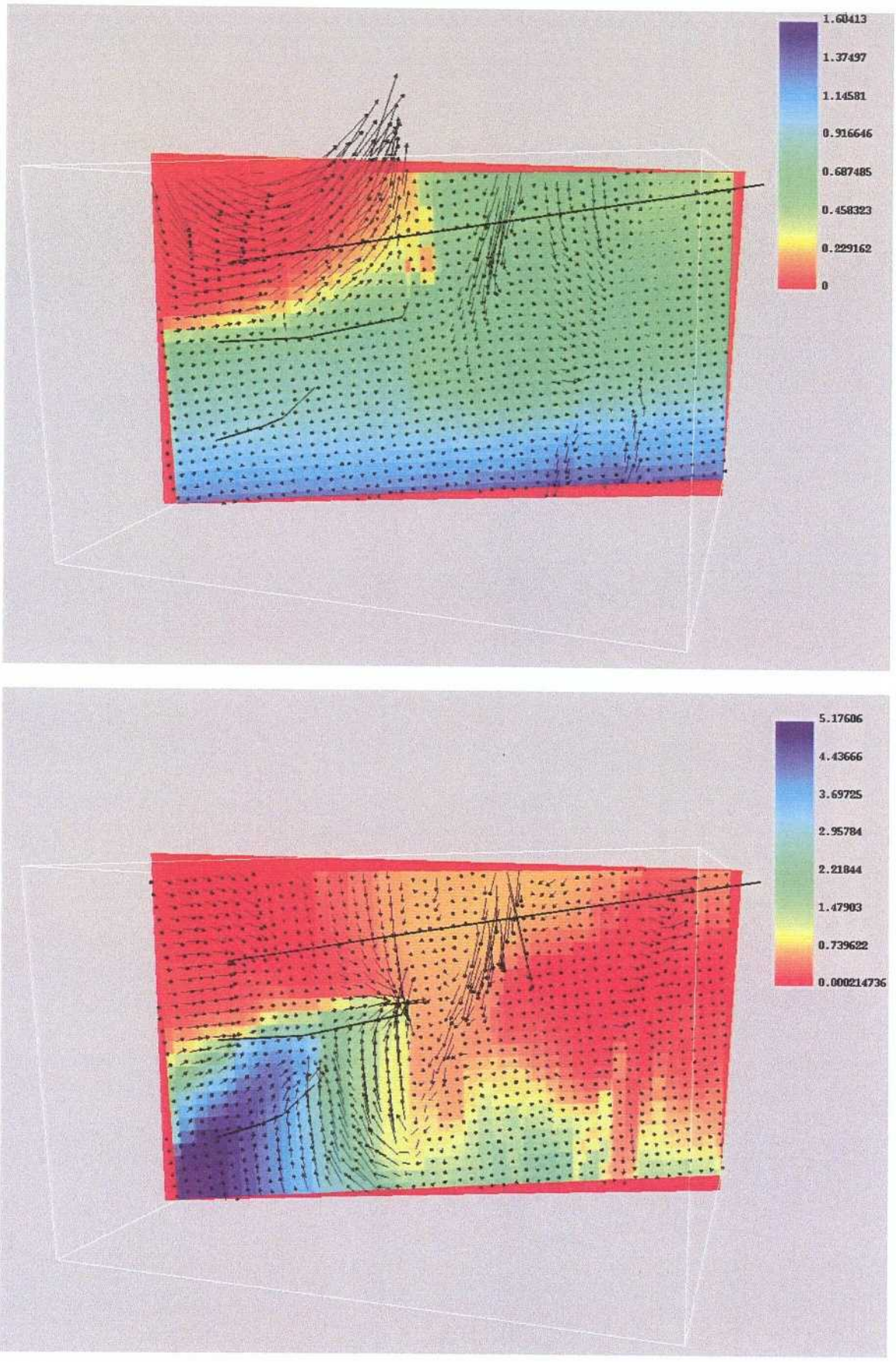

Figure 6-7. *Flow and salinity (in %) distribution in NNW1. View from West. Natural conditions (top) and complete tunnel. Depth interval:* -600 → -200 *metres.*

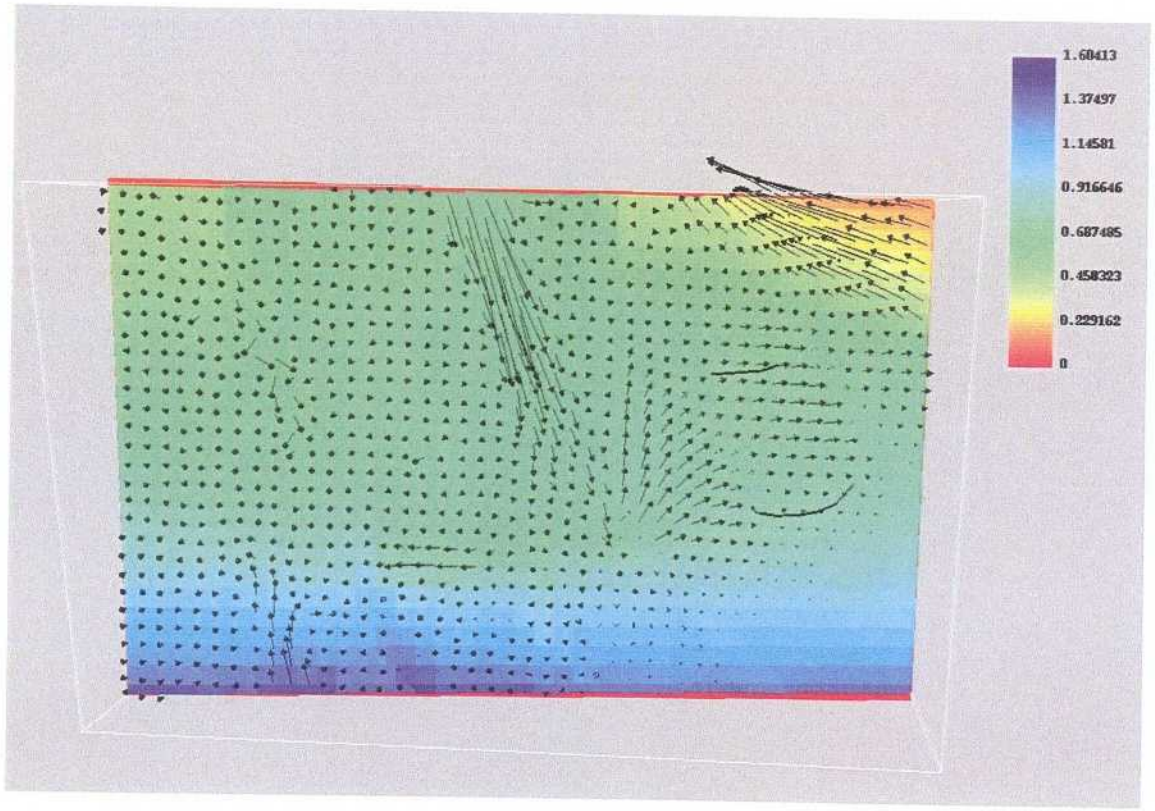

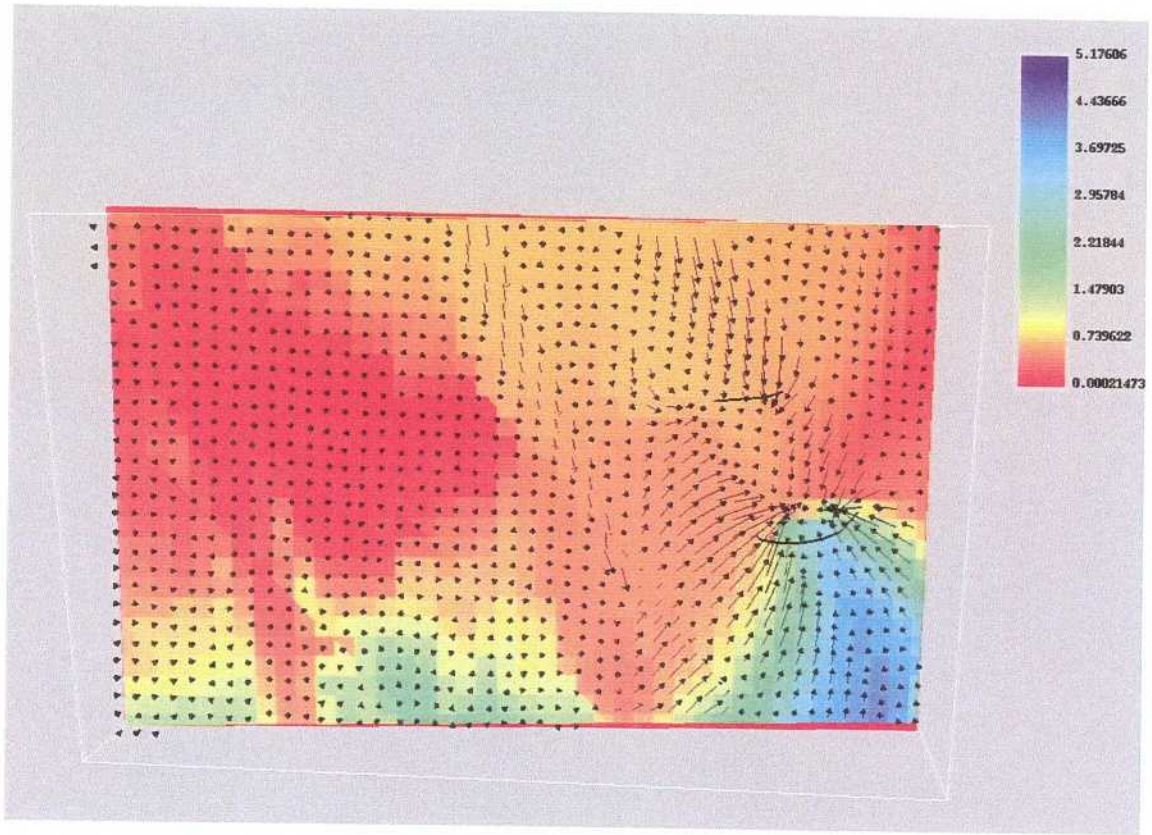

Figure 6-8. *Flow and salinity (in %) distribution in NNW4. View from East. Natural conditions (top) and complete tunnel. Depth interval:* -600 → -200 *metres.*

6.7 TRANSPORT TIMES

The transport time from repository level to ground is a fundamental parameter in a safety assessment study. A brief account of this problem will now be given.

A grid of marked fluid elements is placed below Äspö at a depth of 450 metres. These elements are then tracked for 100 years. The calculation requires an estimate of the kinematic porosity, in order to relate the Darcy velocity to the pore velocity. In Rhén et al (1997) a relation between the hydraulic conductivity (K) and the kinematic porosity (n_e) is suggested:

$$n_e = 34.87K^{0.753} \qquad (6\text{-}1)$$

This equation was used with the constraint that $n_e \leq 0.05$. This will result in an average (arithmetic mean) kinematic porosity of 0.004. The simulation did not include dispersion or any other retardation mechanism.

Results can be found in Figure 6-9. If the particles are placed at a depth of 450 metres roughly 15% will reach ground level in 100 years. If we place the particles at 550 metres depth none will reach ground in 100 years, while roughly 50% will reach ground if we place them at a depth of 350 metres.

The sensitivity to the initial depth is due to the density stratification. This was also found in Svensson (1997).

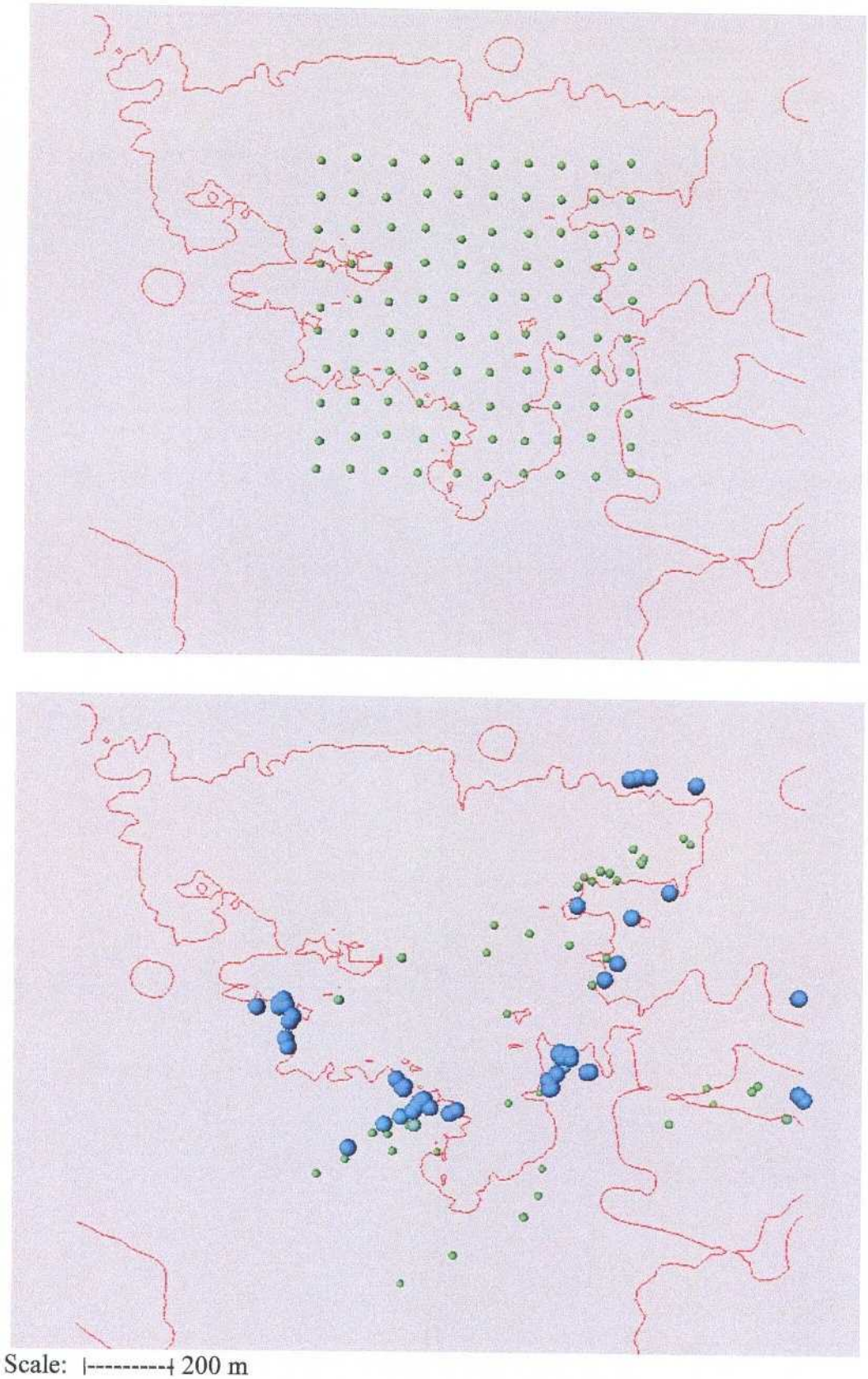

Figure 6-9. *Transport times. Initial positions of particles (top) and positions after 100 years for an initial depth of 350 metres. Big blue particles are close to ground, while smaller ones are at deeper levels.*

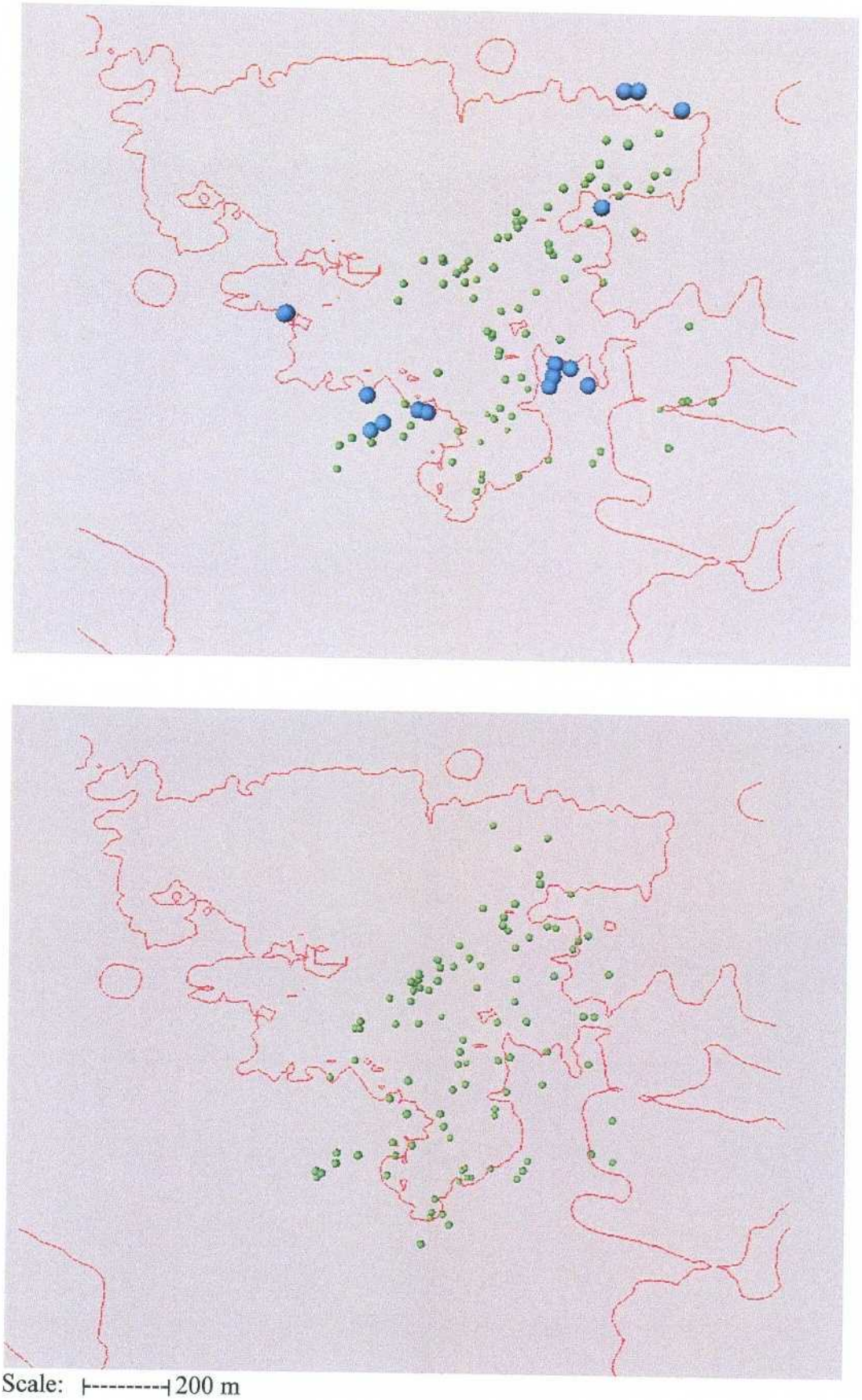

Figure 6-9 cont. *Initial depth 450 metres (top) and 550 metres.*

6.8 THE FRESHWATER LENS

In the sensitivity studies it was found, see Figure 5-2, that the depth of the freshwater lens is depending on the recharge. As the recharge affects the groundwater level, it is more likely that it is the groundwater level that is governing the depth of the freshwater lens.

It is here suggested that the depth of the freshwater lens follows from Archimedes principle. The total mass of fresh water (above and below sea level) should then be equal to the mass of the displaced saline water. If we note the volume above sea level V_1, and the volume below V_2, we can write:

$$(V_1 + V_2)\rho_f = V_2\rho_s \qquad (6\text{-}1)$$

or

$$V_2 = \frac{\rho_f}{\rho_s - \rho_f} V_1 \qquad (6\text{-}2)$$

where ρ_f is the freshwater density and ρ_s the density of the displaced water. To determine ρ_s, we need to assume a salinity of the saline water, which will increase as the depth of the lens increases.

In Table 6-7, the cases with varying recharge are summarised. A salinity of the displaced water has been estimated and V_2 has been obtained from the equation above, based on the Archimedes principle, and compared with the V_2 obtained from the simulations. As can be seen a good agreement is found. It should be noted that the result is not critically dependent on the assumed salinity of the displaced water. If one assumes a salinity of 0.6% (Baltic water) for all recharges the V_2-value for the 200 mm/year recharge will be 2.4×10^8.

This has an interesting implication, as the groundwater level varies over the year and between years. To have a balance the fresh/salt water interface has to adopt to the varying water table and hence move up and down; this could be the explanation to the more dispersed salinity field found from field measurements.

Table 6-7. The freshwater lens and Archimedes principle.

Recharge mm/year	Salinity of displaced water (%)	V_1 from simulation (m^3)	V_2 from Archimedes (m^3)	V_2 from simulation (m^3)
50.	0.60	6.0×10^5	1.3×10^8	1.3×10^8
100.	0.65	8.7×10^5	1.7×10^8	1.7×10^8
200.	0.70	11.3×10^5	2.1×10^8	2.0×10^8

7 DISCUSSION

In this section we will discuss some topics that need to be further analysed. The selection of topics is based on two criteria; either the topic is an interesting physical phenomenon in itself and/or is it a topic that ought to be considered when model improvements are discussed.

- **Conductivities and transmissivities.** As was demonstrated in the sensitivity test all results are very sensitive to the input data. More accurate field data is thus always of value. From the modelling point of view it may however also be other types of data that are needed. In the present technique to include conductive structures we treat about twenty fracture zones deterministically and include all other fractures in a stochastic cell conductivity. Fracture zones with a length scale between the cell size and the twenty fracture zones, i.e. length scales in the interval 20-200 metres, are not well represented with this technique. Improvements can be made and these improvements may also require information from additional field measurements.

- **Surface hydrology.** In the present model the recharge at ground level was set to 100 mm/year and the conductivity of the top five cell layers were determined in the calibration process. It would be useful to have estimates of these values from field measurements.

- **Ten realisations of the conductivity field.** The main results in this report are based on the mean of ten realisations of the stochastic part of the conductivity field. This gives the opportunity to study, for example, the standard deviation distributions of a variable. No results of this kind have however been presented in this report. The reason is that one first ought to consider the representation of fracture zones in the model, as discussed above, in order to have a better understanding of what the stochastic part of the conductivity field really represents.

- **Calibration process.** It would be very useful to have a technique or strategy for how a calibration ought to be carried out. In the present work a trial and error method was used; this can be very time consuming. No systematic method, excluding techniques like inverse modelling, is however known to the author. Another question related to the calibration process is how far the fine-tuning should be taken. In the present

calibration the mean error for both the LPT2 experiment and tunnel front at 2875 metres were reduced to a few centimetres. The mean error for additional realisations of the conductivity field was much larger. Perhaps it can be argued that to much effort was spent on the fine-tuning of transmissivities and conductivities.

- **Freshwater lens below Äspö.** It has in this report been suggested that the depth of the freshwater lens follows from the Archimedes principle; the depth should thus be related to the groundwater level. An interesting question is then what timescale this adjustment has, compared to for example annual variations of the water table. Further, does the adjustment take place only in the fracture zones?

- **Dispersion of salt.** Related to the movement of the fresh/salt water interface is the dispersion of salt. If the interface is displaced several hundred metres, see Figure 5-2, due to seasonal variations in the groundwater level this will probably contribute to the dispersion of salt. A first investigation of this question has been carried out. The product $\beta\Delta$, see equation (7), was increased to simulate the effect of the moving interface. A uniform value of $\beta\Delta$ was set, even if one could argue that the additional dispersion effect ought to be centred around the interface depth and perhaps be proportional to the groundwater level. The result can be studied in Tables 7-1 and 7-2. As can be seen a much closer agreement with field measurements can be achieved by putting $\beta\Delta$ to 300. To firmly establish the dispersion effect of a moving interface a transient analysis is required, possibly also including a double porosity technique for salt in more or less stagnant volumes. The reason for investigating this is not only to understand the observed salinity distribution, it may also point to a general vertical exchange process important also for other substances.

- **Regional flow.** The present model uses boundary conditions from a regional model. Some problems were encountered, see Section 2.5, but the procedure adopted seems to work. However, further studies of the consistency between the two scales are needed. For example, is the flow rate in a fracture zone that crosses the boundary the same in the two models?

Table 7-1. Effect of an increased dispersion coefficient for salt. Measured and calculated salinity in borehole sections for natural conditions.

Borehole section	Depth M b s l	Measured salinity %	Calculated salinity % βΔ=2	Error	Calculated salinity % βΔ=300	Error
KAS02A	52.00	0.38	0.00	-0-38	0.41	0.03
KAS02B	191.00	0.73	0.00	-0.73	0.43	-0.30
KAS02C	311.00	0.95	0.06	-0.89	0.51	-0.44
KAS02D	540.00	0.98	1.08	0.10	091	-0.07
KAS02E	829.00	1.42	2.45	1.03	2.42	1.00
KAS02F	879.00	1.58	2.67	1.09	2.65	1.07
KAS03A	51.00	0.21	0.00	-0.21	0.32	0.11
KAS03B	210.00	0.22	0.00	-0.22	0.39	0.17
KAS03C	349.00	0.86	0.55	-0.31	0.49	-0.37
KAS03D	517.00	0.90	0.86	-0.04	0.81	-0,09
KAS03E	606.00	0.65	1.28	0.63	1.16	0.51
KAS03F	676.00	1.12	1.49	0.37	1.39	0.27
KAS04A	142.00	0.05	0.00	-0.05	0.33	0.28
KAS04B	151.00	0.10	0.00	-0.10	0.33	0.23
KAS04C	185.00	0.12	0.00	-0.12	0.35	0.23
KAS04D	235.00	0.25	0.00	-0.25	0.38	0.13
KAS04E	277.00	0.53	0.00	-0.53	0.41	-0.12
KAS04F	343.00	0.93	0.42	-0.51	0.48	-0.45
KAS05A	81.00	0.08	0.00	-0.08	0.39	0.31
KAS05B	270.00	0.12	0.01	-0.11	0.50	0.38
KAS05C	310.00	0.62	0.12	-0.50	0.54	-0.08
KAS05D	429.00	0.78	0.78	0.00	0.70	-0.08
KAS05E	459.00	0.90	0.82	-0.08	0.73	-0.17
KAS06A	81.00	0.32	0.37	0.05	0.52	0.20
KAS06B	183.00	0.49	0.16	-0.33	0.49	0.00
KAS06C	259.00	1.03	0.26	-0.77	0.51	-0.52
KAS06D	293.00	1.00	0.58	-0.42	0.55	-0.45
KAS06E	334.00	1.01	0.69	-0.32	0.58	-0.43
KAS06F	376.00	1.08	0.70	-0.38	0.60	-0.48
KAS07A	47.00	0.45	0.03	-0.42	0.49	0.04
KAS07B	107.00	0.54	0.01	-0.53	0.47	-0.07
KAS07C	210.00	0.67	0.00	-0.67	0.51	-0.16
KAS07D	295.00	0.66	0.50	-0.16	0.66	0.00
KAS07E	362.00	1.01	0.68	-0.33	0.82	-0.19
KAS07F	463.00	0.85	0.81	-0.04	0.95	0.10
KAS08A	52.00	0.70	0.00	-0.70	0.35	-0.35
KAS08B	148.00	0.66	0.00	-0.66	0.42	-0.24
KAS08C	313.00	0.90	0.68	-0.22	0.60	-0.30
KAS08D	455.00	1.02	0.70	-0.32	0.91	-0.11
Mean error (%)				-0.21		-0.01

Table 7-2. Effect of an increased dispersion coefficient for salt. Measured and calculated salinity of inflows to the completed tunnel. Measured data from Rhén et al (1997)

Tunnel-section (m)	Fracture zone	Measured salinity (%)	Calculated salinity (%) $\beta\Delta$=2	Calculated salinity (%) $\beta\Delta$=300
0-850	NE4	0.50	0.27	0.40
850-1030	NE3	0.61	0.31	0.65
1030-1160	NNW3	0.62	0.33	0.67
1160-1310	NE1	0.69	0.55	0.81
1310-1460	EW3	0.59	0.61	0.84
1460-1584	NE2	0.59	0.79	1.12
1584-1745	NNW7	1.0	0.41	1.25
1745-1883	NNW1 NNW2	0.79 0.79	0.11 0.23	1.24 1.17
1883-2028	NNW4	0.57	0.61	0.97
2028-2178	NNW4	0.59	0.64	0.97
2178-2357	NNW1 NNW2	0.89 0.89	0.89 0.62	1.29 1.00
2357-2496	NE2	1.03	0.97	1.33
2496-2699	NNW7	1.10	2.54	1.49
2699-2875	NNW1 NNW2	1.45 1.45	1.97 1.37	1.52 1.42
2875-2994	NNW4	1.09	1.25	1.22
2994-3179	NNW4	1.18	1.08	1.18
3179-3426	NNW1 NNW2	1.18 1.18	3.04 1.92	1.66 1.51
3426-3600	NNW5	1.07	0.95	1.56
Shaft	NNW7		0.42	1.20

8 CONCLUDING REMARKS

A numerical model of the Äspö site has been developed, calibrated, applied and discussed. The model has the following key features:

- The mathematical formulation of the model is based on relevant conservation laws and embodies all physical processes believed to be important for the problem considered. The importance of gravitational forces is in this context emphasised.

- A high resolution grid, which resolves topographical features and at the same time can simulate the effect of the Äspö HRL, is used.

- Transmissivities and conductivities used in the model are based on field data.

- The model has been calibrated, with good result, using field data for natural conditions, the LPT2 experiment and for tunnel front at position 2875 metres.

- A range of sensitivity studies has been carried out. These demonstrate that the model is quite sensitive to variations in input data. If, for example, the conductivity is multiplied or divided with a factor of two a significant change in the calculated drawdowns will result.

The main objective of the study has been stated as "development of an adequate model of the groundwater flow and salinity distribution in the Äspö area". In the author's view this objective has been fulfilled.

9 REFERENCES

Bear J, Verruijt A, 1987. Modelling Groundwater Flow and Pollution. D. Reidel Publishing Company, Dordrecht, Holland.

Forsmark T, Rhén I, 1994. Information for numerical modelling 1994. General information and calibration cases for the Äspö HRL, tunnel section 700-2545 metres. SKB Progress Report 25-94-16.

Gustafson G, Ström A, 1995. The Äspö Task Force Modelling of Groundwater Flow and Transpot of Solutes. Evaluation report on Task No 1, the LPT2 large scale field experiments. SKB International Cooperation Report 95-05.

Rhén I, Svensson U, Andersson J-E, Andersson P, Eriksson C-O, Gustafsson E, Ittner T, Nordqvist R, 1992. Äspö Hard Rock Laboratory: Evaluation of the combined longterm pumping and tracer test (LPT2) in borehole KAS06. SKB Technical Report 92-32.

Rhén I, Forsmark T, Danielsson P, 1994. Piezometric levels. Evaluation of data from section 2256-2874. SKB Progress Report 25-94-22.

Rhén I (ed), Gustafson G, Stanfors R, Wikberg P, 1997. Äspö HRL – Geoscientific evaluation 1997/5. Models based on site characterization 1986-1995. SKB Technical Report 97-06.

Spalding D.B, 1981. "A general purpose computer program for multi-dimensional one- and two-phase flow". Math. Comp. Sim., 8, 267-276. See also: http://www.cham.co.uk.

Svensson U, 1995. Modelling the unsaturated zone at Äspö under natural conditions and with the tunnelfront at 2874 metres. SKB, Progress report 25-95-24.

Svensson U, 1997. A regional analysis of groundwater flow and salinity distribution in the Äspö area. SKB Technical Report 97-09.

APPENDIX A

Table A-1. Measured and calculated drawdown in borehole sections during the LPT2 experiment.

Borehole section	Depth M b s l	Calculated drawdown (m)	Measured drawdown (m)	Error (m)
K01-A1	-50.35	5.36	6.20	-0.84
K02-B6	-50.35	9.23	6.30	2.93
K02-B5	-190.00	8.71	5.79	2.92
K02-B4	-310.00	8.55	6.30	2.25
K02-B3	-530.00	5.46	5.40	0.06
K02-B2	-830.00	0.84	2.41	-1.57
K02-B1	-870.00	0.53	2.30	-1.77
K03-C6	-50.35	0.14	0.00	0.14
K03-C5	-210.00	0.66	0.00	0.66
K03-C4	-350.00	1.01	0.55	0.46
K03-C3	-510.00	1.17	0.80	0.37
K03-C2	-610.00	1.04	0.83	0.21
K03-C1	-670.00	0.82	0.82	0.00
K04-D6	-130.00	3.30	0.00	3.30
K04-D5	-150.00	3.37	3.27	0.10
K04-D4	-190.00	3.95	3.11	084
K04-D3	-230.00	4.03	3.42	0.61
K04-D2	-270.00	4.37	3.58	0.79
K04-D1	-330.00	4.96	3.33	1.63
KO5-E5	-90.07	3.78	5.58	-1.80
K05-E4	-270.00	4.18	4.97	-0.79
K05-E3	-310.00	4.26	5.45	-1.19
K05-E2	-430.00	4.04	3.30	0.74
K05-E1	-450.00	4.01	3.06	0.95
KO7-J6	-50.35	6.64	15.64	-9.00
K07-J5	-110.00	15.03	16.53	-1.50
K07-J4	-210.00	6.81	5.61	1.20
K07-J3	-290.00	2.77	1.69	1.08
K07-J2	-370.00	1.32	1.88	-0.56
K07-J1	-470.00	1.12	2.54	-1.42
K08-M4	-50.35	2.41	4.73	-2.32
K08-M3	-150.00	5.54	6.58	-1.04
K08-M2	-310.00	4.78	4.70	0.08
K08-M1	-450.00	2.12	3.74	-1.62
K09-AE	-90.07	0.26	0.25	0.01
K09-AD	-110.00	0.32	0.38	-0.06
K09-AC	-150.00	0.42	0.45	-0.03
K09-AB	-210.00	0.44	0.44	0.00
K09-AA	-350.00	0.24	0.25	-0.01
K10-BA	-50.35	0.11	0.63	-0.52
K11-CF	-30.48	0.02	0.49	-0.47
K11-CE	-50.35	0.09	0.57	-0.48
K11-CD	-90.07	0.27	0.58	-0.31
K11-CC	-130.00	0.43	0.69	-0.26
K11-CB	-170.00	0.55	0.90	-0.35
K11-CA	-210.00	0.67	0.55	0.12
K12-DE	-90.07	1.85	3.54	-1.69
K12-DD	-110.00	2.28	3.00	-0.72
K12-DC	-230.00	4.95	4.20	0.75
K12-DB	-270.00	6.27	5.87	0.40
K12-DA	-350.00	7.48	4.13	3.35
K13-EE	-90.07	9.71	5.53	4.18
K13-ED	-150.00	5.94	5.03	0.91
K13-EC	-190.00	4.59	5.06	-0.47
K13-EB	-250.00	3.94	3.43	0.51
K13-EA	-330.00	2.71	2.62	0.09
K14-FE	-70.21	0.17	0.64	-0.47
K14-FD	-110.00	0.34	0.70	-0.36
K14-FC	-110.00	0.34	0.72	-0.38
K14-FB	-130.00	0.38	0.61	-0.23
K14-FA	-150.00	0.43	0.63	-0.20
Mean error (m)	-0.01			

Table A-2. Measured and calculated drawdown for tunnel front position 2875 metres.

Borehole section	Depth M b s l	Calculated drawdown (m)	Measured drawdown (m)	Error (m)
K02-B5	-190.00	40.26	45.10	-4.84
K02-B4	-310.00	37.05	51.50	-14.45
K02-B3	-530.00	26.51	16.90	9.61
K02-B2	-830.00	15.40	18.10	-2.70
K02-B1	-870.00	14.39	17.30	-2.91
K03-C5	-210.00	5.87	1.30	4.57
K03-C4	-350.00	8.49	7.70	0.79
K03-C3	-510.00	8.91	6.90	2.01
K03-C2	-610.00	8.57	6.90	1.67
K03-C1	-670.00	7.82	7.70	0.12
K05-E4	-270.00	47.99	40.40	7.59
K05-E3	-310.00	43.69	39.90	3.79
K05-E2	-430.00	33.83	32.50	1.33
K05-E1	-450.00	32.21	29.20	3.01
K06-F6	-90.07	9.77	9.90	-0.13
K06-F4	-250.00	26.95	33.80	-6.85
K06-F3	-290.00	29.31	13.90	15.41
K06-F2	-330.00	30.23	29.10	1.13
KO6-F1	-370.00	26.94	30.00	-3.06
K07-J5	-110.00	33.83	54.80	-20.97
K07-J4	-210.00	37.58	37.50	0.08
K07-J3	-290.00	33.65	25.20	8.45
K07-J2	-370.00	16.73	11.70	5.03
K07-J1	-470.00	13.06	18.10	-5.04
K08-M3	-150.00	23.55	25.90	-2.35
K08-M2	-310.00	25.13	16.60	8.53
K08-M1	-450.00	16.33	19.50	-3.17
K09-AE	-90.07	14.55	11.40	3.15
K09-AD	-110.00	14.49	12.00	2.49
K09-AC	-150.00	15.03	14.60	0.43
K09-AB	-210.00	19.52	14.00	5.52
K09-AA	-350.00	8.72	11.50	-2.78
K10-BA	-50.35	13.61	13.50	0.11
K11-CF	-30.48	10.61	15.50	-4.89
K11-CE	-50.35	14.01	16.00	-1.99
K11-CD	-90.07	15.09	14.50	0.59
K11-CC	-130.00	17.23	18.60	-1.37
K11-CB	-170.00	23.88	16.80	7.08
K11-CA	-210.00	20.50	20.00	0.50
K12-DE	-90.07	20.32	25.60	-5.28
K12-DD	-110.00	21.33	25.00	-3.67
K12-DC	-230.00	26.22	25.40	0.82
K12-DB	-270.00	28.59	25.30	3.29
K12-DA	-350.00	27.84	24.90	2.94
K14-FE	-70.21	13.37	11.50	1.87
K14-FD	-110.00	14.08	11.50	2.58
K14-FC	-130.00	13.86	11.60	2.26
K14-FB	-130.00	12.22	11.60	0.62
K14-FA	-170.00	11.83	11.90	-0.07
K16-?D	-110.00	10.02	15.20	-5.18
K16-?C	-230.00	19.74	28.00	-8.26
K16-?B	-410.00	13.48	18.60	-5.12
K16-?A	-490.00	12.22	16.70	-4.48
KB2-B6	-50.35	3.79	5.10	-1.31
KB2-B5	-70.21	7.92	8.00	-0.08
KB2-B4	-90.07	9.19	8.60	0.59
KB2-B3	-130.00	11.14	5.30	5.84
Mean error (m):	0.05			

Table A-3. Calculated drawdown during the LPT2 experiment for five realisations of the conductivity field.

Borehole section	Depth m b s l	Realisation				
		1	2	3	4	5
K01-A1	-50.35	5.36	5.03	6.12	3.77	3.92
K02-B6	-50.35	9.23	8.72	8.41	8.49	8.47
K02-B5	-190.00	8.71	7.44	7.51	7.65	6.06
K02-B4	-310.00	8.55	6.45	7.37	7.58	6.70
K02-B3	-530.00	5.46	5.09	5.20	5.19	5.12
K02-B2	-830.00	0.84	0.82	0.84	0.83	0.83
K02-B1	-870.00	0.53	0.52	0.53	0.52	0.53
K03-C6	-50.35	0.14	0.12	0.13	0.15	0.16
K03-C5	-210.00	0.66	0.65	0.70	0.65	0.63
K03-C4	-350.00	1.01	0.92	0.96	0.92	0.92
K03-C3	-510.00	1.17	1.15	1.14	1.14	1.11
K03-C2	-610.00	1.04	1.05	0.95	0.96	0.92
K03-C1	-670.00	0.82	0.90	0.87	0.82	0.84
K04-D6	-130.00	3.30	3.04	3.25	2.90	2.89
K04-D5	-150.00	3.37	3.11	3.27	3.06	3.12
K04-D4	-190.00	3.95	3.79	3.72	3.60	3.82
K04-D3	-230.00	4.03	3.89	3.98	3.84	3.90
K04-D2	-270.00	4.37	4.23	4.25	4.11	4.16
K04-D1	-330.00	4.96	4.72	5.01	4.78	4.50
KO5-E5	-90.07	3.78	3.45	3.64	3.39	3.36
K05-E4	-270.00	4.18	3.86	4.15	3.98	3.87
K05-E3	-310.00	4.26	3.91	3.98	3.58	3.61
K05-E2	-430.00	4.04	3.68	3.85	3.77	3.68
K05-E1	-450.00	4.01	3.66	3.81	3.74	3.65
KO7-J6	-50.35	6.64	7.23	3.09	2.89	3.04
K07-J5	-110.00	15.03	14.17	13.89	13.83	13.75
K07-J4	-210.00	6.81	9.10	6.97	13.26	5.66
K07-J3	-290.00	2.77	2.51	3.40	2.43	2.66
K07-J2	-370.00	1.32	1.32	1.49	1.68	1.31
K07-J1	-470.00	1.12	1.08	1.07	1.07	1.04
K08-M4	-50.35	2.41	1.95	1.48	1.76	1.58
K08-M3	-150.00	5.54	3.02	3.51	3.70	3.86
K08-M2	-310.00	4.78	12.96	12.15	8.45	5.78
K08-M1	-450.00	2.12	2.29	2.15	2.16	2.19
K09-AE	-90.07	0.26	0.24	0.25	0.26	0.24
K09-AD	-110.00	0.32	0.30	0.32	0.32	0.30
K09-AC	-150.00	0.42	0.38	0.40	0.43	0.40
K09-AB	-210.00	0.44	0.45	0.49	0.55	0.47
K09-AA	-350.00	0.24	0.25	0.21	0.26	0.25
K10-BA	-50.35	0.11	0.10	0.11	0.09	0.09
K11-CF	-30.48	0.02	0.03	0.04	0.02	0.02
K11-CE	-50.35	0.09	0.11	0.05	0.09	0.07
K11-CD	-90.07	0.27	0.29	0.28	0.28	0.29
K11-CC	-130.00	0.43	0.42	0.42	0.43	0.44
K11-CB	-170.00	0.55	0.51	0.53	0.54	0.53
K11-CA	-210.00	0.67	0.64	0.66	0.66	0.65
K12-DE	-90.07	1.85	2.16	1.81	1.98	2.07
K12-DD	-110.00	2.28	2.22	2.00	2.16	2.34
K12-DC	-230.00	4.95	5.19	5.08	5.00	5.12
K12-DB	-270.00	6.27	6.54	6.42	6.37	6.50
K12-DA	-350.00	7.48	7.97	7.70	7.81	7.81
K13-EE	-90.07	9.71	9.12	8.89	8.90	8.88
K13-ED	-150.00	5.94	5.41	5.35	4.40	5.12
K13-EC	-190.00	4.59	4.23	4.38	4.25	4.19
K13-EB	-250.00	3.94	3.59	3.53	3.52	3.51
K13-EA	-330.00	2.71	2.59	2.84	2.77	2.64
K14-FE	-70.21	0.17	0.16	0.16	0.17	0.15
K14-FD	-110.00	0.34	0.29	0.33	0.31	0.32
K14-FC	-110.00	0.34	0.29	0.33	0.31	0.32
K14-FB	-130.00	0.38	0.34	0.40	0.35	0.40
K14-FA	-150.00	0.43	0.39	0.44	0.43	0.43
Mean error (m)		-0.01	-0.04	-0.1	-0.15	-0.35

Table A-4. Calculated drawdown for tunnel front at 2875 metres, using five realisations of the conductivity field.

Borehole section	Depth m b s l	Realisation 1	2	3	4	5
K02-B5	-190.00	40.26	42.15	41.72	40.13	45.14
K02-B4	-310.00	37.05	39.88	38.69	37.32	38.62
K02-B3	-530.00	26.51	26.45	26.63	26.32	25.99
K02-B2	-830.00	15.40	15.39	15.43	15.40	15.26
K02-B1	-870.00	14.39	14.38	14.41	14.39	14.28
K03-C5	-210.00	5.87	6.16	6.44	6.18	5.99
K03-C4	-350.00	8.49	8.16	8.39	8.14	8.09
K03-C3	-510.00	8.91	8.97	8.84	8.91	8.71
K03-C2	-610.00	8.57	8.85	8.16	8.15	7.94
K03-C1	-670.00	7.82	8.54	8.38	7.96	8.07
K05-E4	-270.00	47.99	48.45	48.56	47.06	48.16
K05-E3	-310.00	43.69	43.55	44.67	44.07	43.91
K05-E2	-430.00	33.83	33.39	33.87	33.39	32.98
K05-E1	-450.00	32.21	31.89	32.30	31.77	31.44
K06-F6	-90.07	9.77	10.19	9.71	9.37	8.83
K06-F4	-250.00	26.95	26.45	26.35	26.12	26.02
K06-F3	-290.00	29.31	28.68	28.71	28.41	28.33
K06-F2	-330.00	30.23	29.44	29.61	29.32	29.11
KO6-F1	-370.00	26.94	27.95	27.13	27.28	24.81
K07-J5	-110.00	33.83	33.51	34.35	32.75	33.54
K07-J4	-210.00	37.58	40.29	42.15	33.52	36.18
K07-J3	-290.00	33.65	28.79	34.35	28.68	32.50
K07-J2	-370.00	16.73	17.73	17.60	18.49	14.99
K07-J1	-470.00	13.06	12.78	12.79	12.66	11.56
K08-M3	-150.00	23.55	18.97	19.69	19.95	19.55
K08-M2	-310.00	25.13	26.64	25.79	24.74	24.23
K08-M1	-450.00	16.33	16.25	16.16	16.09	15.48
K09-AE	-90.07	14.55	13.59	13.54	13.38	8.47
K09-AD	-110.00	14.49	13.74	14.35	13.17	9.80
K09-AC	-150.00	15.03	14.69	15.29	15.48	14.67
K09-AB	-210.00	19.52	17.86	17.79	16.10	19.46
K09-AA	-350.00	8.72	8.96	8.27	8.69	8.44
K10-BA	-50.35	13.61	12.74	12.66	13.02	9.68
K11-CF	-30.48	10.61	10.86	11.57	10.50	5.55
K11-CE	-50.35	14.01	12.14	11.62	12.76	7.38
K11-CD	-90.07	15.09	14.25	15.01	12.17	8.70
K11-CC	-130.00	17.23	16.14	15.72	16.72	13.91
K11-CB	-170.00	23.88	23.57	22.27	23.01	20.45
K11-CA	-210.00	20.50	20.32	20.04	19.91	17.72
K12-DE	-90.07	20.32	20.96	20.10	20.53	20.36
K12-DD	-110.00	21.33	20.82	20.06	20.70	20.76
K12-DC	-230.00	26.22	26.00	26.13	25.88	25.52
K12-DB	-270.00	28.59	28.24	28.42	28.18	27.78
K12-DA	-350.00	27.84	27.56	27.80	27.61	27.04
K14-FE	-70.21	13.37	12.89	13.01	12.66	9.46
K14-FD	-110.00	14.08	12.86	13.90	11.05	10.48
K14-FC	-130.00	13.86	13.98	14.06	11.51	11.21
K14-FB	-130.00	12.22	11.66	13.42	10.43	11.12
K14-FA	-170.00	11.83	11.91	14.08	14.76	11.06
K16-?D	-110.00	10.02	9.95	9.76	9.49	9.18
K16-?C	-230.00	19.74	19.18	19.18	18.86	18.52
K16-?B	-410.00	13.48	13.28	13.33	13.11	12.30
K16-?A	-490.00	12.22	11.95	11.93	11.80	11.02
KB2-B6	-50.35	3.79	3.04	2.54	0.74	2.59
KB2-B5	-70.21	7.92	7.19	9.57	8.48	8.60
KB2-B4	-90.07	9.19	9.87	8.74	9.75	9.73
KB2-B3	-130.00	11.14	11.31	10.75	11.05	10.79
Mean error (m)		0.05	-0.18	0.00	0.65	-1.30

Table A-5. Comparison of measured and calculated drawdowns in percussion boreholes for LPT2 experiment.

Borehole section	Depth M b s l	Calculated drawdown (m)	Measured drawdown (m)	Error (m)
H01-G1	-30.48	2.23	0.00	2.23
H02-H2	-30.48	0.03	0.00	0.03
H02-H1	-70.21	0.04	0.00	0.04
H03-I2	-1.68	0.01	0.00	0.01
H03-I1	-70.21	0.87	0.00	0.87
H04-K2	-30.48	1.50	4.08	-2.58
H04-K1	-130.00	2.20	2.72	-0.52
HO5-L3	-1.68	0.00	1.87	-1.87
H05-L2	-15.59	1.12	5.68	-4.56
H05-L1	-50.35	8.40	5.75	2.65
HO6-N2	-15.59	0.01	1.57	-1.56
H06-N1	-90.07	0.37	2.37	-2.00
H07-O2	-15.59	0.00	0.96	-0.96
H07-O1	-70.21	0.23	0.96	-0.73
H08-P2	-15.59	0.13	0.00	0.13
H08-P1	-90.07	0.55	0.00	0.55
H09-Q2	-1.68	0.00	0.00	0.00
H09-Q1	-50.35	0.20	0.00	0.20
H10-R2	-2.93	0.02	0.00	0.02
H10-R1	-50.35	0.03	0.00	0.03
H11-S2	-4.66	-0.01	0.00	-0.01
H11-S1	-70.21	0.06	0.00	0.06
H12-T2	-8.14	0.03	0.00	0.03
H12-T1	-70.21	0.06	0.00	0.06
H13-U2	-2.93	0.00	0.58	-0.58
H13-U1	-90.07	1.26	1.10	0.16
H14-V2	-30.48	1.81	0.00	1.81
H14-V1	-70.21	3.56	4.67	-1.11
H15-X2	-4.66	0.11	0.85	-0.74
H15-X1	-70.21	0.65	5.20	-4.55
H16-Y2	-30.48	1.08	1.11	-0.03
H16Y1	90.07	2.59	3.12	-0.53
H17-Z2	-8.14	-0.01	2.16	-2.17
H17-Z1	-70.21	2.78	2.99	-0.21
H18-PB	-30.48	0.81	2.99	-2.18
H18-PA	-50.35	0.86	3.41	-2.55

Table A-6. Comparison of measured and calculated drawdowns in percussion boreholes for tunnel front position 2875 metres.

Borehole section	Depth M b s l	Calculated drawdown (m)	Measured drawdown (m)	Error (m)
H01-G1	-30.48	13.60	1.60	12.00
H02-H2	-30.48	0.09	-0.30	0.39
H02-H1	-70.21	0.38	-0.02	0.40
H03-I2	-1.68	0.01	-0.11	0.12
H03-I1	-70.21	13.19	1.65	11.54
H04-K1	-130.00	35.02	48.20	-13.18
H05-L1	-50.35	28.30	55.90	-27.60
HO6-N2	-15.59	0.02	12.20	-12.18
H06-N1	-90.07	5.14	13.90	-8.76
H07-O2	-15.59	0.00	5.70	-5.70
H07-O1	-70.21	3.27	5.20	-1.93
H08-P2	-30.48	1.16	-0.29	1.45
H08-P1	-90.07	5.61	1.30	4.31
H09-Q2	-1.68	0.00	3.90	-3.90
H09-Q1	-50.35	1.92	1.56	0.36
H10-R2	-2.93	0.00	3.48	-3.48
H10-R1	-50.35	0.40	1.66	-1.26
H11-S2	-4.66	0.25	3.37	-3.12
H11-S1	-70.21	0.84	0.54	0.30
H12-T2	-8.14	0.20	0.38	-0.18
H12-T1	-70.21	0.70	0.96	-0.26
H13-U1	-90.07	13.42	13.86	-0.44
H14-V2	-30.48	3.29	0.39	2.90
H14-V1	-70.21	6.64	6.45	0.19
H15-X1	-70.21	7.77	16.13	-8.36
H16-Y2	-30.48	3.11	10.52	-7.41
H16Y1	-90.07	20.72	31.51	-10.79
H17-Z1	-70.21	22.98	34.65	-11.67
H18-PB	-30.48	11.30	-1.87	13.17
H18-PA	-50.35	15.23	21.69	-6.46
H19-QA	-70.21	12.22	0.91	11.31
H20-RB	-30.48	10.26	-0.08	10.34
H20-RA	-70.21	26.88	0.39	26.49
H21-?B	-15.59	-0.01	5.66	-5.67
H21-?A	-90.07	3.33	6.34	-3.01

Table A-7. Sensitivity to transmissivities. Tunnel front at 2875 metres.

Borehole section	Depth M b s l	Measured drawdown (m)	Calculated drawdown 0.5 x T	Error (m)	Calculated drawdown 2 x T	Error (m)
K02-B5	-190.00	45.10	62.12	17.02	24.05	-21.05
K02-B4	-310.00	51.50	56.49	4.99	22.13	-29.37
K02-B3	-530.00	16.90	36.61	19.71	16.76	-0.14
K02-B2	-830.00	18.10	17.68	-0.42	12.20	-5.90
K02-B1	-870.00	17.30	16.08	-1.22	11.95	-5.35
K03-C5	-210.00	1.30	7.28	5.98	4.05	2.75
K03-C4	-350.00	7.70	10.44	2.74	5.88	-1.82
K03-C3	-510.00	6.90	10.47	3.57	6.38	-0.52
K03-C2	-610.00	6.90	9.57	2.67	6.34	-0.56
K03-C1	-670.00	7.70	8.48	0.78	6.13	-1.57
K05-E4	-270.00	40.40	76.99	36.59	28.09	-12.31
K05-E3	-310.00	39.90	68.82	28.92	25.79	-14.11
K05-E2	-430.00	32.50	50.86	18.36	20.51	-11.99
K05-E1	-450.00	29.20	47.78	18.58	19.68	-9.52
K06-F6	-90.07	9.90	14.29	4.39	6.23	-3.67
K06-F4	-250.00	33.80	43.80	10.00	15.68	-18.12
K06-F3	-290.00	13.90	47.48	33.58	17.08	3.18
K06-F2	-330.00	29.10	48.44	19.34	17.73	-11.37
KO6-F1	-370.00	30.00	42.59	12.59	16.05	-13.95
K07-J5	-110.00	54.80	48.58	-6.22	20.72	-34.08
K07-J4	-210.00	37.50	58.53	21.03	22.54	-14.96
K07-J3	-290.00	25.20	52.44	27.24	20.28	-4.92
K07-J2	-370.00	11.70	25.09	13.39	10.64	..-1.06
K07-J1	-470.00	18.10	18.91	0.81	8.62	-9.48
K08-M3	-150.00	25.90	35.45	9.55	14.24	-11.66
K08-M2	-310.00	16.60	42.06	25.46	14.45	-2.15
K08-M1	-450.00	19.50	24.53	5.03	10.21	-9.29
K09-AE	-90.07	11.40	23.36	11.96	8.93	-2.47
K09-AD	-110.00	12.00	23.06	11.06	8.93	-3.07
K09-AC	-150.00	14.60	22.50	7.90	9.82	-4.78
K09-AB	-210.00	14.00	25.65	11.65	15.31	1.31
K09-AA	-350.00	11.50	12.80	1.30	6.06	-5.44
K10-BA	-50.35	13.50	21.58	8.08	8.39	-5.11
K11-CF	-30.48	15.50	12.17	-3.33	7.09	-8.41
K11-CE	-50.35	16.00	22.43	6.43	8.59	-7.41
K11-CD	-90.07	14.50	24.14	9.64	9.22	-5.28
K11-CC	-130.00	18.60	28.07	9.47	10.34	-8.26
K11-CB	-170.00	16.80	40.97	24.17	13.69	-3.11
K11-CA	-210.00	20.00	34.13	14.13	12.02	-7.98
K12-DE	-90.07	25.60	27.93	2.33	12.72	-12.88
K12-DD	-110.00	25.00	29.33	4.33	13.46	-11.54
K12-DC	-230.00	25.40	38.87	13.47	15.90	-9.50
K12-DB	-270.00	25.30	43.21	17.91	17.14	-8.16
K12-DA	-350.00	24.90	41.94	17.04	16.72	-8.18
K14-FE	-70.21	11.50	21.33	9.83	8.23	-3.27
K14-FD	-110.00	11.50	22.43	10.93	8.66	-2.84
K14-FC	-130.00	11.60	22.04	10.44	8.56	-3.04
K14-FB	-130.00	11.60	19.16	7.56	7.78	-3.82
K14-FA	-170.00	11.90	18.44	6.54	7.59	4.31
K16-?D	-110.00	15.20	15.49	0.29	6.15	-9.05
K16-?C	-230.00	28.00	32.00	4.00	11.67	-16.33
K16-?B	-410.00	18.60	19.87	1.27	8.66	-9.94
K16-?A	-490.00	16.70	17.41	0.71	8.08	-8.62
KB2-B6	-50.35	5.10	5.24	0.14	2.60	-2.50
KB2-B5	-70.21	8.00	10.81	2.81	5.52	-2.48
KB2-B4	-90.07	8.60	13.20	4.60	6.31	-2.29
KB2-B3	-130.00	5.30	17.72	12.42	7.46	2.16
Mean error (m):				10.1		-7.4

Table A-8. Sensitivity to the conductivities. Tunnel front at 2875 metres.

Borehole section	Depth M b s l	Measured drawdown (m)	Calculated drawdown 0.5 x Cond	Error (m)	Calculated drawdown 2 x Cond	Error (m)
K02-B5	-190.00	45.10	29.38	-15.72	30.74	-14.36
K02-B4	-310.00	51.50	28.99	-22.51	28.42	-23.08
K02-B3	-530.00	16.90	22.29	5.39	20.10	3.20
K02-B2	-830.00	18.10	14.09	-4.01	13.08	-5.02
K02-B1	-870.00	17.30	13.37	-3.93	12.61	-4.69
K03-C5	-210.00	1.30	5.37	4.07	4.02	2.72
K03-C4	-350.00	7.70	6.83	-0.87	5.99	-1.71
K03-C3	-510.00	6.90	7.16	0.26	6.56	-0.34
K03-C2	-610.00	6.90	6.97	0.07	6.49	-0.41
K03-C1	-670.00	7.70	6.57	-1.13	6.24	-1.46
K05-E4	-270.00	40.40	41.39	0.99	37.89	-2.51
K05-E3	-310.00	39.90	37.62	-2.28	34.15	-5.75
K05-E2	-430.00	32.50	29.49	-3.01	26.29	-6.21
K05-E1	-450.00	29.20	28.04	-1.16	24.90	-4.30
K06-F6	-90.07	9.90	10.88	0.98	7.46	-2.44
K06-F4	-250.00	33.80	22.52	-11.28	22.16	-11.64
K06-F3	-290.00	13.90	24.82	10.92	24.09	10.19
K06-F2	-330.00	29.10	25.76	-3.34	24.67	-4.43
KO6-F1	-370.00	30.00	23.05	-6.95	21.89	-8.11
K07-J5	-110.00	54.80	19.29	-35.51	24.22	-30.58
K07-J4	-210.00	37.50	32.26	-5.24	28.85	-8.65
K07-J3	-290.00	25.20	32.78	7.58	26.23	1.03
K07-J2	-370.00	11.70	17.92	6.22	13.19	1.49
K07-J1	-470.00	18.10	13.83	-4.27	10.48	-7.62
K08-M3	-150.00	25.90	12.92	-12.98	18.36	-7.54
K08-M2	-310.00	16.60	22.09	5.49	21.35	4.75
K08-M1	-450.00	19.50	15.32	-4.18	13.25	-6.25
K09-AE	-90.07	11.40	16.51	5.11	11.43	0.03
K09-AD	-110.00	12.00	16.45	4.45	11.35	-0.65
K09-AC	-150.00	14.60	18.05	3.45	11.34	-3.26
K09-AB	-210.00	14.00	28.53	14.53	13.22	-0.78
K09-AA	-350.00	11.50	9.85	-1.65	7.42	-4.08
K10-BA	-50.35	13.50	15.51	2.01	10.60	-2.90
K11-CF	-30.48	15.50	9.42	-6.08	10.09	-5.41
K11-CE	-50.35	16.00	15.95	0.05	10.88	-5.12
K11-CD	-90.07	14.50	17.06	2.56	11.87	-2.63
K11-CC	-130.00	18.60	19.13	0.53	13.97	-4.63
K11-CB	-170.00	16.80	25.71	8.91	20.54	3.74
K11-CA	-210.00	20.00	22.18	2.18	17.24	-2.76
K12-DE	-90.07	25.60	7.57	-18.03	14.23	-11.37
K12-DD	-110.00	25.00	8.87	-16.13	14.99	-10.01
K12-DC	-230.00	25.40	17.94	-7.46	19.57	-5.83
K12-DB	-270.00	25.30	21.09	-4.21	21.85	-3.45
K12-DA	-350.00	24.90	21.95	-2.95	21.54	-3.36
K14-FE	-70.21	11.50	15.04	3.54	10.46	-1.04
K14-FD	-110.00	11.50	15.82	4.32	11.14	-0.36
K14-FC	-130.00	11.60	15.60	4.00	10.96	-0.64
K14-FB	-1300.00	11.60	13.99	2.39	9.60	-2.00
K14-FA	-170.00	11.90	13.38	1.48	9.41	-2.49
K16-?D	-110.00	15.20	9.00	-6.20	7.93	-7.27
K16-?C	-230.00	28.00	18.89	-9.11	16.38	-11.62
K16-?B	-410.00	18.60	13.65	-4.95	10.83	-7.77
K16-?A	-490.00	16.70	12.50	-4.20	9.85	-6.85
KB2-B6	-50.35	5.10	4.86	-0.24	2.77	-2.33
KB2-B5	-70.21	8.00	10.38	2.38	5.67	-2.33
KB2-B4	-90.07	8.60	11.47	2.87	6.91	-1.69
KB2-B3	-130.00	5.30	12.45	7.15	9.31	4.01
Mean error (m):				-1.9		-4.2

APPENDIX B

DOCUMENTATION

CONDENSED DESCRIPTION OF GROUNDWATER FLOW MODEL

A site scale analysis of groundwater flow and salinity distribution in the Äspö area Stochastic continuum model	
Scope Groundwater flow and salinity distributions on a site scale	
Process description Conservation of mass, volume and momentum (Darcy´s law)	
CONCEPTS	**DATA**
Geometric framework and parameters	
Domain divided into computational cells to which conservation laws are applied. Subdomains consist of deterministic fracture zones and rock volumes between the fracture zones.	Domain size: 1.8 x 1.8 x 1.0 km^3 Computational grid: 445 500 cells
Material properties	
Hydraulic conductivities (K). Density varies with salinity. Transmissivity for fracture zones (T).	Data from Rhén et al (1997).
Spatial assignment method	
Stochastic conductivity (K) for the rock mass outside the deterministic fracture zones with no correlation between cells. Deterministic fracture zone transmissivities. K modified if cell is intersected by a fracture zone.	Data from Rhén et al (1997).
Boundary conditions	
Boundary conditions from a regional model for bottom and vertical boundaries. Prescribed pressure and salinity below the Baltic and prescribed recharge on land.	Data from Rhén et al (1997). Data from regional model, Svensson (1997)
Numerical tool PHOENICS	
Output parameters Flux, hydraulic head and salinity	

SKB-ÄSPÖ HARD ROCK LABORATORY

Documentation of numerical simulation by Urban Svensson (US) 1997-10-8

OBJECT

SKB purchase order no:52600 97 072 2220
Title of SKB purchase order: Äspölaboratoriet – Grundvattemodell för Äspö
Author of report: US Company: CFE AB
Operator of computer and software: US Company: CFE AB

COMPUTER

Name and version: Silicon Graphics, O2/R10 000.

SOFTWARE

Operative system: IRIX 6.3
Code name: PHOENICS 2.1 Main manual: On line
Program language: FORTRAN
Compiler: F77 for IRIX 6.3
Postprocessor name: EXPLORER Manual:
Postprocessor name: PHOTON Manual:
Subroutine: Report:
Subroutine: Report:
Subroutine: Report:

CODE VERIFICATION

Distributor: Not compiled in a single report.
Report/article:
Report/article:
Other verification
Report/article: See Svensson (1995) and (1997), as referenced in this report.
Report/article:

INPUT DATA

Ref: Rhén et al (1997), see reference list.
Ref: Forsmark and Rhén (1994), see reference list.
Ref:
Ref:

Data file name:	Data of issue:	Stored at:
Data file name:	Data of issue:	Stored at:
Data file name:	Data of issue:	Stored at:

RESULTS

Report/article: All given in this report.
Report/article:

Data file name:	Stored at:
Data file name:	Stored at:

List of SKB reports

Annual Reports

1977-78
TR 121
KBS Technical Reports 1 – 120
Summaries
Stockholm, May 1979

1979
TR 79-28
The KBS Annual Report 1979
KBS Technical Reports 79-01 – 79-27
Summaries
Stockholm, March 1980

1980
TR 80-26
The KBS Annual Report 1980
KBS Technical Reports 80-01 – 80-25
Summaries
Stockholm, March 1981

1981
TR 81-17
The KBS Annual Report 1981
KBS Technical Reports 81-01 – 81-16
Summaries
Stockholm, April 1982

1982
TR 82-28
The KBS Annual Report 1982
KBS Technical Reports 82-01 – 82-27
Summaries
Stockholm, July 1983

1983
TR 83-77
The KBS Annual Report 1983
KBS Technical Reports 83-01 – 83-76
Summaries
Stockholm, June 1984

1984
TR 85-01
Annual Research and Development Report 1984
Including Summaries of Technical Reports Issued during 1984. (Technical Reports 84-01 – 84-19)
Stockholm, June 1985

1985
TR 85-20
Annual Research and Development Report 1985
Including Summaries of Technical Reports Issued during 1985. (Technical Reports 85-01 – 85-19)
Stockholm, May 1986

1986
TR 86-31
SKB Annual Report 1986
Including Summaries of Technical Reports Issued during 1986
Stockholm, May 1987

1987
TR 87-33
SKB Annual Report 1987
Including Summaries of Technical Reports Issued during 1987
Stockholm, May 1988

1988
TR 88-32
SKB Annual Report 1988
Including Summaries of Technical Reports Issued during 1988
Stockholm, May 1989

1989
TR 89-40
SKB Annual Report 1989
Including Summaries of Technical Reports Issued during 1989
Stockholm, May 1990

1990
TR 90-46
SKB Annual Report 1990
Including Summaries of Technical Reports Issued during 1990
Stockholm, May 1991

1991
TR 91-64
SKB Annual Report 1991
Including Summaries of Technical Reports Issued during 1991
Stockholm, April 1992

1992
TR 92-46
SKB Annual Report 1992
Including Summaries of Technical Reports Issued during 1992
Stockholm, May 1993

1993
TR 93-34
SKB Annual Report 1993
Including Summaries of Technical Reports Issued during 1993
Stockholm, May 1994

1994

TR 94-33

SKB Annual Report 1994

Including Summaries of Technical Reports Issued during 1994

Stockholm, May 1995

1995

TR 95-37

SKB Annual Report 1995

Including Summaries of Technical Reports Issued during 1995

Stockholm, May 1996

1996

TR 96-25

SKB Annual Report 1996

Including Summaries of Technical Reports Issued during 1996

Stockholm, May 1997

List of SKB Technical Reports 1997

TR 97-01

Retention mechanisms and the flow wetted surface – implications for safety analysis

Mark Elert

Kemakta Konsult AB

February 1997

TR 97-02

Äspö HRL – Geoscientific evaluation 1997/1. Overview of site characterization 1986–1995

Roy Stanfors[1], Mikael Erlström[2], Ingemar Markström[3]

[1] RS Consulting, Lund

[2] SGU, Lund

[3] Sydkraft Konsult, Malmö

March 1997

TR 97-03

Äspö HRL – Geoscientific evaluation 1997/2. Results from pre-investigations and detailed site characterization. Summary report

Ingvar Rhén (ed.)[1], Göran Bäckblom (ed.)[2], Gunnar Gustafson[3], Roy Stanfors[4], Peter Wikberg[2]

[1] VBB Viak, Göteborg

[2] SKB, Stockholm

[3] VBB Viak/CTH, Göteborg

[4] RS Consulting, Lund

May 1997

TR 97-04

Äspö HRL – Geoscientific evaluation 1997/3. Results from pre-investigations and detailed site characterization. Comparison of predictions and observations. Geology and mechanical stability

Roy Stanfors[1], Pär Olsson[2], Håkan Stille[3]

[1] RS Consulting, Lund

[2] Skanska, Stockholm

[3] KTH, Stockholm

May 1997

TR 97-05

Äspö HRL – Geoscientific evaluation 1997/4. Results from pre-investigations and detailed site characterization. Comparison of predictions and observations. Hydrogeology, groundwater chemistry and transport of solutes

Ingvar Rhén[1], Gunnar Gustafson[2], Peter Wikberg[3]

[1] VBB Viak, Göteborg

[2] VBB Viak/CTH, Göteborg

[3] SKB, Stockholm

June 1997

TR 97-06

Äspö HRL – Geoscientific evaluation 1997/5. Models based on site characterization 1986–1995

Ingvar Rhén (ed.)[1], Gunnar Gustafson[2], Roy Stanfors[4], Peter Wikberg[4]

[1] VBB Viak, Göteborg

[2] VBB Viak/CTH, Göteborg

[3] RS Consulting, Lund

[4] SKB, Stockholm

October 1997

TR 97-07

A methodology to estimate earthquake effects on fractures intersecting canister holes

Paul La Pointe, Peter Wallmann, Andrew Thomas, Sven Follin

Golder Associates Inc.

March 1997

TR 97-08

Äspö Hard Rock Laboratory Annual Report 1996

SKB

April 1997

TR 97-09

A regional analysis of groundwater flow and salinity distribution in the Äspö area

Urban Svensson

Computer-aided Fluid Engineering AB

May 1997

TR 97-10
On the flow of groundwater in closed tunnels. Generic hydrogeological modelling of nuclear waste repository, SFL 3–5
Johan G Holmén
Uppsala University/Golder Associates AB
June 1997

TR 97-11
Analysis of radioactive corrosion test specimens by means of ICP-MS. Comparison with earlier methods
R S Forsyth
Forsyth Consulting
July 1997

TR 97-12
Diffusion and sorption properties of radionuclides in compacted bentonite
Ji-Wei Yu, Ivars Neretnieks
Dept. of Chemical Engineering and Technology, Chemical Engineering, Royal Institute of Technology, Stockholm, Sweden
July 1997

TR 97-13
Spent nuclear fuel – how dangerous is it? A report from the project "Description of risk"
Allan Hedin
Swedish Nuclear Fuel and Waste Management Co,
Stockholm, Sweden
March 1997

TR 97-14
Water exchange estimates derived from forcing for the hydraulically coupled basins surrounding Äspö island and adjacent coastal water
Anders Engqvist
A & I Engqvist Konsult HB, Vaxholm, Sweden
August 1997

TR 97-15
Dissolution studies of synthetic soddyite and uranophane
Ignasi Casas[1], Isabel Pérez[1], Elena Torrero[1], Jordi Bruno[2], Esther Cera[2], Lara Duro[2]
[1] Dept. of Chemical Engineering, UPC
[2] QuantiSci SL
September 1997

TR 97-16
Groundwater flow through a natural fracture. Flow experiments and numerical modelling
Erik Larsson
Dept. of Geology, Chalmers University of Technology, Göteborg, Sweden
September 1997